Thesis submitted in Partial Fulfillment of Requirements for the Degree of Doctor of Philosophy

Updating Failure Probability of a Welded Joint Considering Monitoring and Inspection

For Offshore Wind Turbine Substructures

MAI Anh Quang

September, 2018

Faculty of Applied Sciences
University of Liege

Abstract

Reliability assessment of existing offshore wind turbine (OWT) support structures taking advantage of historical data from inspection and monitoring is crucial for the optimisation of maintenance and life extension. In this thesis, the crack inspection data and the monitoring data are separately considered for updating failure probability of welded joints.

Concerning crack inspection data, this thesis aims at finding advantages of using the fatigue assessment diagram (FAD) in the failure criteria for failure probability estimation and updating. The crack inspection results (no detection or detected) and possible immediate interventions (repair normally or perfectly) are considered. Failure probabilities are calculated using the FAD and then compared with those obtained from the usual critical crack size criteria. The simulation-based approach is used to calculate and update the failure probability. Crack depth and length are simulated simultaneously. The crack propagations are calculated using a bi-linear Paris' law with stress-range value varying over time. Uncertainties come from the crack growth parameters, initial crack sizes, fracture toughness, yield and ultimate strengths, FAD formula, stress intensity factor, stress-range values, and the detectable crack size.

By combining the fracture toughness with the crack size in the failure criteria, the results show that the estimated failure probability of the welded joint is significantly increased in comparison to the case where only critical crack size is considered in the LSF. In comparison with the failure criteria which includes both the critical crack size and fracture toughness, the FAD approach gives similar reliability results when the applied peak tensile stress is small. However, when the applied peak tensile stress is high (the ratio between applied peak tensile stress and yield strength is more than 65%), the FAD approach predicts higher failure probability values. The uncertainty in FAD does not significantly affect the predicted failure probability of the joint as compared to the uncertainties in the ultimate and yield strength. This is because the latter affects directly the cut-off location of the FAD curve where

the plastic failure is defined. The FAD approach can be used to update failure probability considering crack inspections and intervention actions. The calculation shows that reliability of the welded joint increases when no crack is detected, or when a crack is detected and repaired. In comparison with a perfect repair, a normal repair assumption significantly reduces the reliability of the joint.

With regard to the monitoring data, the research questions how to effectively incorporate the measured strain and the oceanographic data (wind, wave) for updating failure probability of a welded joint in fatigue failure mode. To answer the question, the monitoring data is used to update the characteristics of a random variable in the LSF. Consequently, the updated random variable is then used in a reliability analysis to obtain the updated failure probability.

The limit state function (LSF) is based on the Miner's rule and solved using the first order reliability method (FORM). The random variable used to update failure probability is the joint distribution of wind speed, wave height and wave period. The monitoring data consists of strain, 10-minute mean wind speed, significant wave height, and mean wave period. Fatigue damage is summed up from all load combinations, i.e. from all the discretized components of the joint distribution of wind and wave. The measured strain data is used to calculate fatigue damage in each load combination. The probability of each load combination is calculated using its joint distribution, which in turn can be updated using monitoring data. The 10-minute mean wind speed is assumed to follow a Weibull distribution and can be updated using Bayesian approach. Assuming that the scale parameter is a normally distributed random variable with unknown mean and standard deviation, the predictive distribution of this random variable becomes a student's t-distribution.

The proposed methodology has been applied to a monopile support structure of a wind farm in Belgium. The measured strain is used to find the potential hot-spot location. Stresses are derived at the hot-spot location for fatigue analyses. It is assumed that stress-ranges in each load combination follow a Weibull distribution. The stress-range distribution parameters are found by performing least squares fitting method on the fatigue damage.

The results show that the Weibull distribution is generally not very good for fitting stress-ranges in each wind-speed bin for the considered data. However, the integrated fatigue damage for the considered load combination is quite accurate since it is the objective of the fitting procedure. The main influence on the remaining fatigue life is the magnitude of stress-ranges at the hot-spot. So the stress con-

centration factor, the interpolating factor (for example to obtain stresses at under water locations), the correction factor for corrosion effects (if any), and their uncertainties should be estimated with great care. The measured 10-minute wind speed data has a significant effect in adjusting the predicted probability of failure and eventually the remaining fatigue life. The duration of strain measurement should be long enough to be combined with oceanographic data. Longer strain measurement duration, greater number of parameters in the oceanographic data can be considered for the failure probability updating.

Acknowledgments

I would like to acknowledge my indebtedness and render my warmest gratitude to my supervisor, Professor Philippe Rigo, who made this work possible. His friendly approach towards guidance and advice have been invaluable throughout all stages of this work. Through his large professional connections, he guided me to the direction of right people in various industrial, academic and research organisation for advice and collecting data.

I would also wish to express my sincere gratitude to Professor John Dalsgaard Sørensen — Department of Civil Engineering, Aalborg University — for his unwavering support during the four years of my doctoral work. He enriched my knowledge in the field of reliability assessment and constantly motivated me during my research. I have learned a lot from working with him during my stays at Aalborg and I hope to continue this collaboration post my doctorate as well.

I would like to show my deepest gratitude to other members of my thesis committee, Professor Vincent Denoël, and Professor Fredric Collin, Faculty of Applied Sciences - University of Liège for their advice during my four years of doctoral training.

I am profoundly grateful to the Fund for Research Training in Industry and Agriculture (FRIA - FNRS) for having recognised the viability of my research project and financially supported me and my work during the four years.

My sincere thanks to Professor Christof Devriendt — Department of Mechanical Engineering, Faculty of Applied Sciences, Vrije Universiteit Brussel — for his continuous support since the beginning of my doctoral research. This thesis would not have been completed without the help of Professor Devriendt and his colleague, Dr. Wout Weijtjens in the Offshore Wind Infrastructure Application Lab (OWI-Lab), to get access to the measurement data of a real offshore wind farm in Belgium.

I would like to thank all my colleagues in ANAST Research Group for sharing nice moments with me beside the concentrated working hours of the doctoral research. I particularly thank Renaud Warnotte for his Java codes to improve my workflows, Pablo Morato for useful scientific discussions, and Akula Nidarshan for english proofreading.

Finally, I would like to express my gratitude to my family for their encouragement, especially to my wife for sharing responsibilities of parenthood and taking care of my two adorable children.

Contents

List of Figures

List of Tables

Chapter 1.

Introduction

Wind energy has become an important contributor to European electricity generation. In the year 2017, it contributed more than half of renewable energy. More than half of renewable energy produced in 2017 was from this source. As according to the same statistics of the Global Wind Energy Council, wind power provided more than 48% of total power generated in Denmark. In Belgium, two nuclear power plants, Doel and Tihange with a total capacity of 6 gigawatts, are earmarked for closure by 2025 due to technical problems at reactors. To compensate for the shortfall, Belgium will double the available area of its North Sea waters for offshore wind farms after 2020. Germany, with the plan to completely close the country's nuclear plants by 2022 and to gradually stop using fossil power in order to reduce emissions, also promises to ramp up the share of renewables, especially offshore wind energy.

In the organisation's annual 'Global Wind Report 2017', the Global Wind Energy Council states that the prices for offshore wind energy projects to be completed in the next five years will be half of what they were five years ago, and this trend is likely to continue. In 2010, electricity generated through offshore wind in Europe costed around 17 cents per kilowatt hour; more than twice of what utilities were paying for the power derived from burning gas and coal. The price dropped to around 13 cents by the year 2017.

In the near future, the worldwide spread of offshore wind energy is very promising. It results from the advances in sophisticated power electronics, manufacturing and construction of larger scale turbines, planning and overall management. Another factor is the precipitous drop in the battery storage prices. Many new concepts of battery storage have been developed. A recent technology of battery storage, called Power-to-gas technology, helps to convert the overproduced renewable energy into gas (methane–CH_4) and connect to the natural gas system. This is a twofold

'sustainable' battery concept, because for producing CH_4, it takes the emitted CO_2 directly from factories.

The competitiveness of offshore wind energy depends not only on initial costs but also the cost of operation and maintenance (O&M), which is estimated to be about one third of the total lifecycle costs of an offshore wind farm project. The O&M cost of support structures is proportional to the distance from the O&M port to the site. In shallow water, the O&M cost of support structures is similar to that of the turbine. In transitional water, it is twice, and triple in deep water [1]. Therefore, reducing the O&M cost of support structures becomes crucial to maximize the benefit of pushing wind farms further off shore. Changing from preventive maintenance to condition-based maintenance is one of the current research trends to reduce the levelized cost of electricity (LCOE) of offshore wind energy.

In principle, a condition-based maintenance proposes an optimal inspection plan obtained by solving a decision tree for different possible inspection outcomes and intervention actions. The increased focus on the profit of offshore wind farm operations has encouraged mining of historical data and developing modelling tools, which can provide valuable insights into the structural behaviors for the optimisation of maintenance and extended life. Using crack inspection and monitoring data in updating failure probability of a structural component is the subject of this research.

1.1. Research Aims

In using crack inspection data to update failure probability of structural components, a critical crack size value is usually used to justify the failure state of a welded joint. This failure criterion is uncertain because fracture can happen with a smaller crack size subjected to a high applied stress. In contrast, a larger crack size might not lead to component fracture if the applied stress is small. This uncertainty has not yet been treated properly in the reliability assessment. In BS 7910, a British standard for assessing the acceptability of flaws in metallic structures, a Fracture Assessment Diagram (FAD) is used instead of the critical crack size. The benefit of using the FAD concept in the assessment of existing offshore structures is that the knowledge of critical crack size at different values of applied stress is not required, and diferent fracture modes (brittle, plastic, or transition) are already included.

Using monitoring data such as wind, wave, and structural responses (e.g. strain)

in assessment of existing structures is a new demand when offshore wind farms are getting closer to the end of their service lives. The 'design' approach, i.e. using finite element models, contains most of the uncertainties as in the design stage, and is very time consuming for a stochastic analysis. Moreover, measurement data of structural responses may be limited to few years, and it needs to be used efficiently together with wind and wave data in the future to predict failure probability of the structure for inspection planning or life extension purpose.

The aims of this research are, therefore, to quantify advantages of using FAD in reliability updating based on crack inspections, and how a limited monitoring data can be used to update failure probabilities.

1.2. Research Objectives

In order to achieve the research aims, many actions are required:

- Comparing the failure probability obtained using critical crack size and FAD,
- Using FAD in updating failure probabilities when crack inspection and intervention actions are available,
- Formulating a limit state function that contains oceanographic data (i.e. wind, wave) as a basic random variable,
- Updating this basic random variable using data obtained at the design stage,
- Performing reliability analysis using the updated random variable.

1.3. Research Scope

- This thesis aims at reliability assessment of existing offshore wind turbine support structures given that crack inspection data and/or monitoring data are available.
- Only fatigue failure mode is considered since it is the main failure mode in offshore structures.
- The obtained reliability index is at component level, i.e. a welded joint. In a structural system like a monopile, a conclusion about the whole structure can be made if the joint is at a critical level, but it is not usually the case for a redundant structural system;

- Target reliability index optimisation for the existing structure is not in the research scope of this thesis;

The basis assumption of this thesis is the Bayesian interpretation of probability. It is used in updating failure probability of the joint when new information about crack inspection is available. It is also used in updating the 10-minute mean wind speed distribution.

1.4. Thesis Outline

The thesis consists of five chapters. After the introduction (chapter 1), chapter 2 provides an overview of the research ideas and approaches with emphasis on a general framework for risk based assessment, and reliability updating of offshore structures. In chapter 3, FAD is used for updating failure probability of a welded joint considering crack inspection and intervention actions. Then, a methodology is presented in chapter 4 to integrate monitoring data into reliability assessment. The thesis concludes with chapter 5 summarising the main achievements, contributions and perspectives.

Basic state of knowledge is presented in chapter 2. The structural reliability methods are reviewed to see their advantages and disadvantages. Starting with the first order and second order reliability methods, the review continues with Monte Carlo simulation and its important sampling techniques. The response surface methodology is then introduced to consider stochastic variables in finite element analyses. When number of random variables are large, the previous methods may face difficulty to converge. Therefore, for this high dimensional reliability problem, the asymptotic sampling based approach can be used. Considering a random variable that varies with time—a random process—in a reliability analysis is rather complicated and only some solutions for simple problems have been found. Even if the failure probabilities of all the components are available, finding the failure probability of a redundant system is still chanllenging. Chapter 2 continues with a section about reliability assessment of existing offshore structures. Some approximation methods to assess the safety of offshore jacket platforms are reviewed together with some current standards for assessment of existing offshore structures. Discussion about the target safety level for existing offshore structures concludes this chapter.

Chapter 3 presents how the reliability of welded steel details can be updated when data about crack inspection and intervention actions is available. In this chapter, the fatigue failure is modelled by a fracture mechanics model and a FAD is used to

define the limit state function. A two dimensional bi-linear model is considered for the crack growth. Calculation of crack depths and crack lengths are coupled. The stress intensity factors are calculated following the procedure in BS 7910:2013. The initial crack sizes, yield and ultimate strengths of steel, fracture toughness, stress intensity factor, and stress-ranges are considered as uncertain and modelled as random variables. The probability of detection is used to represent the uncertainty in crack inspections. The simulation-based approach is used to update failure probability. Randomly generated stress-ranges are used, not only to calculate crack size but also, together with the calculated stress intensity factors, to check safety condition using FAD. The results of failure probability from FAD approach are compared with the ones using critical crack size. The updating of failure probability is considered for three inspection scenarios: no crack detected; crack detected and repaired imperfectly; crack detected and repaired perfectly.

Chapter 4 covers failure probability updating of a welded joint using the measured oceanogaphic and strain data. Given that they are concurrently measured for a certain period of time, the oceanographic data can be linked to the fatigue damage using the strain data. Oceanographic data is represented by a random variable which is a joint distribution of wind speed, wave height and wave period. New measurement data on wind and wave can be used to update the joint distribution using Bayesian approach. Limit state function for reliability analysis is built using Miner's rule to calculate total fatigue damage. The year-to-year variation of the 10-minute mean wind speed, unrepresentativenesss of the structural response during one year, measurement uncertainty, and corrosion effect are considered together with uncertainties of Miner's rule and S-N curves. The first order reliability method is used to solve the limit state function. The methodology is applied to predict remaining fatigue life of a monopile support structure.

Chapter 2.

State of Knowledge

2.1. Reliability Analysis Methods

The main purpose of reliability analysis is to solve the 'probability integration' of the continous joint density function of basic random variables in the failure space defined by the limit state function. Since this integral cannot be computed analytically, many methods have been proposed during several decades.

The early and widely accepted solution was the second moment reliability concept, proposed by Cornell [2]. The idea of this method is that all random variables are expressed solely in terms of their expected values and covariances. Ditlevsen [3] and Lind [4] independently discovered the invariance problem of the Cornell approach: the reliability index is not constant for certain simple problems when the limit state function is rewritten in an equivalent way. To solve the invariance problem, Hasofer and Lind [5] redefined the linearization point on the failure surface and the reliability index. The drawback of this concept is the inconsistency of the results: different shapes of limit state functions can have the same value of reliability index. Using the Hasofer and Lind's definition of the design point and the reliability index, the First Order Reliability Method (FORM) was introduced by considering the joint distribution of all the basic random variables. A transformation of the random variables is needed to express limit state function in the independent standard normal space. A refined result of reliability index can be obtained by using a quadratic approximation to the failure surface at the design point. That method, developed after FORM, is called the Second Order Reliability Method (SORM). Although FORM/SORM approach is generally efficient, there are cases where a converged solution cannot be found. Besides, it is assumed that the limit state function is differentiable which is not the case if the limit state function involves

expensive external codes such as finite element analyses or experimental crack growth laws.

The Monte Carlo algorithm can be used to solve the 'probability integration' by generating a large series of stochastic experiments. Without any tweaks, the standard Monte Carlo algorithm can only be used to solve a large failure probability problem. Several techniques have been developed to tweak this algorithm. The concept of 'Importance Sampling' was first brought to the attention of the reliability community by Harbitz and Shinozuka [6, 7]. The techniques of Importance Sampling includes, e.g. direct, updating, adaptive, and spherical methods. A review of these Importance Sampling techniques can be found in [8]. The updating Importance Sampling method can be used to update (refine) the reliability index obtained from FORM/SORM and even substitutes them with a little more numerical effort [9]. In general, the Importance Sampling methods will fail or become inefficient if the most likely failure region(s) cannot be identified in advance.

Response Surface Methodology (RSM) is another approach to solve the 'probability integration' where the limit state function is fitted to a linear or quadratic response surface. The response surface can be obtained by many techniques such as interpolation, moving least-squares regression, neural networks, and radial basis functions [10]. The fitting points are selected using experimental design plans. A large variety of experimental designs and methods applying response surfaces can be found in Myers and Montgomery [11]. Some RSM techniques have been implemented in finite element software such as ANSYS [12]. RSM can be used to estimate the LSF in the vicinity of the design point and then the standard gradient reliability optimization method (FORM) is used to search for the exact design point on the LSF approximation [13]. Thöns et al. [14] used a combination of an adaptive response surface method and an Importance Sampling Monte Carlo simulation to estimate reliability of OWT support structures. If an important region of the LSF approximation is fitted from an inaccurate point, the accuracy of this methodology might be difficult to check except that it is a small dimensional uncertainty problem.

When the reliability problem is highly dimensional, some recently developed concepts can be used to approximate the reliability index using Monte Carlo simulations. Bucher [15] proposed the Asymptotic Sampling based on the asymptotic behavior of failure probabilities as the standard deviations of the random variables tend to zero. A similar approach suggested by Naess [16], called Enhanced Sampling, uses the asymptotic behaviour of failure probabilities as the limit states are moved further away from the mean of the random vector. The two mentioned

concepts express reliability index as a function of a single parameter. Monte Carlo simulation is used to find a set of fitting points for the reliability function using different sample sizes. These concepts can be used for reliability assessment of a component with a high dimensional uncertainty space as well as for a system of many components.

For time-dependent reliability, interest lies mainly in the time needed before the first occurrence of an excursion of the random vector out of the safe domain. The probability of the first occurrence of such an excursion (i.e. the outcrossing rate) may be considered to be equivalent to the probability of structural failure during a given period of time. The out-crossing rate calculation involves the full history of the random processes and its solution is rather difficult to obtain. A discretization in time and other approximations have been suggested in [17, 18]. For structural reliability problems, out-crossing rate at a certain time is typically very small, so the out-crossings at different time locations can be considered as independent events. Using a Poisson distribution with zero events for the probability of 'no out-crossing in the first time period', an upper bound and lower bound of the failure probability can be calculated [19].

Concerning the reliability assessment of a system of components, it is often hard to be obtained directly using methods of structural reliability. In principle, standard Monte Carlo simulation methods can be used to predict accurately the system failure probability but the computational burden may be prohibitive. Beside the Importance Sampling and Directional Sampling procedures, the Asymptotic Sampling proposed by Naess [16] can also be used to enhance the efficiency of the Monte Carlo simulation method. In this concept, the reliability problem has been reformulated to depend on a single parameter and exploit the regularity of the tail probability as a function of this parameter. Failure probability of a structural system can only be found using approximation methods. Often, the failure probabilities of a structural system can be found in the form of upper and lower bounds [20]. But the approximated solutions can also be found using artificial limit state functions that are built using response surface approaches [21].

2.2. Probabilistic Evaluation of Existing Structures

With regard to the assessment of existing offshore structures, ISO 19902 [22] procedure includes both a check of the ultimate limit state and the fatigue limit state. The conditions that triggers the need for a structural assessment (assessment ini-

tiators) to demonstrate the fitness-for-purpose of the structures are described, including e.g. damage or deterioration of a primary structural component, changes from the original design, or more onerous environmental conditions. Although the structural reliability analysis is mentioned in the assessment procedure of existing structures, no guidance has been offered.

Developed based on API RP 2A-WSD [23] and ISO 19902:2007 [22], the recommended practice API RP 2SIM [24] details engineering practices for the evaluation, assessment, and inspection of existing fixed offshore structures to demonstrate their fitness-for-purpose. It introduces the concept of risk-based approach to Structural Integrity Management (SIM). However, no specific guidance is provided on how to assess the risk level of the platform.

According to Faber [25], assessment of existing structures can be achieved cost-effectively by using structural reliability methods within the framework of Bayesian decision theory. In general, the term 'assessment of existing structures' covers all assessing aspects of the condition of the structures by mean of inspection, testing, monitoring, and calculation. The assessment process may also involve the consideration of strengthening and repairing or even changing of the use of the structure. A theoretical framework to perform reliability based assessment of existing structures can be found in the Joint Committee on Structural Safety (JCSS) guideline for Probabilistic Assessment of Existing Structures [26]. The fundamental assumption underlying the JCSS framework concerns the Bayesian definition of probability. It is used consistently in the procedure of the guideline to solve decision problems as well as to account for new information in reliability updating.

ISO 2394:2015 introduces formally procedures for estimating target reliability levels by optimisation of the total cost related to an assumed remaining working of a structure.

In the thesis of Ersdal [27], risk evaluation is included in assessment for life extension of existing offshore platforms. Instead of using a target reliability level for the whole structure, the author used a set of indicators such as the reserve strength ratio, the damaged strength ratio, and the reserve freeboard ratio to define failure criteria.

In the thesis of Thöns [28], the adaptive RSM is used together with the Importance Sampling Monte Carlo simulation to find the failure probabilities of every component in the tripod support structure of offshore wind turbines. The ultimate, the fatigue and the serviceability limit states are considered. The result showed that the probability of fatigue failure of a component at the end of service life can

be significantly higher than expected even though it was design to conform with the design code. This might due to the fact that the considered uncertainties in the reliability analysis are different from those in the design code, so the obtained reliability indices are not compatible with the target safety level. This issue will be discussed further in sec. 2.3. Another important result of Thöns [28] is that the reliability index calculated with the measurement data can be higher than with the design data even when the stress-range distributions are identical. It was noted that the measurement uncertainty is an important factor in the fatigue reliability analysis.

2.3. Target Safety Level for Existing Structures

The target safety level is generally interpreted as the minimum allowable reliability index. The reliability index, in turn, is related to failure probability through the inverse of the standardised normal cumulative distribution.

The recommended target safety levels in various documents for new and existing structures are inconsistent with regard to the values as well as the criteria used to find the optimum levels [29]. In general, it is widely agreed that the target safety levels in existing structures should be smaller than in new structures [30, 31, 32, 33]. This is because in existing structures, the costs of safety measures are much higher and the remaining working life is shorter than the design working life.

Although it is still controversial, the reliability of a structure calculated using a given set of probabilistic models for loads and resistances is nominal and has only limited bearing to the real reliability of the structure [25, 27]. Therefore, making a conclusion of the structural safety using the estimated reliability needs a compartible reference value.

There are two main approaches to find target safety levels, according to Faber [25]. The first approach uses an 'optimal' structure to find the reference value for other structures. Being optimal, the structure is considered as a product of the 'best practice' design. Therefore, the reliability index estimated for that structure is already 'optimal'. The second approach uses the economic decision theory, as outlined in Rosenblueth & Mendoza [34] and Hasofer & Rackwitz [35], to find the target safety levels.

In JCSS [26], it is suggested to find the target reliability level by solving a decision problem based on an optimization of generalized benefits and cost including ex-

pected failure costs. The term 'Life Quality Index' is introduced in this document to quantify the cost of human fatalities.

ISO 13822 [36] indicates the possibility of specifying the target reliability levels of existing structures by optimisation of the total cost related to an assumed remaining working life. However, this ISO standard does not provide further guidance for reducing the target reliabilities, e.g. for a shorter residual lifetime.

In case the acceptance criteria with regard to total collapse is set on the structural system level, the assessment of the whole system may be done through the annual probability of joint fatigue failure. This has been done by Faber et al. [37] for jacket structures by using the conditional probabilities of structural collapse given fatigue failure of a joint. As finding the conditional probability is not always feasible in practice, the consequence classes are specified together with the suggested target reliability values, as in EN 1990 [38]. In some current design standards, such as in the FDIS IEC 61400-1 for Wind Turbines [39], the target safety values can be found explicitly for the component level.

2.4. Proposed Principles for Updating Failure Probability

For existing structures, the purpose of reliability assessment is to estimate the remaining lifetime. In order to do that, we need to estimate the failure probability over time given new information, and then refer to the target safety level to see the remaining life before the structure is considered as unsafe.

The new information considered in this thesis is coming from inspection (crack sizes and repair policies) and monitoring data (wind, wave, strain).

Updating failure probability of existing structures is based on Bayes' Theorem. There are two forms of the theorem that can be used for the research questions depending on the type of the new information, named as Event updating and Random Variable updating.

If the new information is about crack inspection, the updating procedure can be expressed as in Eq. (2.1):

$$P\{F|I\} = \frac{P\{F \cap I\}}{P\{I\}} \tag{2.1}$$

where:

F represents a local or global structural failure,

I represents the inspection information, for example 'no crack detected',

$\cap$ indicates the intersection of two events,

$|$ indicates 'conditional upon'.

The probability $P\{F|I\}$ can be solved using FORM/SORM or MCS method.

If the new information is about monitoring data, the measured data can be used to update the individual or multivariate probability distributions, as expressed in Eq. (2.2):

$$f_X(x|I) = C\ P\{I|x\}\ f_X(x) \tag{2.2}$$

where:

X is a basic variable or statistical parameter (such as the scale parameter of the Weibull distribution),

I is monitored data,

$f_X(x)$ is the probability density of X before updating,

C is a normalizing constant,

$f_X(x|I)$ is the probability density of X after updating with information I,

$P\{I|x\}$ is the likelihood to find information I for given value x of X.

Once the basic variable is updated, it can be used in the limit state function to find the updated failure probability using reliability analysis methods shown in sec. 2.1.

Chapter 3.

Updating Failure Probability Considering Inspection Data

3.1. Overview

In the fatigue deterioration models used in inspection planning, a critical crack size is usually considered as a criterion to assess the safety of a welded joint. This is obvious for pipelines and ship structures where a leakage can lead to a catastrophe (or at least a failure of their service limit states). It is not the case for OWT support structures because for such structures both the diameter and thickness are large and a through-thickness crack might not necessarily lead to a failure. As mentioned in DNVGL-RP-C210 [40], for tubular joints, it remains about 40 % of the fatigue life after a crack has grown through the thickness. It seems that using this failure criterion can give conservative results. However, unlike the experimental conditions, real stresses in existing OWT support structures are random. A welded joint might fail in plastic collapse state due to large stresses in harsh environmental conditions even with a moderate crack size, so using a critical crack size criterion might not always be conservative. The idea is, therefore, to find a more suitable failure criteria for reliability analyses and failure probability updatings considering crack inspections and intervention actions.

This chapter explains how the reliability of welded steel details can be updated in the case where the fatigue failure is modelled by a fracture mechanics model and a Fatigue Assessment Diagram (FAD) is used to define the limit state function. Instead of using critical crack size as a criteria, the FAD approach uses the reference stress and the stress intensity factor (which, in turn, depend on crack dimensions and the applied stress) to define the crack state and then compares it with the limit state curve. A two dimensional bi-linear model is used to simulate

the crack growth. Calculation of crack depths and crack lengths are coupled. The stress intensity factors are calculated following the procedure of the standard BS 7910:2013 [41]. The initial crack sizes, the yield and ultimate strengths of steel, the fracture toughness, the stress intensity factor, and the stress-ranges are considered as uncertainties. The probability of detection is used to represent the uncertainty in crack inspections. By using Monte Carlo simulations, stress-ranges are generated randomly and used together with the calculated stress intensity factors to check for failures of the crack state with regard to FAD. The results of failure probability from FAD approach are compared with the 'standard' approach using critical crack size and fracture toughness. Updating of failure probability is considered for three inspection scenarios, no crack detected; crack detected and imperfect repair; crack detected and perfect repair.

The main contributions of the author in this chapter can be summarized as following:

- Identifying the advantages and disadvantages of using Fatigue Assessment Diagram in calculating failure probability of welded joints,
- Proposing a methodology to use FAD in updating failure probability considering crack inspection and repair policies,
- Developing Matlab codes to:
  - compare the failure probability results when FAD and critical crack size are used in the limit state function,
  - update failure probability considering the new information from crack inspection and intervention policies using FAD in the limit state function.

Chapter 3 is organized in 12 subsections, but they can be grouped into 5 main parts. In the first part, sec. 3.2, the current state of art is reviewed. In the second part, sec. 3.3, the basis of FAD is introduced. Sections 3.4 to 3.10 can be grouped into the third part, where the methodology is explained. Results and Discussion, sec. 3.11, forms the fourth part. Finally, chapter 3 is wrapped up by the fifth part about conclusion and perspectives (sec. 3.12 and 3.13).

3.2. Specific Literature Review

New information provided by monitoring of structural responses, load measurement, crack inspections, accidental events or safety measures can be used to up-

date the knowledge about reliability of existing structures. The initally estimated uncertainties of the basic variables, i.e. loads, material properties, and dimensions are reduced thanks to the new collected information. Therefore the reliability of the structure as well as the models of the basic variables should be updated. Based on the updated failure probability, intervention actions can be decided to repair, introduce safety measures, or invest for more information (e.g. crack inspections, load monitoring).

Updating failure probability of welded joints was initially proposed by Madsen [42] using First/Second Order Reliability Methods (FORM/SORM). The idea is then developed by Jiao and Moan [43] to update not only reliability but also the basic random variables. Updating can be done for inequality events (e.g. crack detected or not), equality events (e.g. crack of certain size is measured) or a mix of the two types of event. The distribution type of the updated random variable does not change but the standard deviation is reduced. The introduced updating method is exact only when there is no correlation between the event and the random variable. Zhao and Haldar [44] extended this method, investigated the effect of the detection uncertainties on the updating and applied the updated failure probability to inspection schedule of steel bridges. For offshore structures, applications of FORM to inspection planning can be found in [45, 46].

Since the FORM/SORM approach requires simplifications in crack geometry functions and does not always give a converged solution, the simulation based approach should be used. This approach is used, for example, in [47] for failure probability updating of bridges, or in [37] to perform risk-based inspection planning for jacket structures.

A critical crack size is usually used as a criterion to justify the safety of welded joints. This criterion is reasonable in ship and pipeline structures but it becomes uncertain to define failure of offshore structures such as OWTs. Besides, when the randomness of the stress-range is considered there are possibilities where plastic collapse happens and the critical crack size criterion fails to detect those collapses. In other words, when the small scale yielding (SSY) assumption (i.e. the size of the plastic zone is small compared to the crack length) of linear elastic fracture mechanics (LEFM) is not fulfilled, the popular Paris' law used to describe crack propagations is not valid and it may underestimate the crack size [48]. Therefore, Failure Assessment Diagram, which accounts for the two extremes failures (brittle fracture and plastic collapse) can be used in those reliability analyses.

Failure Assessment Diagram has been used to assess failure probabilities of bridges

[49]. In this reasearch, the FAD is used as a failure criterion to estimate the fatigue life distribution of a welded joint on a bridge. By comparing a linear with a bi-linear fracture mechanics models, it is concluded that the latter gives higher fatigue life estimates. This is useful for the case of offshore wind turbine support structures since their stress-range histograms contain a high number of low amplitude cycles [50].

The FAD criterion is also suggested by JCSS [51] for reliability analysis of existing offshore structures. This FAD approach recently has been used in [52] to update failure probability of OWT support structures accounting for inspection and repair. In this research, the authors assume that the crack size follows a lognormal distributed random variable. The reference stress—the stress at the net area—is simplified as a product of the geometry function and the stress-range. This simplification ignores the variation of crack size in the reference stress since the geometry function is considered as a constant.

To the best of the author's knowledge, no indication has been reported in literature about the advantages and disadvantages of using FAD in reliability updating in comparison with the critical crack size criteria. This information might be useful in choosing a suitable fatigue deterioration model for reliability assessment in inspection planning and life extension of existing offshore wind turbine support structures.

3.3. Basis of Failure Assessment Diagram

3.3.1. The Fatigue Assessment Diagram

Failure Assessment Diagram is a method to determine if a crack may cause a structural failure, using two criteria: brittle fracture and plastic collapse. Detail of this method can be found in textbooks, for example by Anderson [48], Webster et al. [53], Milne et al.[54], and British Standard BS 7910 [41].

The FAD curve is an assessment line describing the relationship $K_r = f(L_r)$, and a cut-off value of L_r, $L_{r(\max)}$. The cut-off is to prevent plastic collapse, defined as in Eq.(3.1):

$$L_{r(\max)} = \frac{\sigma_Y + \sigma_u}{2\sigma_Y} \tag{3.1}$$

where σ_Y corresponds to the offset yield point (or proof stress), having a 0.2%

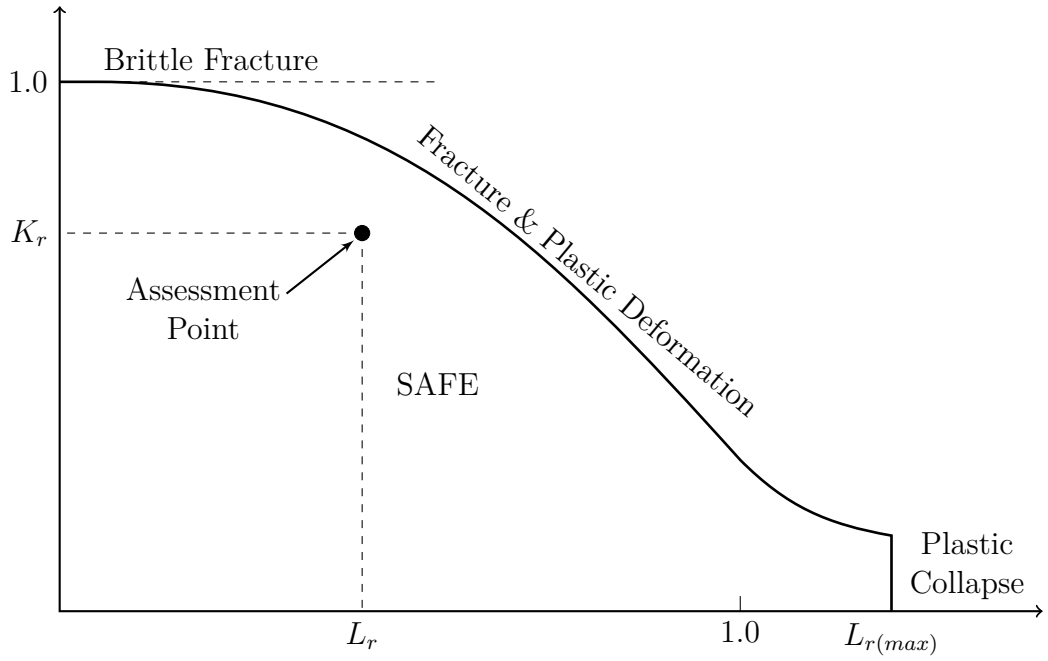

Figure 3.1.: Definition of FAD curve

plastic strain on the stress-strain curve (Fig. 3.2); σ_u is the tensile strength (or ultimate strength on the engineering stress-strain curve).

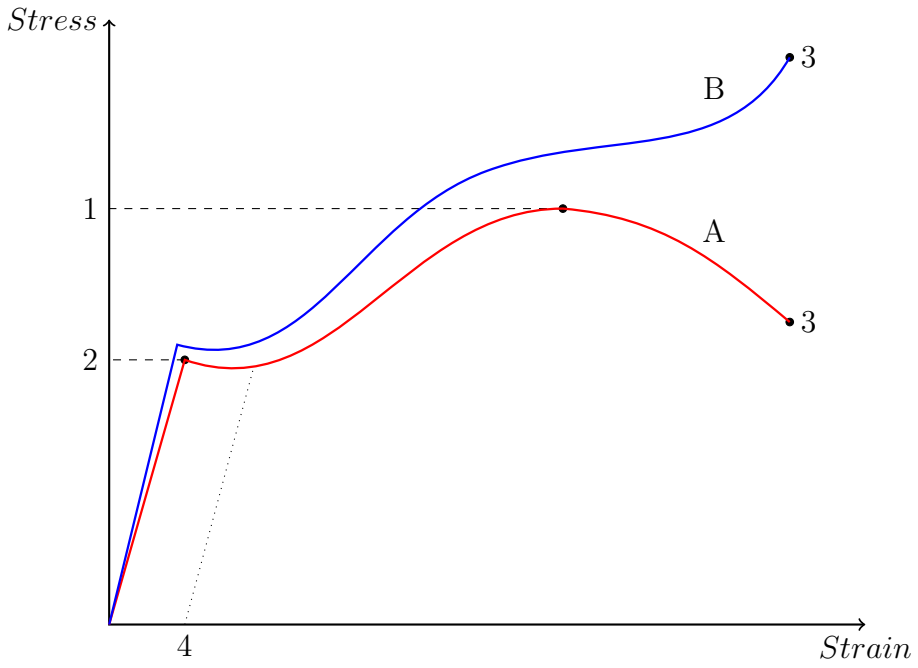

Figure 3.2.: 'Engineering' (A) and 'true' (B) stress–strain curves of typical structural steel. 1: Ultimate strength σ_u; 2: Yield strength; 3: Rupture; 4: Offset strain of 0.2%

A crack size is acceptable if the calculated assessment point, as shown in Fig. 3.1 and defined in the following section, lies within the area bounded by the two axes, the assessment curve and the vertical cut-off line corresponding to $L_{r(\max)}$. Otherwise, it is unacceptable.

The most thorough method to determine a FAD curve is to perform an elastic-plastic J-integral analysis and obtain K_r by Eqs. (3.2) to (3.3). This method is used in BS 7910:2015 as 'Option 3' for fatigue assessment.

$$K_r = \frac{K_I}{K_J} \tag{3.2}$$

$$K_J = \sqrt{\frac{JE}{1-\nu^2}} \tag{3.3}$$

where:

K_I is the stress intensity factor in mode I, (or a factor to predict the stress state near the tip of a crack),

J is the strain energy release rate per unit fracture surface area, calculated using J-integral method. Detail of J-integral method can be found in, for example, Anderson [48],

E is the Young's modulus,

ν is the Poisson's ratio.

Since building the FAD curve using Eq.(3.2) is complicated and time consuming, simplified approximations of the FAD curve are usually used in initial assessments. Simplified forms of a FAD curve can be found because for a given material, this curve is geometry independent [54], i.e. it is not very sensitive to crack sizes.

The first simplified approach, as shown in Eq.(3.4), utilizes the true stress – true strain curve of the material. A true stress – strain curve is the one considering the reduced cross-sectional area of the test sample. This approach is used in BS 7910:2015 [41] as 'Option 2' for fatigue assessment.

$$f\left(L_r\right) = \left(\frac{E\ \varepsilon_{\text{ref}}}{L_r\ \sigma_{_Y}} + \frac{L_r^3\ \sigma_{_Y}}{2E\ \varepsilon_{ref}}\right)^{-1/2} \text{ for } L_r \leq L_{r(\max)} \tag{3.4}$$

where ε_{ref} is the reference strain, inferred from the true stress – true strain curve at various σ_{ref} values, who in turn is calculated from L_r as in Eq.(3.5); $\sigma_{_Y}$ is the

0.2% proof strength of the material.

$$\sigma_{ref} = L_r \sigma_{_Y} \tag{3.5}$$

Using Eq.(3.4), an unique FAD curve can be obtained for each material. By considering a range of stress-strain curves for different materials, an empirical formula is found from the curve fitting for the lower bound of several FAD curves [54]. Such empirical formula is shown in Eq.(3.6), more detail can be found in [48, 53].

$$f\left(L_r\right) = \left[1 + 0.5\left(L_r\right)^2\right]^{-1/2} \left\{0.3 + 0.7\exp\left[-0.6\left(L_r\right)^6\right]\right\} \quad \text{for } L_r \leq L_{r(\max)} \tag{3.6}$$

The simplified form in Eq.(3.6) is material and geometry independent. A similar form is used in BS 7910:2015, known as 'Option 1' for fatigue assessment, as shown in Eqs. 3.7 to 3.9. This FAD method is used in this chapter to assess the failure probability of a welded joint. It is clear that an assessment point located outside the safe region of 'Option 1' may not nescessarily imply that the crack is not safe as more complex analyses in terms of the required material and stress analysis data may show the opposite.

$$f\left(L_r\right) = \left(1 + \frac{1}{2}L_r^2\right)^{-1/2} \left[0.3 + 0.7\exp\left(-\mu L_r^6\right)\right] \quad \text{for } L_r \leq 1 \tag{3.7}$$

$$f\left(L_r\right) = f\left(1\right) L_r^{(N-1)/(2N)} \quad \text{for } 1 < L_r < L_{r,\max} \tag{3.8}$$

$$f\left(L_r\right) = 0 \quad \text{for } L_r \geq L_{r(\max)} \tag{3.9}$$

where

$$\mu = \min\left(0.001\frac{E}{\sigma_{_Y}},\ 0.6\right)$$

$$N = 0.3\left(1 - \frac{\sigma_{_Y}}{\sigma_u}\right)$$

3.3.2. The Assessment Point

The assessment point represents the crack state (see Fig. 3.1). To define an assessment point, it is required that crack length ($2c$), crack depth (a), and the corresponding stress intensity factors (K_a, K_c) are known. The latter implies that the applied stress is also required, in addition to the stress-ranges used in crack growth simulation.

Location of the assessment point on the FAD is defined by its two coordinates: the fracture ratio K_r and the load ratio L_r as in Eqs. (3.10) and (3.11), respectively.

$$K_r = \frac{K_I}{K_{mat}} \tag{3.10}$$

$$L_r = \frac{\sigma_{ref}}{\sigma_Y} \tag{3.11}$$

where

K_I is the stress intensity factor at the current crack dimensions, calculated as a function of structural geometry (Y), applied stress (σ), and instantaneous crack size (a) as in (3.12). In BS 7910:2015 [41], K_I is separated into K_I^p and K_I^s to consider the effects of primary loads and secondary loads. Stresses that are typically classified as secondary may include displacement-controlled loads such as thermal expansion as well as weld misalignment stresses and they are not considered in this thesis for the purpose of simplicity of the methodology illustration;

$$K_I = Y(\sigma)\sqrt{(\pi a)}, \tag{3.12}$$

K_{mat} is the facture toughness—the critical stress intensity factor above which the crack growth becomes unstable and rapid failure occurs. Fracture toughness can be obtained using either J-integral or crack-tip openning displacement (CTOD) methods [48];

σ_Y is the yield stress;

σ_{ref} is the reference stress. For surface cracks in a plate (as shown in Fig. 3.3) under combined tension and bending, σ_{ref} is defined as:

$$\sigma_{ref} = \frac{P_b + \left[P_b^2 + 9P_m^2\left(1-\alpha''\right)^2\right]^{0.5}}{3\left(1-\alpha''\right)^2} \tag{3.13}$$

where P_m, P_b are the primary membrane stress and the primary bending stress; and α'' is calculated as in Eq.(3.14) for the crack dimensions shown in Fig. 3.3.

$$\begin{cases} \alpha'' = (a/t) \,/\, \{1 + (t/c)\} & \text{for } W \geq 2\,(c+t) \\ \alpha'' = (2a/t)\,(c/W) & \text{for } W < 2\,(c+t) \end{cases} \tag{3.14}$$

In (3.14), a is crack depth, $2c$ is crack length, W is the plate width, t is the plate thickness (see Fig. 3.3).

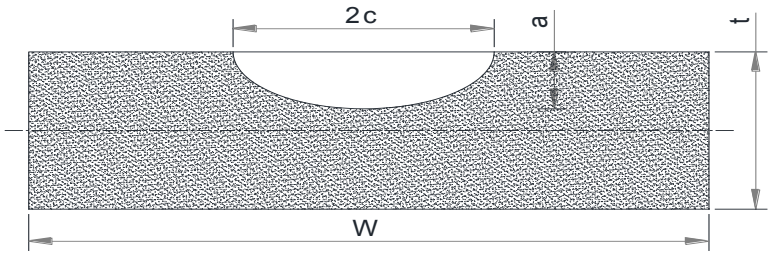

Figure 3.3.: Dimensions of a surface crack in a plate.

3.3.3. Deterministic Use of Fatigue Assessment Diagram

The aim of this section is to show how FAD is used to deterministically check the acceptance condition of a certain crack size. The result is the remaining fatigue life before fracture happens. The procedure can be summarized as follows:

1. Select crack growth parameters for the crack propagation simulation. In an elliptical crack, the same relationship can be assumed for crack growth in both the crack depth and crack length directions.
2. Obtain stress-ranges using a cycle counting method for a given stress history.
3. For the actual or assumed crack dimensions, the stress intensity factor range ΔK (corresponding to the applied stress-range) should be estimated for both crack depth (a) and crack length ($2c$) for each stress cycle.
4. With the ΔK value in each direction, the crack increment Δa and Δc can be calculated. The new crack dimensions are then calculated by adding the crack increment (Δa and Δc) to the previous crack sizes.
5. The new crack sizes are used together with the peak value of the tensile stress to calculate stress intensity factor K, as in (3.12).

6. The coordinate of the assessment point can be found by using (3.10) and (3.11) and then compare with the FAD curve.

7. If acceptable, the next stress cycle should be considered and the procedure from step 3 is repeated. The actual crack size (the one being assessed) should be regarded as acceptable if the specified fatigue design life is reached and the limit to growth (based on the FAD curve) is not exceeded. For surface cracks on pipelines or side shell of ship structures, the procedure can stop when crack depth reaches the wall-thickness because leakage occurs. However on offshore wind turbine support structures, it should be treated as a through-thickness crack of length $2c$ and the process of incremental growth can then be continued.

Some remarks about stress intensity factor calculations:

- ◇ While in the stress-life (S-N curve) approach for fatigue assessments, membrane and bending stresses are usually not distinguished, in the Fracture Mechanics approach, the stress intensity factor (K) solution differentiates between membrane and bending stresses. So a detailed stress analysis is needed to separate stress components at the hot spot, or if it is not possible, an assumption is needed for the degree of bending ratio.

- ◇ For a variable amplitude loading, a Markov matrix (a matrix stores the stress-range and the mean stress of each cycle) of cycle counting can be obtained from the stress time series using a cycle counting algorithm, e.g. the rain flow counting method [55]. Using this Markov matrix (see Tab. 3.1), for each stress-range considered in crack propagation, a corresponding maximum stress value can be traced back. So using FAD method for a long-term measured stress time series would be straight forward. This is not the case if the measured stress is not available and the stress-range distribution is calibrated from the design fatigue factor of the joint. In that case, an assumption about the peak value of the tensile stress of each stress-range is needed to calculate the stress intensity factor K.

3.4. Crack Growth Modelling

When Fracture Mechanics is used to assess fatigue damage, welded joints are considered as imperfect even before they are put in service. This is because of the inherent uncertainty/imperfections in material properties and manufacturing. Those imper-

Stress Range	Mean Stress [MPa]				
[MPa]	−1.0	−0.5	0	0.5	1.0
10	...	...	...	...	...
9	...	...	...	0.5	...
8	...	...	0.5	...	0.5
7	...	0.5	...	1.0	0.5
6	1.0	...	0.5	...	...

Table 3.1.: Example of a Markov matrix—results of cycle counting [55]

fections work as initial cracks, which may grow under cyclic loading and become critical for the failure of the joint as well as the whole structure.

To model the crack growth over time, the Paris-Erdogan law [56] is used. Although this crack propagation law is only valid for long cracks in Linear Elastic Fracture Mechanics (LEFM) and uniaxial loading conditions, it is widely used in offshore practice [41, 57, 58, 59] thanks to its simplicity in input parameters and sufficiently accuracy.

To consider the fatigue damage caused by small stress-ranges, a bi-linear Paris-Erdogan crack growth model can be used, as shown in Fig. 3.4, suggested by [51]. This crack growth model will be applied to find both crack length (a) and half crack depth (c). To find the crack length, the corresponding equations are shown in Eqs. (3.15) to (3.17).

No crack propagation:

$$\frac{\mathrm{d}a}{\mathrm{d}N} = 0 \quad \text{for } \Delta K_a \leq \Delta K_0 \tag{3.15}$$

Crack propagation in region I, see Fig. 3.4, ranges from ΔK_0 to ΔK_{tr} with Paris' law parameters ($C_1,\ m_1$):

$$\frac{\mathrm{d}a}{\mathrm{d}N} = C_{1a}\left(\Delta K_a\right)^{m_1} \quad \text{for } \Delta K_0 < \Delta K_a < \Delta K_{tr} \tag{3.16}$$

Crack propagation in region II, see Fig. 3.4, with parameters ($C_2,\ m_2$) ranges from ΔK_{tr} to the point where $K = K_{mat}$, with:

$$\frac{\mathrm{d}a}{\mathrm{d}N} = C_{2a}\left(\Delta K_a\right)^{m_2} \quad \text{for } \Delta K_a \geq \Delta K_{tr} \tag{3.17}$$

Since crack depths a and crack length $2c$ are interrelated and need to be simulated

simutaneously, similar equations for half crack length c are shown from (3.18) to (3.20), with:

$$\frac{\mathrm{d}c}{\mathrm{d}N} = 0 \quad \text{for } \Delta K_c \leq \Delta K_0 \tag{3.18}$$

$$\frac{\mathrm{d}c}{\mathrm{d}N} = C_{1c} \left(\Delta K_c\right)^{m_1} \quad \text{for } \Delta K_0 < \Delta K_c < \Delta K_{tr} \tag{3.19}$$

$$\frac{\mathrm{d}c}{\mathrm{d}N} = C_{2c} \left(\Delta K_c\right)^{m_2} \quad \text{for } \Delta K_c \geq \Delta K_{tr} \tag{3.20}$$

In Eqs. (3.15) to (3.20):

N is number of cycles;

ΔK_0 is the threshold of the stress intensity factor range, below which the crack is assumed to be non-propagating. This parameter is a material property;

ΔK_{tr} is the transition value of stress intensity factor between the two crack growth regions. This parameter can be obtained by finding the intersection of the two linear crack growth models;

ΔK_a is the stress intensity factor range of a, calculated as a function of a, c, and stress-ranges;

ΔK_c is the stress intensity factor range of c, calculated as a function of a, c, and stress-ranges.

$C_i,\ m_i$ (where $i = 1, 2$), are the parameters of Paris' law model in two regions.

The stress intensity factor ranges ΔK_a and ΔK_c are calculated using the general formula:

$$\Delta K = Y \left(\Delta \sigma\right) \sqrt{\pi a} \tag{3.21}$$

where the stress-range $\Delta\sigma$ is separated into membrance and bending components, and the geometry function Y is a function of the crack type (embeded, surface, through-thickness, etc.), crack dimensions (a and c), stress types (membrance or bending), and other correction factors. Detailed formulas are shown in Appendix D.

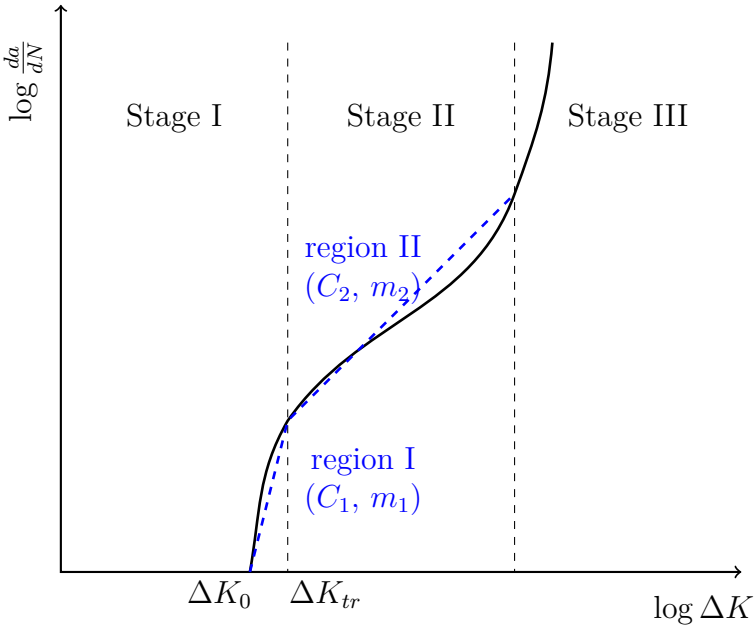

Figure 3.4.: Bi-linear crack growth using Paris' law. The solid curve represents the real crack growth curve; the dashed blue lines represent the bi-linear crack growth.

3.5. Uncertainties

3.5.1. Uncertainty in Paris' Law Parameters

In the Paris' law equations used in the previous section (as shown in Eqs. (3.15) to (3.20) and Fig. 3.4), C is the intercept of the line $\mathrm{d}a/\mathrm{d}N$ versus ΔK on the log–log plot, when the line is extended until it meets the $\mathrm{d}a/\mathrm{d}N$ axis at $\Delta K = 1$. The exponent parameter m is the slope of that line. The parameters C and m are generally regarded as being interdependent.

Many authors [60, 61, 62, 63] experimentally observed a stable relationship between C and m, as shown in the following empirical formula:

$$C = A\ B^m \tag{3.22}$$

or in a logarithmic form:

$$\ln C = \ln A + m \cdot \ln B \tag{3.23}$$

Different values of C and m for offshore steel can be found in fatigue handbooks, for example, in Almar-Næss [64].

Concerning the uncertainty of the Paris crack growth model, Lassen [63] suggested that it is better to use a model that assumes a fixed value of m, which is independent of C to predict crack growth when the stress-ranges are not constant amplitude. The value of m ranges from 2 to 4, according to Irving and McCartney [61].

In DNV guidelines and standards [65, 66], it is suggested to use the values of Paris' law parameters as shown in Tab. 3.2. The recommendations are based on collected data from various investigations and are recommended when other relevant information is not available. The unit of $\ln C$ in Tab. 3.2 is in N, mm.

Environment	m	$\ln C$(mean, std.)
In air	3.1	$\mathcal{N}(-29.84, 0.55)$
In sea water	3.5	$\mathcal{N}(-31.01, 0.77)$

Table 3.2.: Modelling of $\ln C$ and m, according to DNV [65]. $\mathcal{N}$ denotes a normal distribution.

Using the reference formula given in Gurney [67], the mean value of C can be calculated as:

$$\ln C = -15.84 - m \cdot 3.34 \tag{3.24}$$

In case the fatigue design of the existing structure is done by using the stress-life (S-N) approach (Miner's rule and SN curves), a common practice is to calibrate the mean value of $\ln C$ so that the difference between the reliability curve obtained from the SN approach and the fracture mechanics approach is minimized [68, 69].

In a coupled crack propagation simulation (i.e. crack depth a and half crack length c are considered simultaneously), the intercept parameter C_c of crack length propagation can be deduced from the one of crack depth C_a, following Newman and Raju[70]:

$$C_c = 0.9^m \times C_a \tag{3.25}$$

In DNV-GL-RP-0001 [57], C_a and C_c are assumed to be fully correlated and equally distributed, where $\log_{10} C$ is normally distributed with the distribution parameters shown in Tab. 3.3.

The conversion of standard deviations between $\log_{10} C$ and $\ln C$ are as follows:

$$\sigma_{\ln C} = \frac{1}{\log_{10} e} \sigma_{\log_{10} C} \tag{3.26}$$

Environment	Position of potential crack	Mean of C μ_C	Standard deviation $\log_{10} C$	Standard deviation $\ln C$	m
In air	base material	1.83×10^{-13}	0.11	0.25	3.0
	weld metal	1.83×10^{-13}	0.22	0.50	3.0
Sea water with cathodic	base material	(1)	0.11	0.25	3.0
	weld metal	(1)	0.22	0.50	3.0
free corrosion	base & weld metal	8.35×10^{-13}	0.22	0.50	3.0

Note: (1) = air value multiplied with factor from Eq. (3.28);

Table 3.3.: Modelling of $\ln C$ and m, according to [57].

Given the values of μ_C and $\sigma_{\ln C}$, the value of $\mu_{\ln C}$ can be calculated as:

$$\mu_{\ln C} = \ln(\mu_C) - \frac{1}{2}(\sigma_{\ln C})^2 \tag{3.27}$$

The ratio between crack growth in sea water with cathodic protection and air is calculated as in (3.28). This relationship is derived from S-N data and valid from 1 to 1000 years [57].

$$f(F,h) = \left(0.07A^3 - 0.275A^2 - 0.245A + 2.38\right)^{2.0429-1.1523h}, \tag{3.28}$$

where $A = \log_{10} F$; F is the calculated fatigue life; h is Weibull shape parameter of the stress-range distribution.

In this chapter, the parameters shown in Tab. 3.3, in sea water with cathodic protection are used for the Limit State Function (LSF) comparisons. Data for reliability updating is taken from Tab. 3.4.

	Variables	Distr.	Mean (Scale)	C_V (Shape)	– (Location)	Sources
ν	No. of cycles per year	D	1×10^7	–	–	
B	Steel thickness [mm]	D	40	–	–	
R	Outer radius [mm]	D	5000	–	–	
L	Joint length [mm]	D	120	–	–	
DoB	Degree of Bending	D	0.5	–	–	
$\Delta\sigma$	Stress range [MPa]	W	$\mathcal{N}(6, 0.2)$	3.0	–	
ΔK_0	SIF range threshold [N/mm$^{3/2}$]	LN	140	0.4		
K_{mat}	Fracture toughness [MPa m$^{1/2}$]	3p W	A_k	4	20	
$\ln C_{1a}$	Paris' law, 1^{st} line [N, mm]	LN	4.8×10^{-18}	1.7	–	[51]
$\ln C_{2a}$	Paris' law, 2^{nd} line [N, mm]	LN	5.86×10^{-13}	0.6	–	[51]
m_1	Paris' law, 1^{st} line	D	5.1	–	–	[51]
m_2	Paris' law, 2^{nd} line	D	2.88	–	–	[51]
C_a/C_c	C ratio between a and c	D	0.9^m	–	–	[70]
a_0	Initial crack depth [mm]	LN	0.15	0.66	–	[51, 71]
a_0/c_0	Initial aspect ratio	LN	0.62	0.40	–	[51]
B_{sif}	Uncertainty in SIF	LN	1	0.05	–	[51]
M_u	Uncertainty in FAD	3p W	0.97	1.11	−0.06	[72]
σ_Y	Uncertainty in yield strength	LN	368.75	0.07	–	[26]
σ_U	Uncertainty in ultimate strength	LN	750	0.04	–	[26]

Note: Deter. = Deterministic; W = Weibull distribution; 3p W = Three-parameter Weibull distribution; LN = Lognormal distribution;

Table 3.4.: Summary of input data

3.5.2. Uncertainties in Initial Crack Sizes

The initial defects in modern fabricated welds are assumed to be extremely small, typically less than 10 µm (0.01 mm). These cracks are too small that LEFM is not applicable. Before reaching a depth of 100 µm they grow faster than LEFM can predict. Typically, the time for a crack depth to reach 100 µm (the short crack propagation) is about 20 % to 30 % of the fatigue life [63]. For welded joints in substructures of offshore wind turbines, it is sufficient to consider only crack depths above 100 µm—long crack propagation—where LEFM is applicable to model the propagation phase until failure is reached.

However, it is mentioned in [51, 71] that the mean value and standard deviation of initial crack depth a_0 can be estimated to be 0.15 mm and 0.10 mm, respectively, for 'sound' quality welds. The initial crack depth data fits well to either a lognormal, an exponential, or a Weibull distributions.

For the initial crack length c_0, it is suggested to use initial defect aspect ratio, which is defined as the ratio of initial crack depth to semi-crack length (a/c). This quantity may also be modelled as a lognormal random variable with a mean of 0.62 and $C_V = 0.4$ as suggested in [51].

For cracks that need to be repaired after inspection, this chapter considers two cases for the new initial crack depth—either crack is repaired perfectly (i.e. $a_0 = 0$) or as after-fabricated state (as at its origin after manufacturing).

3.5.3. Uncertainties in Yield Strength and Ultimate Strength

Uncertainties of Yield Strength and Ultimate Strength are often assumed to follow a normal, lognormal, or a Weibull distribution [73, 74, 75]. By fitting an extensive data set of the yield strength from the materials database to normal, lognormal, and Weibull distributions, it was found that the lognormal distribution was the most appropriate one [75].

According to [74, 76], the parameters of the lognormal distribution for yield and ultimate tensile strengths can be calculated in two cases:

a) If only measured mean values for yield strength $\left(\mu_{\sigma_Y}\right)$ and ultimate tensile strength $\left(\mu_{\sigma_u}\right)$ are available, the standard deviation values are determined as:

◇ yield strength:

$$\sigma_{\sigma_Y} = 0.03\mu_{\sigma_Y} \tag{3.29}$$

◇ ultimate tensile strength:

$$\sigma_{\sigma_u} = 0.05\mu_{\sigma_u} \tag{3.30}$$

b) If only the standardized values for yield strength (R_e) and the ultimate tensile strength (R_m) are available, the mean and standard deviation values are determined as:

◇ yield strength:

$$\mu_{\sigma_Y} = R_e + 70 \text{ MPa} \quad \text{and} \quad \sigma_{\sigma_Y} = 30 \text{ MPa} \tag{3.31}$$

◇ ultimate tensile strength:

$$\mu_{\sigma_u} = R_m + 70 \text{ MPa} \quad \text{and} \quad \sigma_{\sigma_u} = 30 \text{ MPa} \tag{3.32}$$

Following the suggestion of JCSS [26], the mean and coefficient of variation values of yield and ultimate tensile strengths are calculated as:

◇ yield strength:

$$\mu_{\sigma_Y} = f_{ysp} \cdot \alpha \cdot \exp\left(-u \cdot C_V\right) - C \tag{3.33}$$

$$C_V = 0.07 \tag{3.34}$$

◇ ultimate tensile strength:

$$\mu_{\sigma_u} = B_t \cdot \mathrm{E}\left[f_u\right] \tag{3.35}$$

$$C_V = 0.04 \tag{3.36}$$

where:

f_{ysp} the code specified or nominal value for the yield,

α spatial position factor ($\alpha = 1.05$ for webs of hot rolled sections and $\alpha = 1$ otherwise),

u is a factor related to the fractile of the distribution used in describing the distance between the code specified nor nominal value and the mean value; u is found to be in the range of -1.5 to -2.0 for steel produced in accordance with the relevant EN standards; if nominal values are used for f_{ysp}, the value of u needs to be appropriately selected.

C is a constant reducing the yield strength as obtained from usual mill tests to the static yield strength; a value of 20 MPa is recommended,

B_t is a factor, $B_t = 1.5$ for structural carbon steel; $B_t = 1.4$ for low alloy steel; $B_t = 1.1$ for quenched and tempered steel.

The calculation performed in this chapter follows the method suggested by JCSS [51] to find the parameters of the lognormal distributions of yield and ultimate tensile strengths:

- $f_{ysp} = 350$ MPa is chosen as the nominal value of the yield strength, with $\alpha = 1$ and $u = -1.5 \Rightarrow \mu_{\sigma_Y} = 368.75$ MPa;
- $B_t = 1.5$, $\mathrm{E}[f_u] = 500$ MPa $\Rightarrow \mu_u = 750$ MPa.

3.5.4. Fracture Toughness Uncertainties

Fracture toughness is a property describing the ability of a material containing a crack to resist fracture. The fracture toughness can be represented either by K_{mat}—the critical stress intensity factor for brittle failure or by J_{Ic}—the critical energy for a ductile failure. For weld-toe cracks of offshore structures, the K_{mat} is of interest. When the stress intensity factor K exceeds fracture toughness, the crack growth becomes unstable and rapid failure occurs.

Fracture toughness is found by doing laboratory tests at various temperatures. Over a large range of temperatures from $-269\,^{\circ}\mathrm{C}$ to $27\,^{\circ}\mathrm{C}$ and grain sizes from $1\,\mu\mathrm{m}$ to $16\,\mu\mathrm{m}$, the fracture toughness K_{mat} varies from $632.46\,\mathrm{MPa\,mm^{1/2}}$ to $3162.3\,\mathrm{MPa\,mm^{1/2}}$ with an average value of $1897.4\,\mathrm{MPa\,mm^{1/2}}$ [77, 78]. In the lower shelf and transition region of temperature, Wallin [79] and others have argued for the use of Weibull distribution for the tested results.

A three-parameter Weibull distribution is proposed to describe fracture toughness related to the cleavage fracture mode [51, 76, 80]:

$$F_{K_{mat}}(k) = 1 - \exp\left[-\left(\frac{k - K_0}{A_k}\right)^{B_k}\right] \tag{3.37}$$

where:

B_k is the shape parameter, taken a 4 on the basis of experiments [76],

K_0 is the threshold parameter, a recommended value is $20\,\mathrm{MPa\,m^{1/2}}$[80],

A_k is the scale parameter $[\mathrm{MPa\,m^{1/2}}]$, calculated as:

$$A_k = \left\{11 + 77\left[\exp\left(\frac{T - T_{27J} + T_0}{52}\right)\right]\right\}\left(\frac{25}{t}\right)^{1/4} \tag{3.38}$$

T is operating temperature (°C),

T_{27J} is temperature (°C) corresponding to a Charpy V-Notch of 27 J, chosen to be e.g. $-50\,°\mathrm{C}$,

T_0 is modelling variability of T_{27J}: e.g. Normal distributed with mean of $18\,°\mathrm{C}$ and standard deviation of $15\,°\mathrm{C}$,

t is plate thickness, chosen to be 40 mm.

3.5.5. Stress Intensity Factor Uncertainties

As the Stress Intensity Factor (SIF) parameter is determined from experiments, it should be considered as an uncertainty while calculating the failure probability of the joint. Using the suggestion of JCSS [51], it can be modelled as lognormal distributions with mean of 1 and CoV of 5%.

3.5.6. Threshold Value and Transition Value of the Stress Intensity Factor

As suggested in [51], the threshold ΔK_0 (Fig. 3.4) is assumed to follow a lognormal distribution with a mean of $140\,\mathrm{N/mm^{3/2}}$ and CoV of 0.4. The transition value ΔK_{tr} also varies since it is calculated as the intersection of the two linear crack growth lines (the C parameter of each line is a random variable).

3.5.7. Uncertainty in FAD

As mentioned in sec. 3.3, an assessment point located outside the fatigue assessment diagram does not necessarily represent a failure at a certain crack size. It might be possible to either refine the stress analysis or to re-characterize the flaw, or use an alternative FAD.

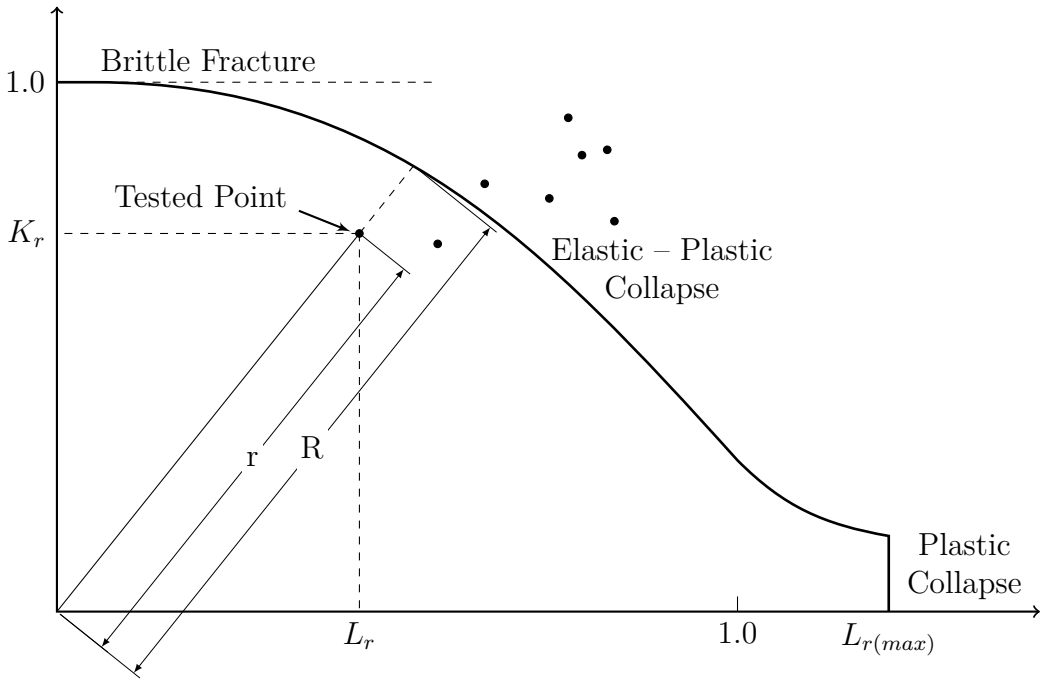

Figure 3.5.: Illustration of FAD uncertainty quantification

In the Offshore Technology Report 2000/021 published by HSE [72], the uncertainty of the FAD method is quantified using data from [81]. By plotting assessment points of the tested specimens at their failure states on the 'Option 1' FAD curve (Fig. 3.5), the error of the FAD is defined as:

$$M_u = R - r \tag{3.39}$$

where r, R are the distances from the origin to the assessment point and the corresponding intersection on the FAD curve, respectively. The statistics of M_u shows that, on average, the safety margin of the FAD curve is minimum in the middle (elastic-plastic) region, slightly higher in the 'plastic collapse' region, and maximum in the 'brittle fracture' region.

In general, it is concluded that a 3-parameter Weibull distribution can be used to represent M_u as follows:

$$F_{M_u}(m) = 1 - \exp\left[-\left(\frac{m - M_0}{A_m}\right)^{B_m}\right] \tag{3.40}$$

where:

- ◇ location parameter: $M_0 = -0.06$
- ◇ scale parameter: $A_m = 0.97$

◇ shape parameter: $B_m = 1.11$

It is noted that M_u is unitless and it is quantified for the case of a 'Option 1' FAD only, and that a limit state function defined similar to the definition of M_u is required to have a valid application in reliability analysis.

3.5.8. Probability of Detection

The probability of detection, POD, expresses the probability of detecting a crack of a given length, i.e. the crack length $2c$. It is a parameter to evaluate the accuracy of an inspection technique. In general, there are three different types of POD curve [82], as illustrated in Fig. 3.6. Curve 1 incorporates the possibility of non-detection of large cracks. Curve 2 incorporates false call probability—it is the fraction of time that an un-cracked joint will be incorrectly classified as being cracked. Curve 3 ignores the possibility of false calls and non-detection of large cracks and normally used as a cumulative distribution function in Bayesian updating for failure probability of a joint.

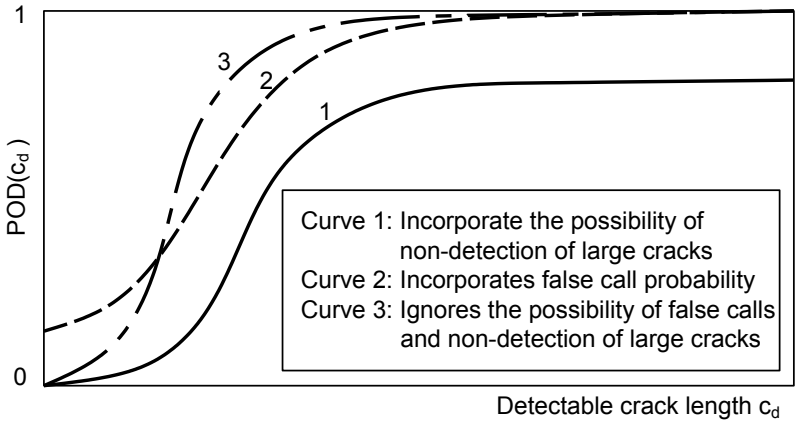

Figure 3.6.: Types of POD curve

Although Curve 1 and Curve 2 are not in the form of a cumulative distribution function, they can easily be incorporated in updating the failure probability of the joint using a simulation method.

In the DNV General Guideline [83], typical POD curves for different inspection scenarios are shown in the form:

$$\mathrm{P}\left(c_d\right) = 1 - \frac{1}{1 + \left(\frac{c_d}{x_0}\right)^b} \tag{3.41}$$

where the parameters x_0 and b can be found in Tab. 3.5 for some inspection scenarios:

Inspection Scenario	x_0	b
MPI under water	2.950	0.905
MPI above water ground test surface	4.030	1.297
MPI above water not ground test surface	8.325	0.785
Eddy current	12.28	1.790

Note: MPI = Magnetic particle inspection

Table 3.5.: POD parameters taken from [83].

For illustration purpose, this chapter uses the POD defined in Eq.(3.42). This function shows the probability of the smallest detectable crack length in [mm] with the parameter $\lambda = 1.95$ [mm] corresponding to a quite good inspection technique for welded joints in sea water [84].

$$\mathrm{POD}\left(c_d\right) = 1 - \exp\left[-\frac{c_d}{\lambda}\right] \tag{3.42}$$

3.6. Limit State Functions

Traditionally, reliability problems for fatigue crack growth can be solved in both serviceability and ultimate limit states. In the serviceability limit state, a critical crack size is selected to justify the acceptability of the crack size, as shown in Eq. (3.43).

$$g_1\left(N\right) = a_c - a \tag{3.43}$$

The ultimate limit state, on the other hand, considers the fracture toughness K_{mat} as an upper limit for the stress intensity factor K_{max}. The crack growth becomes unstable and rapid failure happens when K_{max} exceeds K_{mat} , as in Eq. (3.44).

$$g_2\left(a\right) = K_{mat} - K_{max} \tag{3.44}$$

In fracture mechanics, the critical crack size a_c is the crack size at which the stress intensity factor reaches the fracture toughness, so the two equations above express

the same failure state of the crack. In pipelines and ship structures, a_c is defined considering only the serviceability condition—failure is considered to happen when crack depth is larger than the wall-thickness because leakage can happen.

In reliability analyses of offshore structures, normally only the crack size condition in Eq. (3.43) is used for the purpose of failure probability updating, considering crack inspection and repair. This approach is widely utilized for inspection planning using a calibrated FM model based on the SN model [68, 85, 57].

To accurately predict the remaining fatigue life when the parameters of the crack growth model are known, the constraint on the material strength (i.e. fracture toughness) and the validity of the crack growth model should also be considered. The popular Paris' law model is valid only if the small scale yielding (SSY) condition is satisfied. This condition is to ensure that the plastic zone around the crack tip is small in comparison to the relative dimensions of the structure in which it is contained. Although it is crucial to check the SSY condition, especially when the applied stress-range is assumed to be a random variable, it is not possible to do that if the LSF as Eqs. (3.43) and (3.44) are used.

The fracture assessment diagram is an useful tool to control the crack propagation process, using not only the brittle fracture condition (i.e. fracture toughness condition), but also the plastic collapse and the transition region. Given the L_r parameter of the assessment point calculated as in (3.11), the corresponding value of K_{rFAD} of the FAD curve can be calculated (as in Eqs. (3.7) to (3.9)) and then compared with the K_r parameter of that assessment point (as in Eq. (3.10)). This comparison is the basis of the limit state function shown in Eq. (3.48).

$$g_3\left(L_r\right) = K_{rFAD} - K_r \tag{3.45}$$

The FAD limit state function in Eq. (3.45) can be rewritten as in Eq. (3.46):

$$g_4\left(\phi\right) = R_{FAD} - r \tag{3.46}$$

where r is the distance from the assessment point to the origin; ϕ is the angle between the X-axis and the line from the origin to the assessment point; R_{FAD} is distance from the intersection of that line with the FAD curve to the origin. r and ϕ are calculated as in Eqs. (3.47) and (3.48), respectively.

$$r = \sqrt{L_r^2 + K_r^2} \tag{3.47}$$

$$\phi = atan\left(\frac{K_r}{L_r}\right) \tag{3.48}$$

R_{FAD} can be found by using the ϕ value of the assesment point and the FAD curve in the polar coordinate system.

3.7. Reliability Updating

The limit state functions introduced in the previous section are used to calculate failure probabilities of a welded joint. When new information coming from crack inspections and intervention actions is available, the updated failure probability of the joint is the failure probability conditioned on those new events.

The detection event is defined as:

$$I_d = 2c - c_d \tag{3.49}$$

where $2c$ is the crack length and c_d is the detectable crack size of the inspection technique. $I_d < 0$ means no detection, $I_d \geq 0$ means crack detected.

Since a crack detected may not be necessary to be repaired immediately, the repair action can be separated from the detection event by assigning a minimum crack size to repair (c_r):

$$I_r = 2c - c_r \tag{3.50}$$

There are two intervention actions to be considered, to repair 'imperfectly' denoted as R_n, or to repair 'perfectly' denoted as R_p.

For a perfect repair, the inital crack size after repair is set to zero. For a normal repair, the initial crack size after repair is generated from the initial crack size distribution with an upper truncation at the detectable crack size value. The truncation is to ensure that the new initial crack size is smaller than the detectable crack size.

The updated failure probabilities considering inspection and repair are expressed in conditional probabilities forms as follows:

◇ No detection:

$$p_f = P\left[g \leq 0 \mid I_d < 0\right] \tag{3.51}$$

◇ Detected and repaired imperfectly if $c \geq c_r$: a_r can be a certain crack size that is equal to or larger than the detectable crack size a_d.

$$p_f = P\left[g \leq 0 \mid I_r \geq 0 \bigcap R_n\right] \tag{3.52}$$

◇ Detected and repair perfectly

$$p_f = P\left[g \leq 0 \mid I_r \geq 0 \bigcap R_p\right] \tag{3.53}$$

The conditional probabilities in Eqs. (3.51) to (3.53) can be rewritten in the Bayesian form, as illustrated in Eq. (3.54), to solve a parallel system problem using FORM/SORM methods. However, a combination of intervention actions and the detection event might cause convergence difficulties in those approaches, not to mention the necessity to simplify the interrelated crack dimensions as well as the FAD curve.

$$P\left(A \mid B\right) = \frac{P\left(A \cap B\right)}{P\left(B\right)} \tag{3.54}$$

For those reasons, a simulation based approach—crude Monte Carlo simulation is used in this chapter to estimate the failure probability:

$$\hat{p}_f = \frac{1}{N}\sum_{j=1}^{N} I\left[g\right] \tag{3.55}$$

where N is the number of simulations and $I\left[g\right]$ is the indicator function, defined by:

$$I\left[g\right] = \begin{cases} 0 & \text{if } g > 0 \\ 1 & \text{if } g \leq 0 \end{cases} \tag{3.56}$$

Failure probability at the end of each year, either updated or before updating, is calculated based on the relizations of crack sizes and the corresponding ΔK, K values that are implicitly or explicitly used in the limit state functions in (3.43) to (3.46), or (3.60).

It is noted that Eqs. (3.51) to (3.53) show inequality updating events. The equality events, for example when cracks are measured a certain value, are not considered in this thesis.

3.8. Updating Procedure

The procedure to update failure probability in simulation based approach is summarized in Fig. 3.7. For each set of random variable generated (including initial crack depth a_0, initial aspect ratio a_0/c_0, SIF uncertainty, yield strength σ_Y, ultimate strength σ_U, fracture toughness K_{mat}, SIF threshold ΔK_0, and Paris' law parameters C of each crack growth region) one series of crack propagation can be obtained by solving differential equations (Eqs. (3.15) to (3.17)). Each series of crack propagation is one crack growth scenrio for the whole lifetime. Several crack growth scenarios of the welded joint are needed in the simulation based approach to find the failure probability. The whole stress-range distribution is considered for each crack growth scenario by assuming that each day the welded joint is subjected to a constant stress amplitude loading with a random value of stress-range generated from its distribution.

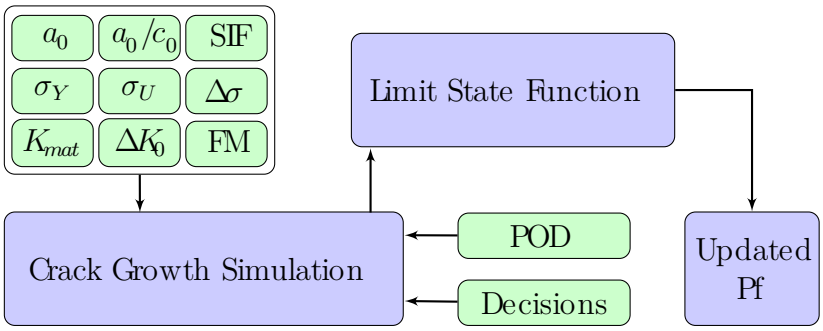

Figure 3.7.: Procedure to update failure probability in simulation based approach.

For each crack growth realization, at each inspection time, a random value of detectable crack size is generated from the POD curve. This detectable crack size c_d is used to compare with the current crack length $2c$ of that crack growth realization. The crack state of the joint from the current inspection time to the end of the service life may need to be changed according to the current inspection result and intervention action:

- ◇ In case of no detection:

  - if $2c < c_d$ then no need to change the crack state (both the crack length and the crack depth);
  - if $2c \geq c_d$ then crack states from the current inspection time need to be recalculated with an initial crack size smaller than the detectable crack size. A new set of a_0 and a_0/c_0 are to be generated with a constraint that $2c_0 < c_d$.

- ◇ In case of crack detected and repaired imperfectly with repair threshold size c_r:
  - if $2c < c_r$ then no need to change the crack state;
  - if $2c \geq c_r$ then crack states from the current inspection time need to be recalculated with an initial crack size randomly generated from the a_0 and a_0/c_0 distributions as shown in Tab. 3.4.

- ◇ In case of crack detected and repaired perfectly with repair threshold size c_r:
  - if $2c < c_r$ then no need to change the crack state;
  - if $2c \geq c_r$ then the following crack states are set to zero.

In Fig. 3.8, the continous line represents a crack growth scenario where no crack detected at the inspection i^{th} while the dashed line illustrates how a crack growth scenario is modified after being detected and repaired.

Figure 3.8.: Modifying the crack growth realization considering intervention actions. The continuous line represents a crack growth scenario where no crack is detected; the dashed line illustrates how a crack growth scenario is modified after being detected and repaired.

By applying the above updating procedure to every crack growth realization at every inspection time, all the crack growth scenarios which can be detected, are modified to be suitable with the given inspection result and intervention action.

The updated failure probability is then obtained for every year by simply using Eq. (3.55) with the chosen limit state function.

3.9. Details of The Studied Welded Joint

The considered joint is a butt weld of a monopile support structure (Fig. 3.9) with following parameters:

- ◇ Steel thickness: B=40 mm
- ◇ Outer radius: R=5000 mm
- ◇ Joint length: L=120 mm

It is assumed that the degree of bending—the ratio between bending stress component and the total stress—is $DoB = 0.5$.

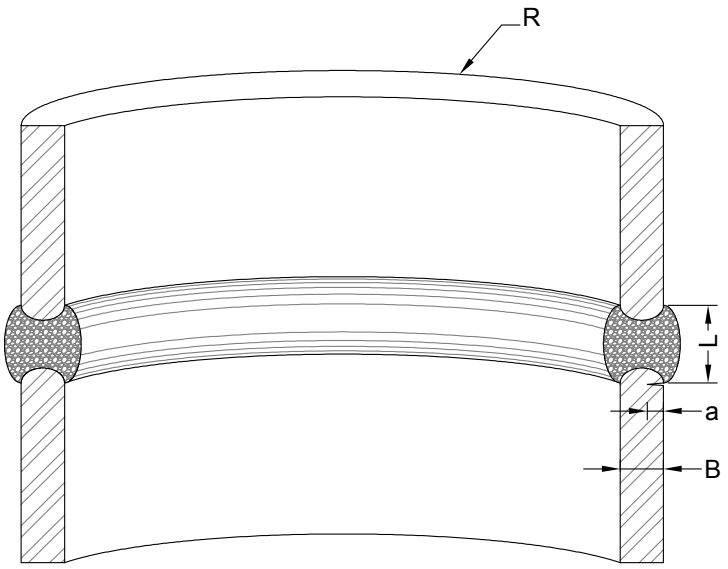

Figure 3.9.: Detail of the welded joint.

3.10. Maximum Stress and Stress-ranges

It is assumed that the long-term stress-ranges are represented by a two-parameter Weibull distribution. To consider the randomness of stress-range in crack propagations, one value of stress-range is generated from the distribution and kept constant during a certain period of time.

For the purpose of demonstrating the updating methodology, the Weibull stress-range distribution used in this chapter is assumed to have a shape parameter of 0.8 and the scale parameter is calibrated to get the exact value of the design fatigue factor (DFF) of the joint.

The uncertainty in stress-range can be assumed to be a normal distribution with CoV of 15%. This uncertainty is assigned to the scale parameter. The mean value is the calibrated scale value as explained above.

By using a S-N curve as in Eq. 3.57 and assuming that the joint is designed with a DFF of 3, the mean value of scale parameter is 5.792 MPa.

$$\begin{cases} \log K_{1c} = 11.764; & m_1 = 3 \\ \log K_{2c} = 15.606; & m_2 = 5 \end{cases} \tag{3.57}$$

The maximum stress (peak tensile stress) is used in calculating stress intensity factor. In [46], Madsen used the average far field stress (S_{ave}) and stress-range ($\Delta\sigma$) to calculate this peak tensile stress value, as shown in Eq. (3.58).

$$S_{max} = S_{ave} + \frac{\Delta\sigma}{2} \tag{3.58}$$

The assumption in Eq. (3.58) might not be able to include the extreme peak tensile stresses. So it might lead to an under-estimation of the failure probability because fracture can happen with realizations of such extreme stresses when the crack sizes are relatively large at the end of the design lifetime. On the other hand, assuming that the peak tensile stress follows the distribution of the annual maximum stress might over-estimate the failure probability. The ideal solution could be to model the peak tensile stress as a random process, but the reliability problem becomes quite complex and numerically very expensive to solve.

In this chapter, to find the updated failure probability results, the peak tensile stress is assumed to be the maximum value of the generated stress-range in one month. For other calculations such as comparing LSFs or sensitivity analyses, this variable is kept constant.

3.11. Results & Discussion

Based on the assumption that the loading condition can be obtained by measurement or calculation from wind and wave condition, the aim of the chapter is to

assess the benefit of using FAD approach to update failure probability of a welded joint on existing OWT support structures. Although FAD method has the ability to consider the secondary load effects and make distinction between bending stresses and membrane stresses in calculating stress intensity factors, in the following calculations the secondary load effects (such as thermal expansion or weld misalignment stresses) are not considered for the purpose of simplicity of the methodology illustration, and an unique value of degree of bending (DOB) is assumed.

After each simulation step, the crack state of every crack growth scenario is checked using FAD criteria. If the crack state fails to meet the safety criteria, the crack propagation process will end for that crack growth scenario.

For comparing LSFs and sensitivity analyses, there are about 10^5 crack growth scenarios, some of which might be disregarded in the failure probability calculation if the random initial values are not realistic.

3.11.1. Effect of K_{mat} Constraint in a Critical Crack Size Criteria

To see the effect of using the fracture toughness constraint in the LSF on the reliability result, three different values of K_{mat} are used (see Fig. 3.10). They represent the minimum, maximum and average fracture toughness of a typical offshore steel. First, only critical crack size is considered in the LSF. Then the fracture toughness criterion is included for each case of K_{mat}.

Fig. 3.10 shows that adding the fracture toughness constraint in the LSF reduces the estimated reliability index of the joint. Smaller the value of K_{mat}, lower will be the reliability curve. The difference depends on the peak tensile stress that is used to calculate the stress intensity factor K_{max}. In this figure, the applied peak tensile stress is assumed to be 120 MPa. This result implies that using only the critical crack size criterion in the limit state function will lead to an overestimated fatigue life result.

In current practice of inspection planning, the parameters of the crack growth model are usually calibrated from the S-N model without considering the applied stress and the fracture toughness of the material. This practice might be oversimplified and not conservative because under a high applied stress, the stress intensity factor can be higher than the fracture toughness even when the crack size is small. When only the design data of the structure is available, this practice is

sufficient to find the deterioration model for inspection planning. For a life extension or a reliability updating problem using measured loads of existing structures, a limit state function considering the applied stress and fracture toughness are necessary to obtain a real safety state of the joint.

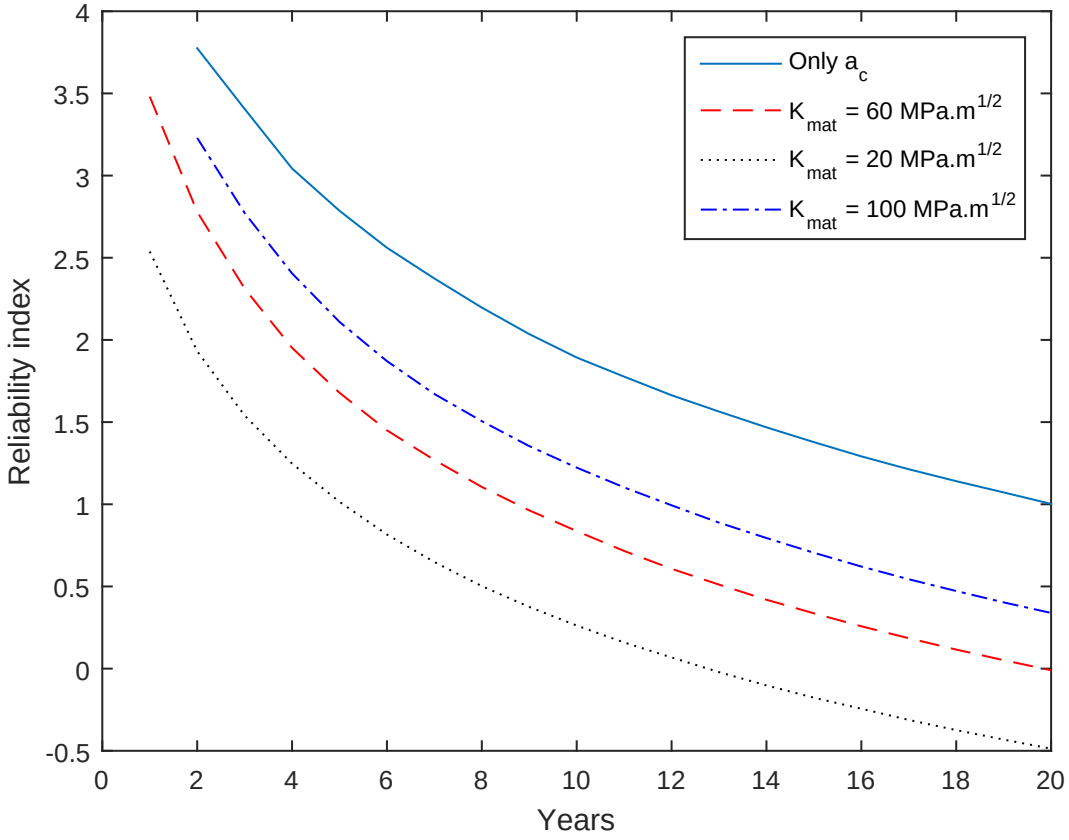

Figure 3.10.: Effects of fracture toughness K_{mat} on the annual reliability index result. The applied peak tensile stress is 120 MPa. 'Only a_c' is the case where only critical crack size is considered in the LSF. For other cases, the fracture toughness constraint is added in the LSF. Only three sources of uncertainty are considered: C, a_0, and a_0/c_0.

3.11.2. FAD vs. Critical Crack Size

The aim of this section is to see the change of the reliability curve when the conventional failure criteria is replaced by the FAD. The term 'conventional failure criteria' in this section is used to imply the combination of Eqs. (3.43) and (3.44), while the FAD limit state function is in the form of Eq. (3.45).

In Fig. 3.11, there are three groups of reliability curves corresponding to three different values of K_{mat}. A unique value of peak tensile stress of 120 MPa is used

for each curve. The result shows that there is no significant difference in using these two LSFs for a given value of fracture toughness. The reason behind this result can be the fact that the brittle fracture is dominant, so the two LSFs are equivalent.

Since the FAD approach can identify not only the brittle fractures but also the plastic collapses and failures in the transition region between the two failure modes, different values of peak tensile stress can be used to see the advantage of FAD approach. In Fig. 3.12, four cases of the peak tensile stress values are considered for comparison, as shown in Eq. (3.59). The result shows that when $\frac{S_{max}}{S_Y} > 0.5$, plastic collapse starts to occur and the reliability curve of the FAD approach starts to be different from the one using the critical crack size.

The four cases of the peak tensile stress values are:

$$S_{max} = \begin{bmatrix} 60 & 120 & 240 & 320 \end{bmatrix} \text{ MPa} \tag{3.59}$$

This result indicates that the applied peak tensile stress is important in assessing reliability of existing structures and that using the critical crack size criteria is not always conservative.

3.11.3. Effect of FAD Uncertainty

The fracture assessment diagram (FAD) is uncertain because its formula is originated from a curve fitting on experimental data. To consider the FAD uncertainty, the limit state function in Eq. (3.46) needs to be modified as follows:

$$g_{4a}(\phi) = R_{FAD} - r - M_u \tag{3.60}$$

where M_u is the general FAD uncertainty, quantified by taking the radial distance of the assessment point minus the radial distance of the intersection point with FAD [72].

To see the effect of FAD uncertainty, a reference case with only three sources of uncertainty C, a_0, and a_0/c_0 is considered. The two reliability curves (the reference case and the case with M_u uncertainty) are plotted among others in Fig. 3.13. It shows that the effect of FAD uncertainty on the reliability of the joint is not significant.

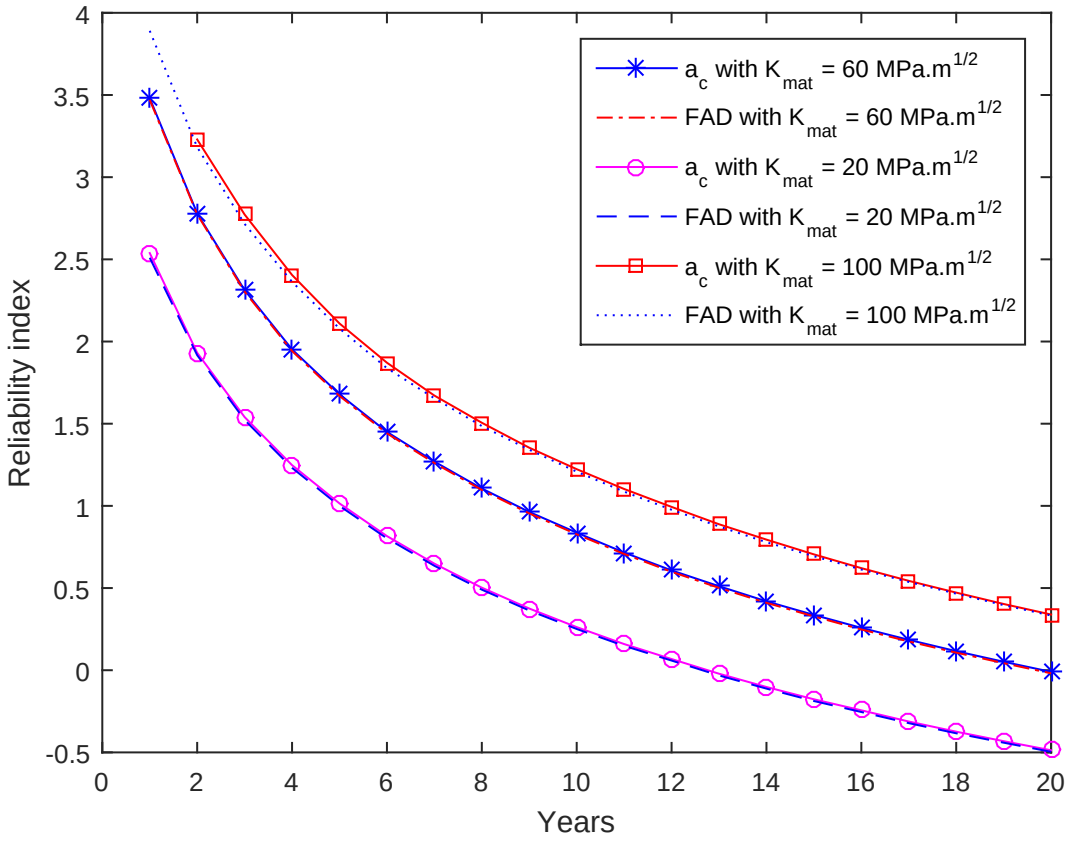

Figure 3.11.: Compare the FAD and the critical crack size LSFs with regard to the annual reliability index. The applied peak tensile stress is 120 MPa. The fracture toughness constraint is included in the critical crack size LSF. Only three sources of uncertainty are considered: C, a_0, and a_0/c_0.

3.11.4. Effect of Yield Strength and Ultimate Strength Uncertainties

As can be seen in Fig. 3.14, the uncertainties of the yield strength (S_Y) and the ultimate strength (S_U) induce significant changes of the plastic failure region. The reliability curves before (the reference case) and after considering these two uncertainties are shown in Fig. 3.13. The result shows that even with a moderate value of peak tensile stress $S_{max} = 60$ MPa, the difference in reliability is significant. The difference becomes more important at the end of the service life since crack sizes become larger and therefore the plastic failure is more probable.

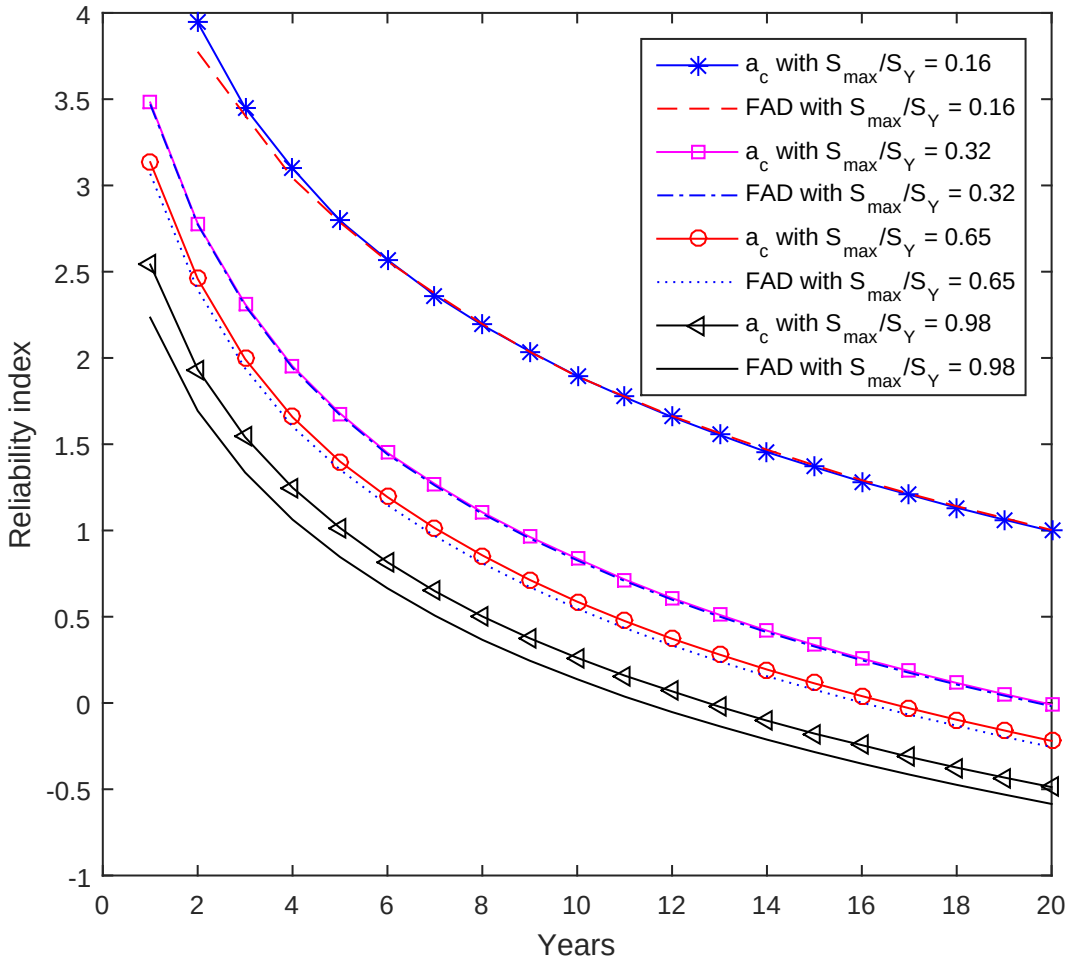

Figure 3.12.: Compare the FAD and the critical crack size LSFs with regard to the annual reliability index. S_{max} is the applied peak tensile stress; S_Y is the yield strength, assumed to be the mean value in Tab. 3.4. The fracture toughness is fixed to $K_{mat} = 60\,\mathrm{MPa\,m^{1/2}}$. Only three sources of uncertainty are considered: C, a_0, and a_0/c_0.

3.11.5. Effects of Fracture Toughness

Fracture toughness is used to calculate the K_r parameter of the assessment point in the FAD approach, as shown in Eq. (3.10). The effect of K_{mat} uncertainty on the reliability, as shown in Fig. 3.14, is significant. This uncertainty becomes more important when the structure reaches the end of its service life.

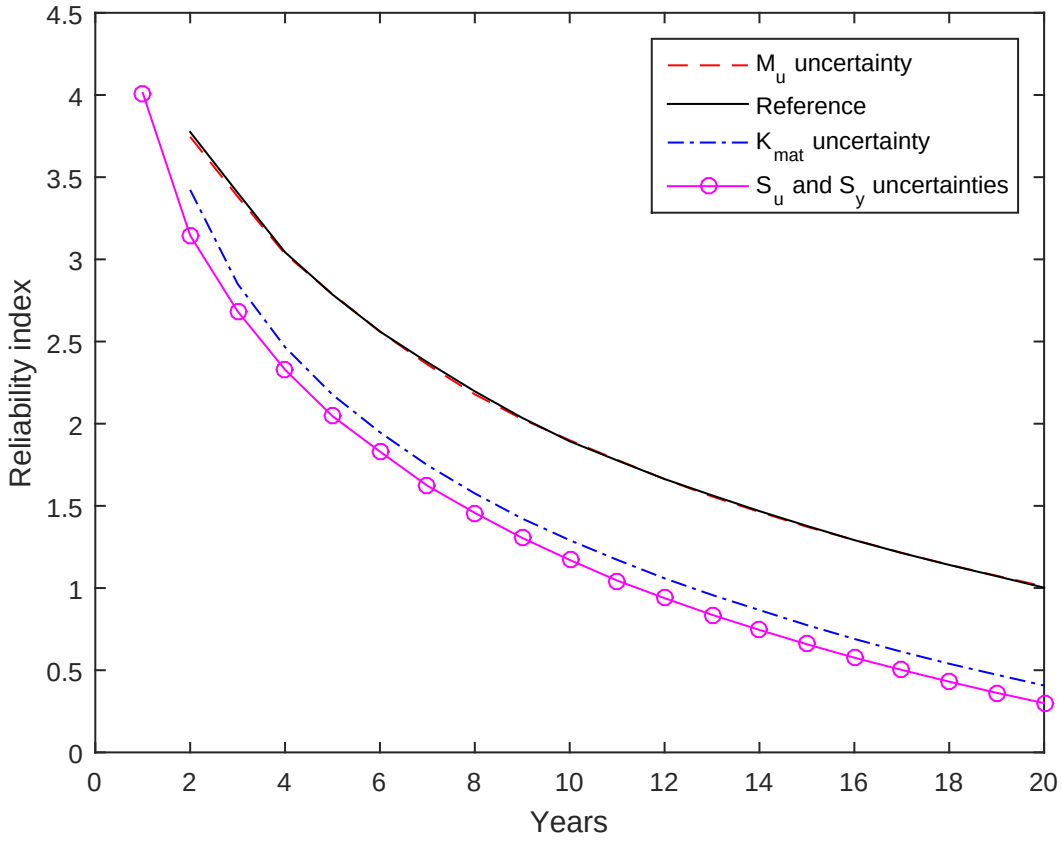

Figure 3.13.: Compare the effects of different uncertainty on the annual reliability index. The applied peak tensile stress is $S_{max} = 60$ MPa; the fracture toughness is $K_{mat} = 60$ MPa.m$^{1/2}$; three sources of uncertainty are commonly considered in each case: C, a_0, and a_0/c_0.

3.11.6. Updated Failure Probabilities

The updated failure probabilities are done using the input variables shown in Tab. 3.4, except the FAD uncertainty.

As explained in sec. 3.8, updating failure probability of the joint is performed on crack propagation samples. At the time of inspection, if the crack size of a crack propagation sample is larger than a detectable crack size—a random value generated from the POD curve—then a crack is detected and an intervention action can be introduced to modify that crack propagation sample.

An amount of 1×10^6 samples of crack propagations are simulated for the chosen joint for failure probability assessment. As seen in Fig. 3.15, crack grows with different rates during the entire lifetime of each sample. Figures Fig. 3.16 and Fig. 3.17 show that the solution converges for the chosen number of samples.

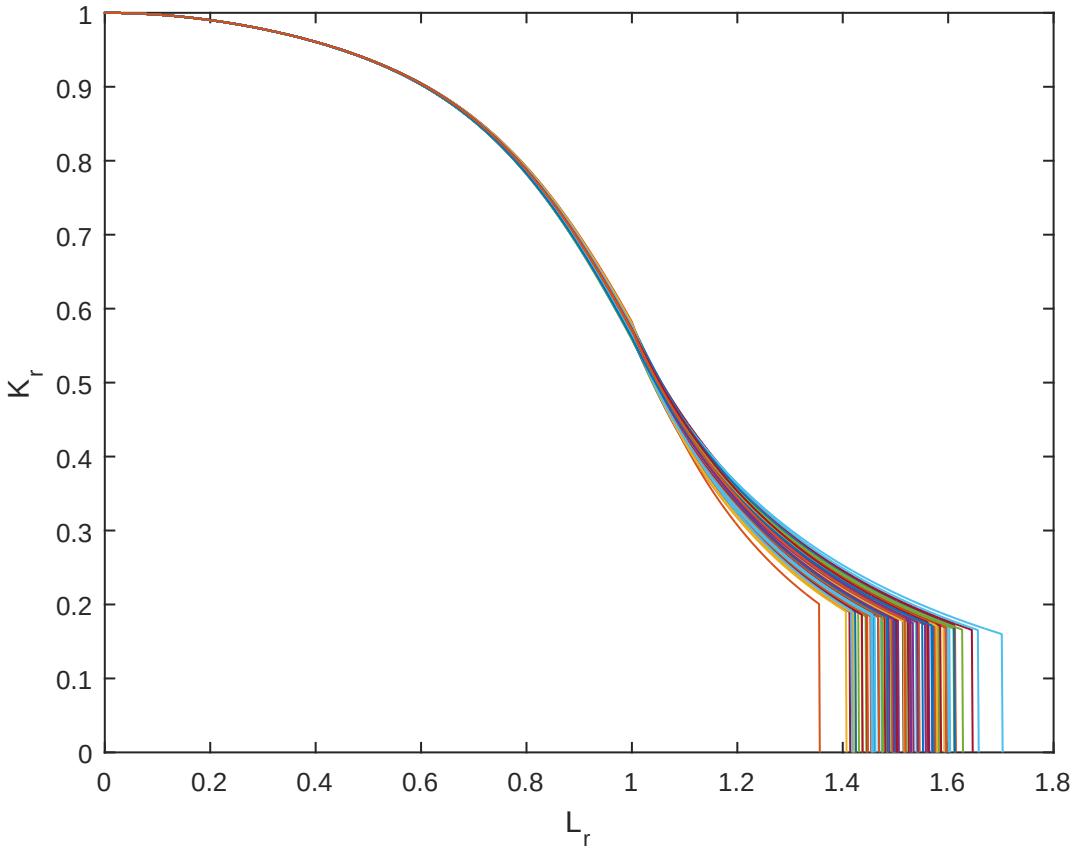

Figure 3.14.: Effects of the yield strength (S_Y) and the ultimate strength (S_U) on the shape of FAD.

Hereafter, the results of updated failure probabilities are shown for an equidistant inspection times approach but the same simulation method can be used for a constant threshold approach. This is because the FAD criteria checks for failures of crack states at every timestep. Consequently, failure probability can also be determined at the timestep level. It allows to perform inspection and repair actions as soon as the failure probability reaches the threshold value.

When no crack is detected: As can be seen from Fig. 3.18 and Fig. 3.19, the failure probability of the joint is updated assuming that crack inspections are done at years 5, 10, and 15. The updated failure probability curve is plotted on the 'No inspection' curve for comparison. As expected, the annual failure probability curve after updating is reduced, even when no crack detected.

When cracks are detected and repaired: When crack is detected, a typical decision is to repair immediately because of the high transportation cost in performing

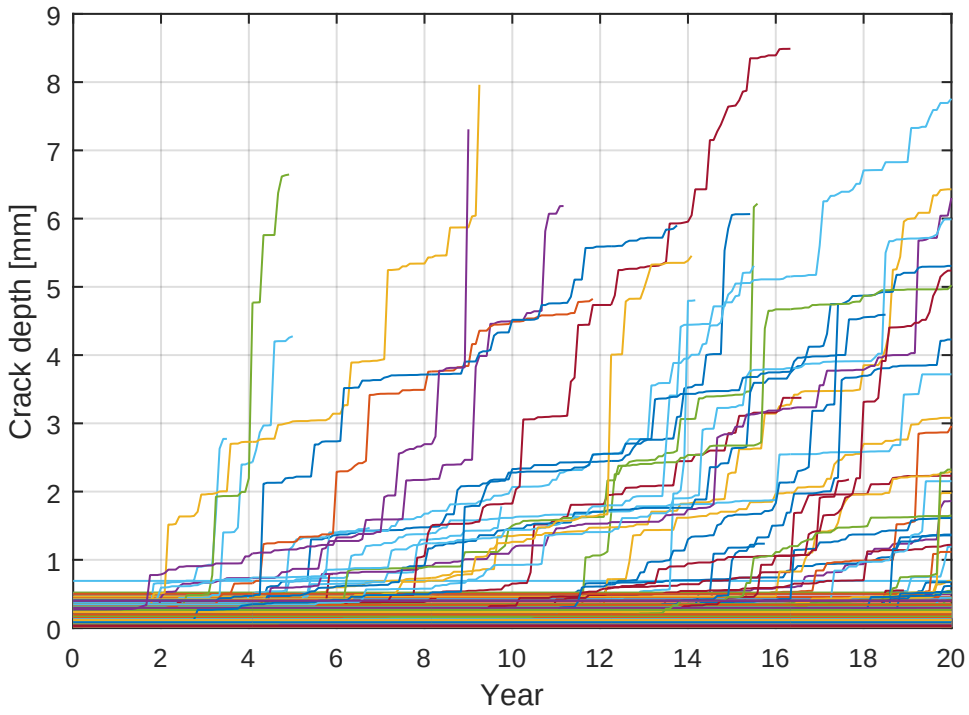

Figure 3.15.: Illustration of crack propagations

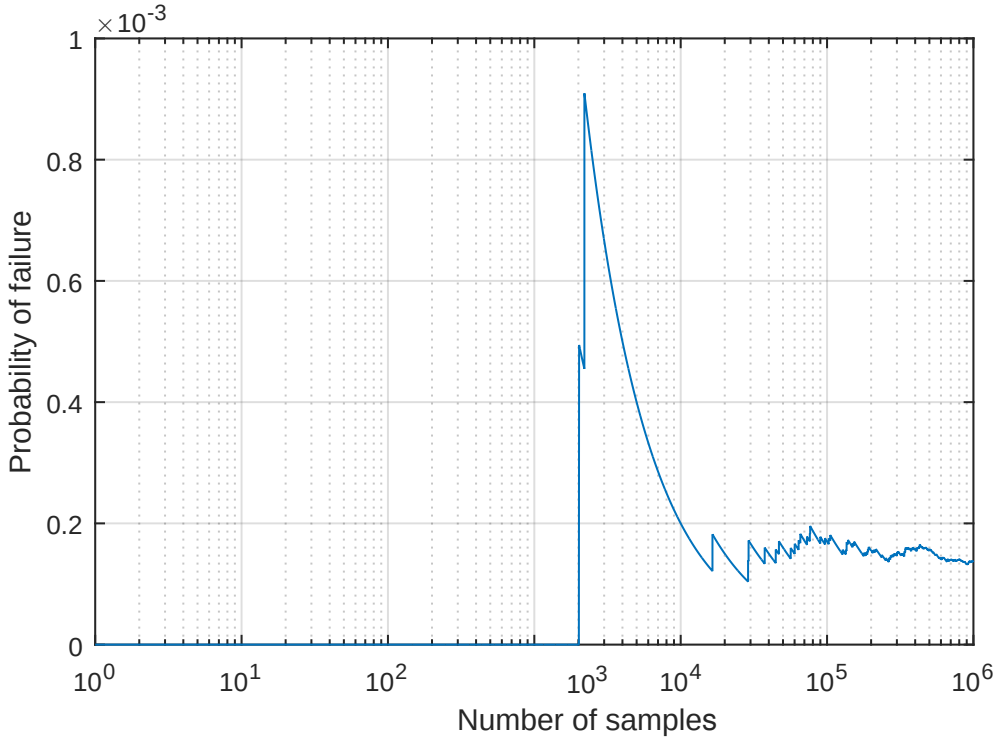

Figure 3.16.: Convergence of Cumulative p_f after the first year

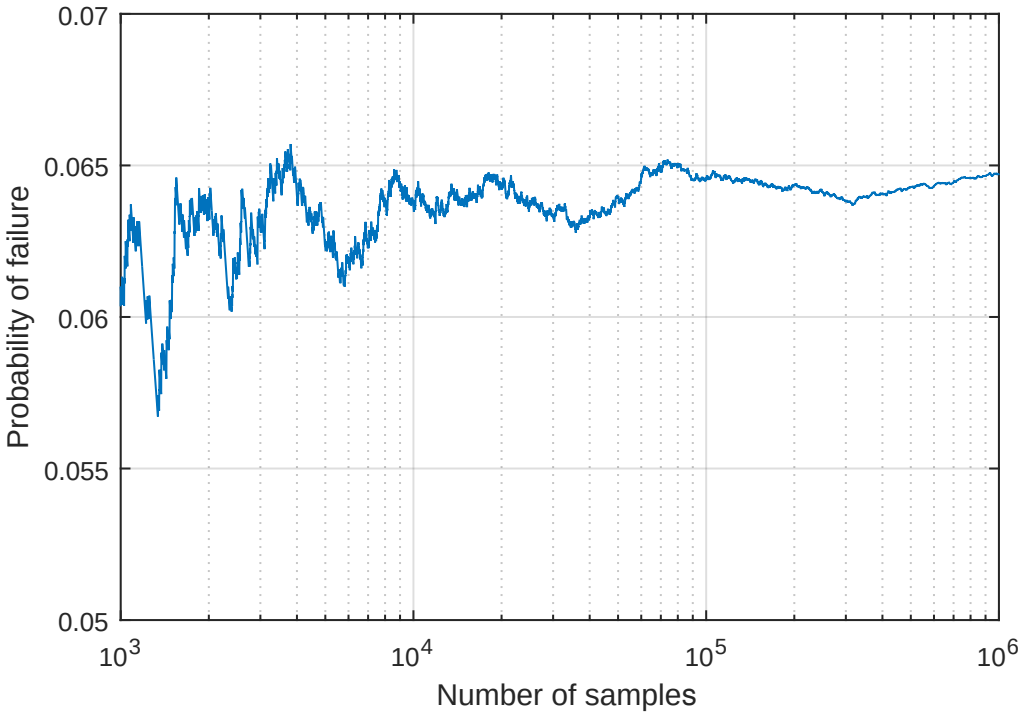

Figure 3.17.: Convergence of Cumulative p_f after the 20^{th} year

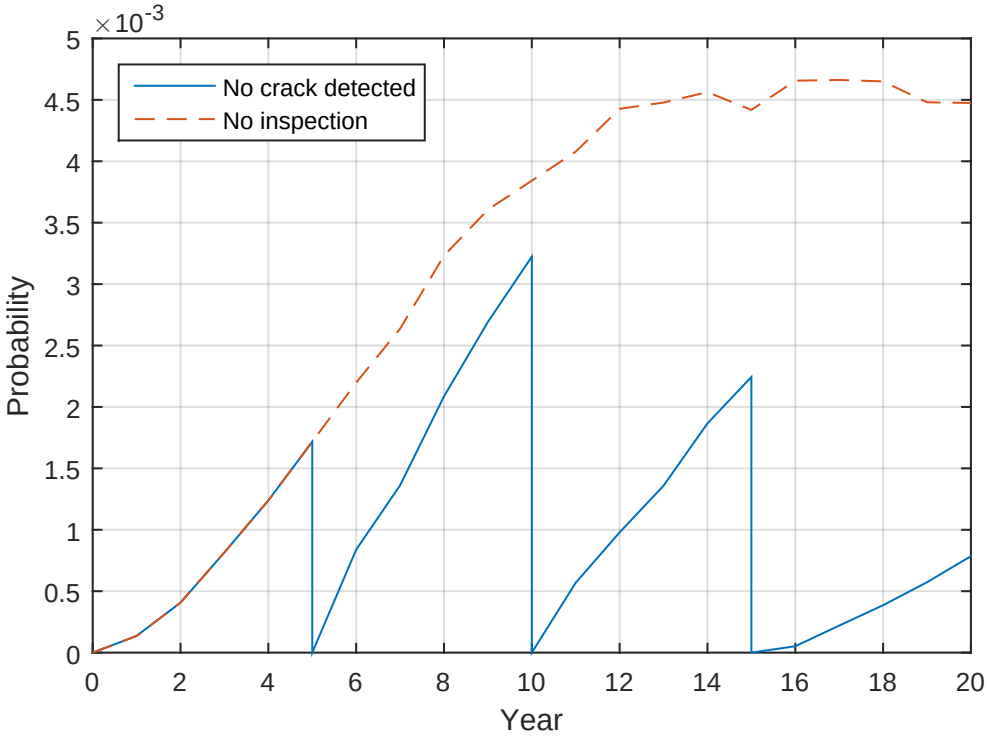

Figure 3.18.: Annual failure probability—No crack detected.

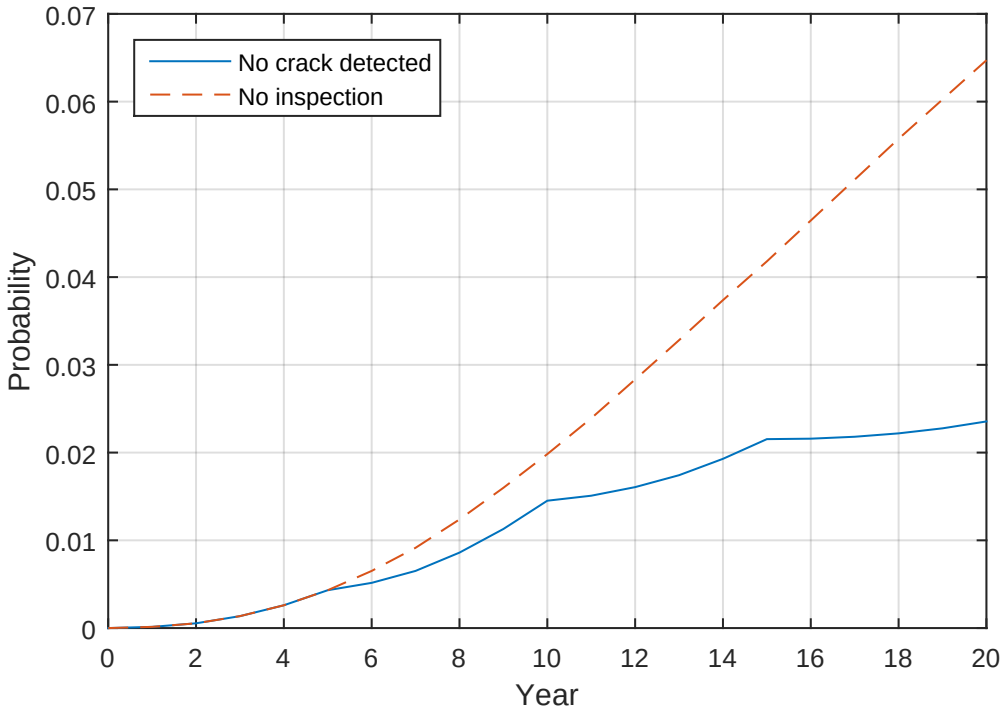

Figure 3.19.: Cumulative failure probability—No crack detected

inspection. In this section, the material properties after repair are considered unchanged, but the intial crack sizes are reset at the time of inspection. Concerning repair quality, a 'normal' repair and a 'perfect' repair scenarios are considered.

As explained in sec. 3.7, in a perfect repair the inital crack size after repair is set to zero, while in a normal repair, the initial crack size after repair is generated from the initial crack size distribution with an upper truncation at the detectable crack size value.

The following results (Fig. 3.20 and Fig. 3.21) are done assuming that the threshold crack size for repair is equal to the detectable crack size. The normal repair curve is plotted on top of the perfect repair curve. As expected, compared to the case repaired imperfectly, when crack is repaired perfectly, the updated failure probability is significantly reduced.

It is noted that separating repair quality into imperfect and perfect cases are reasonable because a repair operation (by grinding or welding, for example) may cause a new problem in the weld. Considering an imperfect repair scenario would give a conservative updated failure probability for decision making, for example in inspection planning.

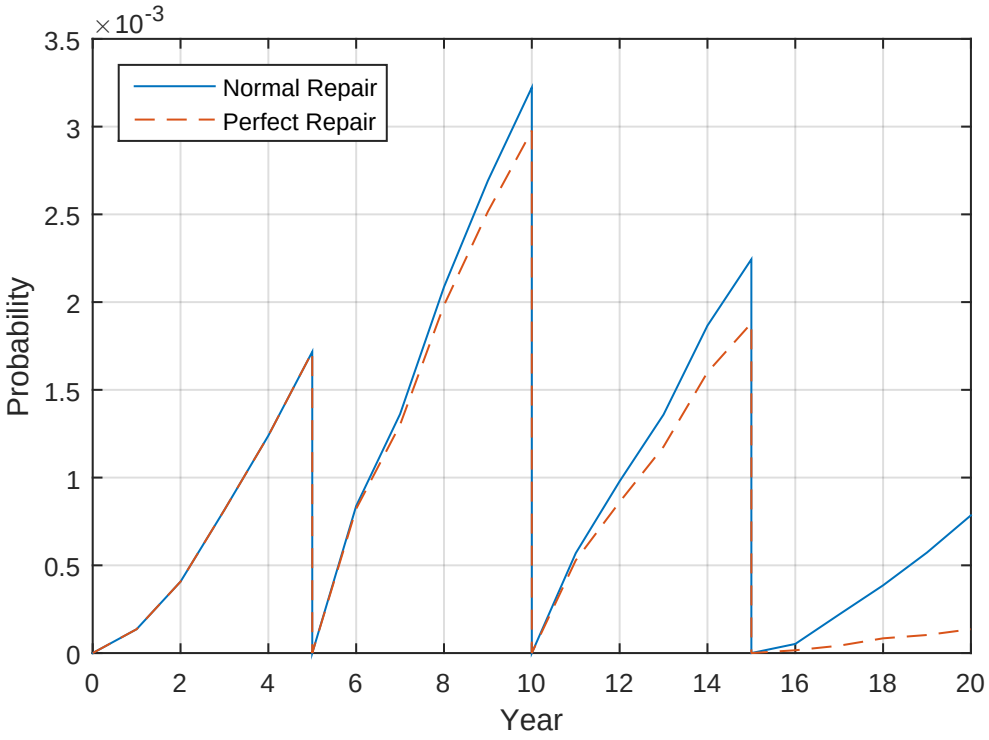

Figure 3.20.: Annual failure probability—Crack detected and repaired.

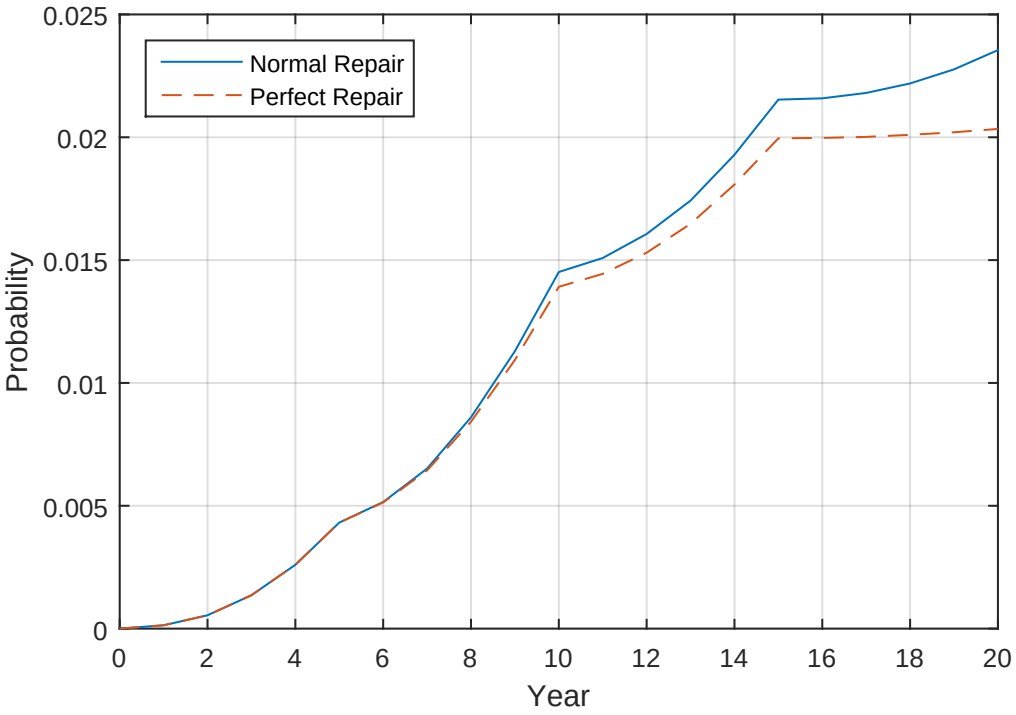

Figure 3.21.: Cumulative failure probability—Crack detected and repaired.

When cracks are detected and not repaired In this event, crack is measured a certain size and the intervention action is 'do not repair'. This scenario might be important for decision makers to economically chose a threshold for crack repair. However, solving this equality event is not possible by using simulation based approach because a lot of samples are required to accurately estimate this very small magnitude of failure probability. A solution would be to reduce the number of uncertainties considered in the LSF to simplify the problem. An example can be found in [86], where both the simulation based approach and the dynamic bayesian network approach have been used.

3.11.7. About Potential Use of FAD

As seen from the results in comparing failure probabilities obtained from an FAD approach and a critical crack size approach, there is no significant difference as long as the applied stress is small.

For an existing structure, there exist a threshold for the ratio between the peak tensile stress and yield strength, above which the FAD approach should be used to catch the possibility of failure due to plastic collapse. For the degree of bending and the FAD parameters assumed in this chapter, this threshold is 65%.

When FAD is used to calculate failure probability, it is required that failure is checked after each stress cycle if the peak tensile stress is random. That causes FAD approach more computationally expensive than using critical crack size criterion (without considering the fracture toughness K_{mat}).

Despire the limitation mentioned above, the fact that FAD approach is capable of releasing the 'critical crack size' assumption and considering plastic collapse makes it an attractive option for reliability assessment and for life extension of existing structures.

3.12. Conclusion

In this chapter, fatigue failure probabilities of welded joints of OWT support structures are updated considering 'crack inspections' and 'intervention actions'. Failure probabilities are calculated using the Fracture Assessment Diagram (FAD) and compared with the usual critical crack size approach. The crack propagation are calculated using a bi-linear Paris' law with stress-range values varying over time. Calculation of crack length and crack depth are coupled.

Fracture toughness should always be included in addition to the critical crack size in the failure criteria to accurately predict remaining fatigue life of existing offshore steel structures. The predicted failure probability increases when the fracture toughness reduces.

In comparison with the critical crack size approach, the FAD approach gives higher failure probability when the applied peak tensile stress is high—the ratio S_{max}/σ_U is more than 65%.

The uncertainty in FAD does not affect significantly the failure probability of the joint as compared to the uncertainties in the ultimate and yield strength. This is because they directly affect the cut-off location of the FAD curve where the plastic failure is defined.

The FAD approach can be used to update failure probability considering crack inspections and intervention actions. New information obtained from crack inspections improves the knowledge about the inspected structure. The calculation shows that reliability of the welded joint increases when no crack detected, or when crack detected and repaired. An imperfect repair assumption significantly reduces the reliability of the joint in comparison with a perfect repair.

3.13. Perspective

The peak tensile stress is one of the variables that determine the failure. It is used not only in FAD approach but also in critical crack size approach where the condition on fracture toughness is included. Instead of using a deterministic value for reliability assessment, the randomness in time of the peak tensile stress should be considered, i.e. the time when high peak tensile stress occurs. This is because a high value of this stress occurs at the beginning of the service life can lead to failure.

The bottleneck in computational time of the simulation based method for updating is the calculation of geometry function values for crack depth and crack length. To handle this bottleneck, for a specific joint and a given DoB value of the stress, a pre-simulation can be done to quantify the uncertainty of the geometry functions, in relation with crack sizes for example.

Since FAD approach is capable of assessing the safety of a through-thickness crack, it should be used to assess reliability of existing structure for a life extension purpose or an inspection planning.

Chapter 4.

Updating Failure Probability Considering Monitoring Data

4.1. Overview

Currently some offshore wind farms are close to or have already passed half of their designed lifetime. Fatigue assessment of their support structures becomes more and more crucial for operation, maintenance, and life extension.

The existing support structures may have completely different dynamic responses from those expected in the design due to many reasons. It can be the corrosion of steel or soil foundation, the unpredicted harsh loading conditions, hidden manufacturing defects, etc.. Therefore the predicted fatigue damage from the design might not be realistic, leading to a different fatigue life of the welded joints.

Many researches have assessed the integrity of existing structures by simulating the dynamic behaviour using coupled or de-coupled wind and wave effects but the as-constructed state of the existing structure, for example the material property, connections, especially the damping ratios are not easy to simulate.

The objective of this chapter is to update failure probability of welded joints using the measured oceanographic and strain data. The oceanographic data can be linked to the fatigue damage by using the strain data, provided that they are concurrently measured. The year-to-year variation of the 10-minute mean wind speed, unrepresentativeness of the structural response during one year measurement, strain measurement uncertainty, and the corrosion effect are considered together with uncertainties of Miner's rule and S-N curves.

The present methodology can be used not only for the strain measuring locations but also for other nearby locations, especially those under water, provided that the

interpolating factors and the corresponding uncertainties are known.

The measurement data used in this chapter comes from OWI-Lab (Vrije Universiteit Brussel).

The main contributions of the author in this chapter can be summarized as following:

- ◇ The formula to derive a resultant stress history from measured data at a set of three strain gauges for each wind direction. More specifically, a resultant moment is obtained for any location on the measuring circumference by projecting normal bending and lateral bending moments on the perpendicular direction of the diameter at the considered location. By doing that, fatigue damage caused by each 10-minute wind speed record can be calculated for any location on the measuring circumference;
- ◇ Propose a methodology to combine oceanographic data with measured strain to update failure probability of the existing support structures;
- ◇ Propose a methodology to fit stress-range distribution with respect to the fatigue damage.
- ◇ Develop a Matlab code to:
  - clean the measured strain data and perform cycle counting,
  - perform least square fitting for stress-range distribution, and for wind speed distribution given the shape parameter of the Weibull distribution.
  - calculate failure probability using the First Order Reliability Method for the specific limit state function;
- ◇ Identify related uncertainties and their importances to the reliability of the existing support structures.

Chapter 4 is organized in three main parts. First, the current state of art is reviewed, then the methodology is explained in detail, and finally a case study is shown for a real wind farm.

4.2. Specific Literature Review

Reliability updating of welded joints is necessary to establish an inspection plan, especially for offshore structures where large number of welded joints are prone to crack and corrosion. Since fatigue fracture is the main failure mode of offshore

structures, it is widely used to identify the critical locations for inspection and maintenance. By using Paris' crack propagation law, different combinations of inspection and repair policies can be described in limit state equations to find failure probabilities and eventually optimize the inspection plan considering relevant costs [87], [85].

Since the stress life (S-N) model is normally used in the fatigue design of offshore wind turbines, parameters of the Fracture Mechanics (FM) model for inspection planning are usually obtained through a calibration process based on the reliability curve [68, 69]. This process can also be applied for existing structures where failure probabilities are updated considering the measured loading conditions or corrosion state.

The accumulated fatigue damage and failure probability of a welded joint on existing structures can be accurately estimated using measured strain. However, it is economically not possible to measure everywhere and for the whole lifetime of the structure. Strain at the under-water locations on the monopile support structures can be found by structural identification methods, for example in [88]. It opens an opportunity to find the most probable hot-spot location on the support structure for fatigue fracture with some limited measurement locations. Since a monopile structure has no structural redundancy, a fatigue crack through the monopile wall will potentially result in the end-of-life for the structure.

Although measured strain data contains errors, as it has been quantified by Thöns [89], real strain data on existing structures reduces the uncertainty on stress-ranges and reflects the real structural responses. Despite the fact that the variance of stress-range uncertainty is smaller, investing on strain measurement does not necessarily improve the reliability index of the structure since the real loading condition might be different from the one predicted in the design stage. From the economic point of view, a pre-posterior Bayesian decision problem should be solved to see if a monitoring system is needed [90, 91].

Using loading conditions (wind, wave) to estimate the accumulated fatigue damage of the structure has been widely studied, both for design and existing structures. In [92], a joint distribution of measured wind speed and wind direction has been used to link fatigue damage to wind data. This is valid only for structures that are not exposed to wave loads, such as bridges, onshore wind turbines, etc.. For offshore wind turbines, since wave loads significantly affect the ultimate and fatigue limit states, wave data should also be considered. In [93] and [94], one can find a method to link wave data to fatigue damage of offshore platforms and wave energy

converters, respectively. For offshore wind turbines, a joint distribution of wind and wave data as proposed in [95] can be used to consider the effects of wind speed together with wave height and wave period.

Concerning the relation between loading conditions (i.e. wind and wave data) and fatigue damage, the corresponding stress-ranges are either implicitly or explicitly involved. For example, in bridges and wave energy converters, the stress can be calculated using a closed-form expression of loading data, but in offshore wind turbines, simulations are needed to find dynamic responses by coupling or de-coupling wind and wave loads. Therefore, reassessing remaining fatigue life using simulation methods is not recommended because it requires enormous load combinations, without mentioning the model uncertainty related to the mathematical models for load calculation, damping ratios assumed, and boundary conditions which may differ from the real structure, especially parameters characterizing the soil conditions.

In conclusion, there is a gap in the literature about how to perform reliability assessment of existing offshore wind turbine support structures using directly monitored data. The objectives of this chapter are to calculate failure probability of a welded joint of a support structure using monitoring data, and to update the failure probability when more data is available.

4.3. Methodology

The limit state function for calculating failure probability is built using the Miner's rule. Based on this cumulative fatigue model, fatigue damage is summed up from different loading combinations. The total fatigue damage is the product of the probability of each loading combination and the corresponding fatigue damage of that loading combination. The measured oceanographic data is used to find the probabilities of load combinations. The measured strain data is used to find the potential hot-spot and eventually the fatigue damage in each loading combination. The methodology is summarized in Fig. 4.1 and explained in the following subsections.

4.3.1. Choosing Oceanographic Parameters

To link oceanographic data to fatigue damage, one needs to discretize its continuous joint distribution into load combinations and then use the measured strain corresponding to each load combination to calculate fatigue damage.

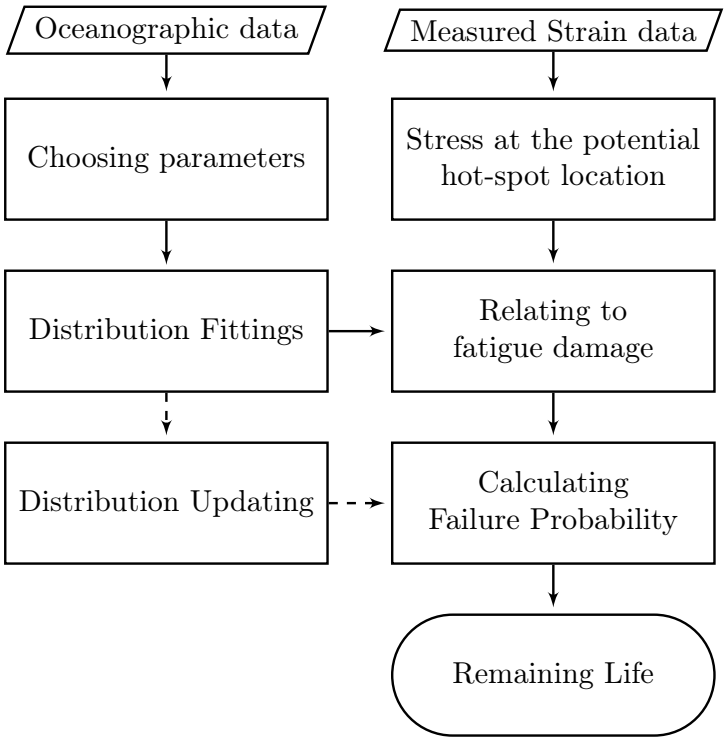

Figure 4.1.: Updating failure probability using monitoring data

Since the duration of strain measurement is limited, it is preferable to limit the number of parameters of the oceanographic data being considered to keep a sufficiently large number of stress cycles in each load combination to guaranty the quality of the stress-range distribution. A small number of parameters also helps to reduce the computational cost.

The joint density distribution of the wind speed, significant wave height, and wave period can be written as in Eq.(4.1), as suggested in [95].

$$f\left(U_{10}, H_s, T_p\right) = f\left(U_{10}\right) \times f\left(H_s|U_{10}\right) \times f\left(T_p|H_s\ U_{10}\right) \tag{4.1}$$

where:

$f\left(U_{10}\right)$ is the marginal distribution of the 10-minute mean wind speed, normally assumed to be a two parameter Weibull distribution whose cumulative distribution function is shown in Eq.(4.2), with k_w and λ_w denote the scale and shape parameters, respectively;

$$F_W\left(U_{10}\right) = 1 - \exp\left(-\left(\frac{U_{10}}{k_w}\right)^{\lambda_w}\right) \tag{4.2}$$

$f(H_s|U_{10})$ is the conditional distribution of significant wave height. By dividing the wind speed data into classes, the H_s data in each class of U_{10} is fitted to a two parameter Weibull distribution whose scale and shape parameters are expressed as functions of wind speeds;

$f(T_p|H_s\ U_{10})$ is the conditional distribution of mean wave periods for given wave heights and mean wind speed. It is assumed to be lognormal distributed with mean and standard deviation calculated from H_s and U_{10}.

For the reason discussed in sec. 4.3.2.3 to guaranty the fitting quality of the stress-range distribution, the remaining stress-ranges in each bin of oceanographic data should be sufficiently large, so the number of the included parameters should be proportional to the duration of strain measurement.

Since the 10-minute mean wind speed is widely collected at wind farms, using the wind speed distribution is recommended if, at least, one year of strain measurement is available. Access to more than one year strain measurements enables U_{10}, H_s, and T_p to be considered together with suitable bin sizes.

4.3.2. Relating Fatigue Damage to Oceanographic Data

4.3.2.1. Cycle Counting

From the time series of measured strain, one needs to perform cycle counting to get stress-ranges for fatigue assessment. Counting stress cycles for a narrow band time series (Fig. 4.2a) is not complicated and most generally accepted counting methods give almost the same results. This is not the case for a broad band time series (Fig. 4.2b) where the large cycles are interspersed with small cycles. As pointed out in [96], for this type of time series, the rain-flow counting method is most suitable because it can identify stress cycles that are compatible with constant amplitude fatigue data (i.e. closed hysteresis loops of strain) and it is capable of identifying stress cycles associated with low frequency components.

The quality of cycle counting depends also on the data cleaning process, i.e. removing unrealistic, duplicated, and redundant recorded values. Unrealistic values are easy to be removed by checking the corresponding weather conditions. Duplicated and redundant recorded values (Fig. 4.3) are the results of having too high resolution monitoring system. Though it is necessary to avoid missing data, this monitoring system may reduce the number of large stress-ranges if the recorded data is not treated properly before performing cycle counting.

(a) Narrow band **(b)** Broad band

Figure 4.2.: Different types of time series

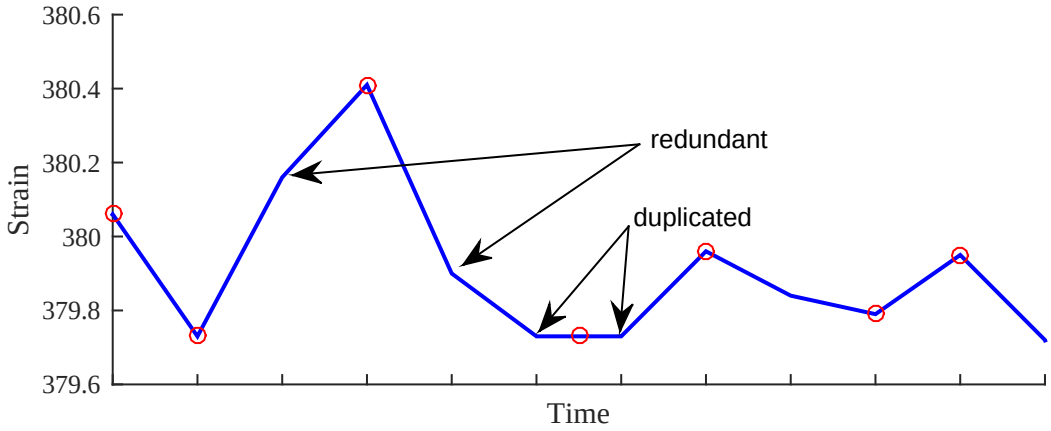

Figure 4.3.: Illustration of redundant and duplicated recorded strain values. Circles represent remaining points after cleaning.

Detail procedure of the rain-flow counting method can be found in [55], a filtering procedure to clean measured strain data is shown in Appendix A.

4.3.2.2. Fatigue Damage

To relate the fatigue damage to oceanographic data, the widely used cumulative damage model — Miner's rule [97], as shown in Eq.(4.3) — can be used.

$$D = \sum_{i=1}^{n} \frac{1}{N_i} \tag{4.3}$$

where:

D is fatigue damage,

n is number of stress cycles during the interested period of time,

N_i is fatigue life of the welded joint corresponding to a constant-amplitude-fatigue

test at the i^{th} stress-range ($\Delta\sigma_i$). The relationship between N_i and $\Delta\sigma_i$ is shown in Eq.(4.4) when a bi-linear S-N curve is used,

$$N_i = \begin{cases} K_{1c} \cdot \Delta\sigma_i^{-m_1} & \text{if } \Delta\sigma_i \geq \Delta\sigma_q \\ K_{2c} \cdot \Delta\sigma_i^{-m_2} & \text{otherwise} \end{cases} \tag{4.4}$$

$\log K_{1c},\ \log K_{2c}$ are the intercept of the characteristic values of the tested data with the $\log N$ axis,

$m_1,\ m_2$ are the negative slopes of the S-N curve,

$\Delta\sigma_q$ is the stress-range at the slope transition, calculated as in Eq.(4.5).

$$\Delta\sigma_q = \left(\frac{K_{2c}}{K_{1c}}\right)^{1/(m_2-m_1)} \tag{4.5}$$

Provided that the measured strain and oceanographic data are concurrent, this cumulative damage rule allows to calculate total fatigue damage by summing up fatigue damages of every bin of the oceanographic data. Detail of calculating total fatigue damage considering oceanographic data is shown in sec. 4.3.3.

4.3.2.3. Fitting Method of Stress-range Distributions

The measured strain data from one or few years may not be representative of the lifetime structural response. For instance, loading conditions during the measurement period may be too mild or too severe compared to the nominal behaviour. In order to consider this uncertainty in updating failure probability, the Weibull distribution model is used to describe stress-range in each bin of the oceanographic data, and subsequently, its scale parameter is considered as a random variable.

The scale k_s and shape λ_s parameters of the Weibull distributions are found for each bin of the oceanographic data by the least squares method as shown in Eq.(4.6).

$$\min_{k_s,\ \lambda_s} \sum_{i=1}^{n_b} \left(\frac{D_{mea}\,(i)}{D^*_{mea}} - \frac{D_{gen}\,(i; k_s, \lambda_s)}{D^*_{gen}\,(k_s, \lambda_s)} \right)^2 \tag{4.6}$$

where:

n_b is number of bin of stress-range;

$D_{mea}\,(i)$ is the 'measured' fatigue damage, calculated by summing up the fatigue damages of the 'measured' stress-ranges in the i^{th} bin of the oceanographic data;

$D_{gen}\,(i; k_s, \lambda_s)$ is the 'generated' fatigue damage, calculated by summing up the fatigue damages of the generated stress-ranges in the i^{th} bin of the oceanographic data. The stress-ranges are generated from the Weibull distribution with the trial values of k_s and λ_s during the optimization process;

$D^*_{mea} = \sum_{i=1}^{n_b} D_{mea}\,(i)$

$D^*_{gen} = \sum_{i=1}^{n_b} D_{gen}\,(i; k_s, \lambda_s)$

For fitting the stress-range distribution using fatigue damage as a constraint, the number of stress-cycles available should be sufficiently large so that in each loop of the optimization process, the quantity $\sum_{i=1}^{n_{cj}} \Delta\sigma_i^m$ converges (where $m = m_1$ or m_2 in the bi-linear S-N curve, and n_{cj} is total number of stress cycles in the j^{th} bin of the oceanographic data). Depending on the distribution parameters, the minimum number of stress-cycles vary for each specific case.

4.3.3. Total Fatigue Damage

For a sufficiently large number of stress cycles, a Weibull distribution of stress-ranges, and a stress-life relationship following a bi-linear curve, the cumulative fatigue damage calculated in Eq.(4.3) can be rewritten as:

$$D = T \sum_{j=1}^{n_{cl}} \left[\frac{\alpha_f^{m_1}}{K_{1c}} k_{s,j}^{m_1} \Gamma\left(\frac{m_1}{\lambda_{sj}} + 1, \left(\frac{\Delta\sigma_q}{k_{s,j}} \right)^{\lambda_{s,j}} \right) + \cdots \right.$$
$$\left. \frac{\alpha_f^{m_2}}{K_{2c}} k_{s,j}^{m_2} \gamma\left(\frac{m_2}{\lambda_{s,j}} + 1, \left(\frac{\Delta\sigma_q}{k_{s,j}} \right)^{\lambda_{sj}} \right) \right] n_{c,j} \tag{4.7}$$

where:

T is number of years in service;

n_{cl} is number of bins of the oceanographic data;

$n_{c,j}$ is number of stress cycles in the j^{th}bin;

α_f is the load factor, a product of the stress concentration factor and a safety factor in fatigue design. The safety factor can be the product of partial safety factors used in the design or an equivalent factor on the design stress-range to meet the required design fatigue factor;

$k_{s,j}$, $\lambda_{s,j}$ are the fitted Weibull scale and shape parameters of the j^{th} bin;

$\Gamma\,()$, $\gamma\,()$ are the upper and lower incomplete gamma functions, respectively.

Typically, the measured strain in support structures of existing offshore wind turbines is rather small, the damage contribution of the upper branch of the stress-life curve is insignificant. If this is the case, one can use Eq.(4.8) for simplification. However, the proposed methodology is not limited to a linear stress-life case.

$$D = T \sum_{j=1}^{n_{cl}} \frac{\alpha_f^{m_2}}{K_c} k_{s,j}^{m_2} \Gamma \left(\frac{m_2}{\lambda_{s,j}} + 1 \right) n_{c,j} \tag{4.8}$$

To include the joint distribution of the oceanographic data in Eq.(4.1) into Eq.(4.8), one simply needs to convert the number of stress cycles in each bin into number of oceanographic records (i.e. number of 10-minute records, for example) as:

$$D = \sum_{i=1}^{T} \sum_{j=1}^{n_{U_{10}}} \sum_{k=1}^{n_{H_s}} \sum_{l=1}^{n_{T_p}} \frac{\alpha_f^{m_2}}{K_c} k_{s,jkl}^{m_2} \Gamma \left(\frac{m_2}{\lambda_{s,jkl}} + 1 \right) \mathrm{P}\left(U_{10,j}, H_{s,k}, T_{p,l} | k_{w,i}\right) \frac{n_{c,jkl}}{n_{m,jkl}} n_m^* \tag{4.9}$$

where:

$n_{cj} = n_{U_{10}} \times n_{H_s} \times n_{T_z}$ is total number of bins;

$n_{c,jkl}$ is number of stress cycles in the bin number jkl;

$n_{m,jkl}$ is number of oceanographic records in the bin number jkl;

$n_m^* = \sum_{j=1}^{n_{cl}} n_{m,j}$ is total of observed oceanographic data per year;

$\mathrm{P}\left(U_{10,j}, H_{s,k}, T_{p,l} | k_{w,i}\right)$ is the probability of the bin jkl given the scale parameter of the wind speed distribution $k_{w,i}$ in the i^{th} year, calculated using Eq.(4.1) considering edges of classes in wind speed, wave height, and wave period.

4.3.4. Calculating Failure Probability

Calculating failure probability of a welded joint of an OWT support structure involves many sources of uncertainty, including:

Critical fatigue damage Δ: This is the threshold to justify when fatigue fracture happens. In a deterministic fatigue assessment, this quantity is set to 1. However, in a fatigue test where different load sequences are used, the tested results showed that the critical fatigue damage value can be larger than one for a low-to-high loading sequence, and smaller than one for a high-to-low loading sequence [98]. A lognormal distribution with median equals 1.0 and CoV equals 0.3 was proposed in [99] and has become a standard model;

Scattering of stress-life tested results: This is the nature of experimental data. However, a representative standard deviation for each specific S-N curve is not available. This is because the test specimens are most often more perfect than real structures with less amount of residual stresses, and the stress-ratios are different in real structures. When there is a lack of tested data established for specific design and fabrication, a typical standard deviation $s_{\log K} = 0.2$ is suggested by DNV-RP-C203 [100]. This uncertainty is represented by random variable K, whose characteristic value is K_c in Eq.(4.4).

The final stress-range values at the hot-spot: they are uncertain because they may contain (1) the measurement uncertainty; (2) the uncertainty in the stress concentration factor (SCF); (3) the uncertainty in the method used to transfer stresses from measuring locations to the hot-spot location, and the uncertainty in the correction factor for corrosion effects.

(1) Measurement uncertainty: Concerning the strain measurement uncertainty, Thöns [101] suggested to use a normal distribution with mean of 1 and a standard deviation of 0.05 to represent. When no experimental data is available to determine the measurement uncertainty for a specific measurement setup, this uncertainty model can be used. Measurement uncertainty is represented by random variable X_m hereafter.

(2) SCF uncertainty: When the hot-spot stress approach needs to be used, the uncertainty in the stress concentration factor is introduced, represented by random variable X_{SCF} hereafter. Since the stress concentration factor can be included in the load factor (α_f) (see Eq.(4.9), for example), random variable X_{SCF} can take the mean value of 1 and the CoV can be chosen regarding the complexity of the joint and the method to calculate stress concentration factor. Some reference values of this uncertainty can be found in Tab. 4.1, taken from [102]. A lognormal distribution is usually chosen for X_{SCF}, as explained in [103], to have a closed form for the expression of the probability of failure since experimental data on Δ and K are also well fitted to a lognormal distribution. In DNVGL-RP-C210 [40], X_{SCF} can be considered to be normally distributed and a CoV of 5% can be used for butt welds, assuming that thickness transitions are properly accounted for by relevant SCF.
In this chapter, a lognormal distribution is used for modelling the uncertainty of X_{SCF}, following the background document to IEC 61400-1 ed 4 [39].

CoV_{SCF}	Fatigue critical detail
0.00	Use of FEM tools at the considered location for statically determinate systems with simple fatigue critical details (e.g. girth welds)
0.05	Use of FEM tools at the considered location for statically determinate systems with complex fatigue critical details (e.g. multi-planar joints)
0.10	Use of FEM tools at the considered location for statically in-determinate systems with complex fatigue critical details (e.g. doubler plates)
0.15	Use of SCF parametric equations for simple fatigue critical details
0.20	Use of SCF parametric equations for complex fatigue critical details

Table 4.1.: Examples of CoV_{SCF}, according to [102].

(3) Other uncertainties: The two last sources of uncertainty are not in the scope of this chapter. They are relevant to specific methods for load extrapolation and consideration of corrosion effects.

The year-to-year variation of loading conditions: This uncertainty can be considered by using the scale parameter k_{wi} (Tab. 4.2) of wind speed distribution at the year i^{th} as a normal random variable. Since the wind measurement period is shorter than the service life, the mean and standard deviation of this normal random variable are unknown and can be updated using measurement data. In this thesis, it is assumed that waves are mainly wind-driven, that the wind induced loads are dominating and that wave height and wave period are wind dependent variables; and therefore considering year-to-year variation in wind speed is sufficient.

Statistical uncertainty: Given that the fluctuation of strain over years is represented by the year-to-year variation of wind speed, the duration of strain measurement may still not be long enough to find a representative of the mean fatigue damage over the whole 20 year lifetime. This statistical uncertainty can be considered by assigning a normally distributed random variable on the scale parameter of the fitted stress-range distribution $k_{s,jkl}$ of the bin jkl of oceanographic data (Tab. 4.2). The coefficient of variation is assumed to be 0.1 based on IEC/FDIS recommendations related to site assessment uncertainty in [39] and can be reduced when several years of measurement data are available.

Random Variables		Dist.	Mean or Median	CoV or std.
Δ	Critical damage	LN	$\tilde{m} = 1$	0.3
X_m	Measurement unc.	N	1	0.05
X_{SCF}	SCF uncertainty	LN	1	0.15
$\log K$	S-N curve unc.	LN	16.006	$\sigma_{\log K} = 0.2$
k_{sjkl}	Statistical unc.	N	fitted	0.1
k_{wi}	Unc. in wind	S	updated	updated

LN: lognormal; N: normal; S: Student's t-distribution;

Table 4.2.: Details of input random variables

Fatigue failure happens when the total fatigue damage calculated in Eq.(4.9) is larger than the critical fatigue damage Δ, so the limit state function can be written as in Eq.(4.10).

$$g(T) = \Delta - \sum_{i=1}^{T} \sum_{j=1}^{n_{U_{10}}} \sum_{k=1}^{n_{H_s}} \sum_{l=1}^{n_{T_p}} \frac{(\alpha_f X_m X_{SCF})^{m_2}}{K} k_{s,jkl}^{m_2} \Gamma\left(\frac{m_2}{\lambda_{s,jkl}} + 1\right) \cdots \times \mathrm{P}\left(U_{10,j}, H_{s,k}, T_{p,l} | k_{w,i}\right) \frac{n_{c,jkl}}{n_{m,jkl}} n_m^* \tag{4.10}$$

The limit state function in Eq.(4.10) can be solved using FORM/SORM as well as simulation techniques. Details of FORM/SORM solution can be found in, for example, [104]. In solving Eq. (4.10) using FORM/SORM, the 'importance factor' of each random variable can be obtained. The 'importance factor' of a random variable is a measure of the sensitivity of the reliability index to randomness of that random variable at the design point. The 'importance factors' offer a way to rank the importance of the input variables with respect to the failure event of the welded joint. The vector of 'importance factors' is denoted as $\boldsymbol{\alpha}$, and defined in Eq.(4.11):

$$\boldsymbol{\alpha} = -\frac{\nabla g(\boldsymbol{x})}{|\nabla g(\boldsymbol{x})|} \tag{4.11}$$

where $\nabla g(\boldsymbol{x})$ is the gradient vector of the limit state function at the design point $\boldsymbol{x}$, which is assumed to exist, as shown in Eq.(4.12):

$$\nabla g(\boldsymbol{x}) = \left(\frac{\partial g}{\partial x_1}(\boldsymbol{x}), \quad \cdots, \quad \frac{\partial g}{\partial x_n}(\boldsymbol{x}) \right) \tag{4.12}$$

It is noted that Eq.(4.10) is also used to calculate the failure probability considering the updated joint distribution of oceanographic data since the updated predictive distribution for k_{wi} is used to obtain $\mathrm{P}\left(U_{10,j}, H_{s,k}, T_{p,l}|k_{w,i}\right)$.

If only wind speed is considered in load combinations, $\mathrm{P}\left(U_{10,j}, H_{s,k}, T_{p,l}|k_{w,i}\right)$ becomes $\mathrm{P}\left(U_{10,j}|k_{w,i}\right)$ and is calculated as shown in Eq.(4.31) below. Otherwise, $\mathrm{P}\left(U_{10,j}, H_{s,k}, T_{p,l}|k_{w,i}\right)$ can be calculated using a numerical integration method with respect to the joint density function in Eq. (4.1).

4.3.5. Updating Distribution of the Oceanographic Data

The oceanographic data consists of wind speed, wave height, and wave period. During the service life, the oceanographic data is collected, the wind speed distribution can be updated through its scale parameter (k_w). The distribution parameters of other dependent quantities (i.e. H_s and T_p) can be updated by redoing the regression for each bin of wind speed.

The scale parameter of wind speed distribution (k_w) is considered normally distributed with unknown mean (μ) and unknown standard deviation (σ), as shown in Eq.(4.13). This distribution will be updated using Bayesian approach considering the 'measured' data $\left(\hat{\mathbf{k}}_w\right)$— the fitted scale parameters of the 10-minute wind speed for each year of measurement. The updating procedure follows [26] and [105] and is explained here below.

$$\begin{aligned} f_{K_w}\left(k_w|\mu,\sigma\right) &= f_N\left(k_w|\mu,\sigma\right) \\ &= \frac{1}{\sigma\sqrt{2\pi}}\exp\left(-\frac{1}{2}\left(\frac{k_w-\mu}{\sigma}\right)^2\right) \end{aligned} \tag{4.13}$$

Assuming a normal distribution for the mean μ given σ, as shown in Eq.(4.14),

$$f_N\left(\mu|\mu',\frac{\sigma}{\sqrt{n'}}\right) = \frac{\sqrt{n'}}{\sigma\sqrt{2\pi}}\exp\left(-\frac{n'}{2}\left(\frac{\mu-\mu'}{\sigma}\right)^2\right) \tag{4.14}$$

and an Invers-Gamma-2 distribution for the standard deviation σ, as shown in Eq.(4.15)

$$f_{i\gamma 2}\left(\sigma|s',\nu'\right) = \frac{\left(\nu'/2\right)^{\nu'/2}}{\Gamma\left(\nu'/2\right)}\frac{2}{s'}\left(\frac{s'^2}{\sigma^2}\right)^{(\nu'+1)/2}\exp\left(-\nu's'^2/\left(2\sigma\right)\right) \tag{4.15}$$

the joint prior density function of μ and σ becomes a Normal-Invers-Gamma-2

distribution, as shown in Eq.(4.16)

$$f'_{\mu,\sigma}(\mu,\sigma) = f_N\left(\mu|\mu', \frac{\sigma}{\sqrt{n'}}\right) \; f_{i\gamma 2}(\sigma|s',\nu') \tag{4.16}$$

and the posterior density function is also a Normal-Invers-Gamma-2 distribution, as shown in Eq.(4.17)

$$f''_{\mu,\sigma}\left(\mu,\sigma|\hat{\mathbf{k}}_w\right) = f_N\left(\mu|\mu'', \frac{\sigma}{\sqrt{n''}}\right) \; f_{i\gamma 2}(\sigma|s'',\nu'') \tag{4.17}$$

In Eqs. from (4.14) to (4.17):

- μ', s', n', and ν' are prior parameters that represent the prior estimation of the expectation of μ, the expectation of σ, sample size n, and degrees of freedom ν, respectively.

- μ'', s'', n'', and ν'' are their posterior parameters, calculated as following:

$$\begin{aligned}
n'' &= n' + n \\
\mu'' &= \left(n'\mu' + n\bar{k}_w\right)/n'' \\
s''^2 &= \left(\nu' s'^2 + n'\mu'^2 + \nu s^2 + n\bar{k}_w^2 - n''\mu''^2\right)/\nu'' \\
\nu'' &= \nu' + \delta(n') + \nu + \delta(n) - \delta(n'')
\end{aligned}$$

- the statistical $\bar{k}_w$ and s^2 are calculated for a vector of n-year 'measured' data $\hat{\mathbf{k}}_w = \left(\hat{k}_{w1}, \hat{k}_{w2}, \cdots, \hat{k}_{wn}\right)$ — each component corresponds to one year of data — as following:

$$\begin{aligned}
\bar{k}_w &= \frac{1}{n}\sum_{i=1}^{n} \hat{\mathbf{k}}_{wi} \\
s^2 &= \frac{1}{n-1}\sum_{i=1}^{n}\left(\hat{k} - \bar{k}_w\right)^2 \\
\nu &= n - 1
\end{aligned}$$

The predictive density function of k_w given measured data becomes a Student'

t-distribution as shown in Eq.(4.18).

$$
\begin{aligned}
f_{K_w}\left(k_w|\hat{\mathbf{k}}_w\right) &= f_S\left(k_w|\mu'', s''\frac{n''+1}{n''}, \nu''\right) \\
&= \frac{\Gamma\left(\frac{\nu''+1}{2}\right)}{s''\sqrt{\nu''\pi}\Gamma\left(\frac{\nu''}{2}\right)}\left[\frac{\nu''+\left(\frac{k_w-\mu''}{s''}\right)^2}{\nu''}\right]^{-\left(\frac{\nu''+1}{2}\right)}
\end{aligned}
\tag{4.18}
$$

With the updated mean wind speed distribution thanks to its updated scale parameter Eq.(4.18), and new regression parameters for H_s and T_p (if any), Eq.(4.1) can be used to calculate values of $\mathrm{P}\left(U_{10,j}, H_{s,k}, T_{p,l}|k_{w,i}\right)$ in the limit state function in Eq.(4.10). It is worth mentioning that random variable k_w is part of the limit state function, and should be treated properly in the reliability analysis.

4.4. Application to Remaining Fatigue Life Prediction of a Monopile Support Structure

4.4.1. Measurement Setup

Measurements are conducted by VUB at a monopile support structure of a 3 MW offshore wind turbine with a hub height of approximately 71m. The monopile has a diameter of 5.2 m and is installed at a water-depth of approximately 19 m. Three strain gauges, arranged as shown in Fig. 4.4, are used to measured strain and calculate bending moments.

The current set-up uses optical Fiber Bragg Gratings (or FBGs). These optical sensors use variations of the reflected spectrum to infer strain, and reach a resolution of about 1 micro-strain. These glass-fiber sensors have advantages over classic (resistive) strain gauges that they are not prone to corrosion or electrical interference. The major advantage is that several FBG sensors can be inscribed in a single fiber, thus reducing the required wiring. While the price of the fiber and the sensors is acceptable the measurement hardware, a so-called interrogator, currently is still far more expensive than the hardware required for classic resistive strain gauges.

Similar to strain gauges, FBG sensors require to be temperature compensated, preferably using temperature sensors positioned exactly next to the set-up to ac-

count for solar radiation. No additional filter is applied to the time series. To prepare the data for fatigue damage assessment the time series are processed using the rain-flow cycle-counting algorithm. As a result, for each ten-minute interval a histogram is available for the occurring stress ranges within the considered ten-minute period.

Measured data available for the application is:

- ◇ One-year strain data;
- ◇ Three-year oceanographic data: 10-minute mean wind speed, wind direction, significant wave height, wave direction;
- ◇ 15 year data of 10-minute mean wind speed at the similar site;
- ◇ Design wind speed distribution;
- ◇ Other SCADA: pitch, rpm to identify operational cases.

4.4.2. Deriving Stress Histories

Strain is measured at the three locations G_{090}, G_{210}, and G_{330} as shown in Fig. 4.4. In order to find the most probable fatigue fracture location on the plane of the three strain gauges, it is necessary to derive stress histories for any location on the circumference from the three known strain gauge locations.

Using the known angle of the wind (β_w), the tower normal bending moment in the wind direction (M_{tn}), the tower lateral bending moment in the cross-wind direction (M_{tl}) (as shown in Fig. 4.5 and Fig. 4.4), and the normal load (N) acting on the plane of the measurement are calculated from the three strain gauge data by solving Eq.(4.19).

$$\begin{bmatrix} \varepsilon_{090} \\ \varepsilon_{210} \\ \varepsilon_{330} \end{bmatrix} = -\frac{1}{E} \begin{bmatrix} \frac{1}{A} & -\frac{R_i}{I_c}\sin(90-\beta_w) & -\frac{R_i}{I_c}\cos(90-\beta_w) \\ \frac{1}{A} & -\frac{R_i}{I_c}\sin(210-\beta_w) & -\frac{R_i}{I_c}\cos(210-\beta_w) \\ \frac{1}{A} & -\frac{R_i}{I_c}\sin(330-\beta_w) & -\frac{R_i}{I_c}\cos(330-\beta_w) \end{bmatrix} \begin{bmatrix} N \\ M_{tl} \\ M_{tn} \end{bmatrix} \tag{4.19}$$

in which E is Young's modulus of structural steel at 210 GPa and:

$$A = \pi\left(R_o^2 - R_i^2\right) \tag{4.20}$$

$$I_c = \frac{\pi}{4}\left(R_o^2 - R_i^2\right) \tag{4.21}$$

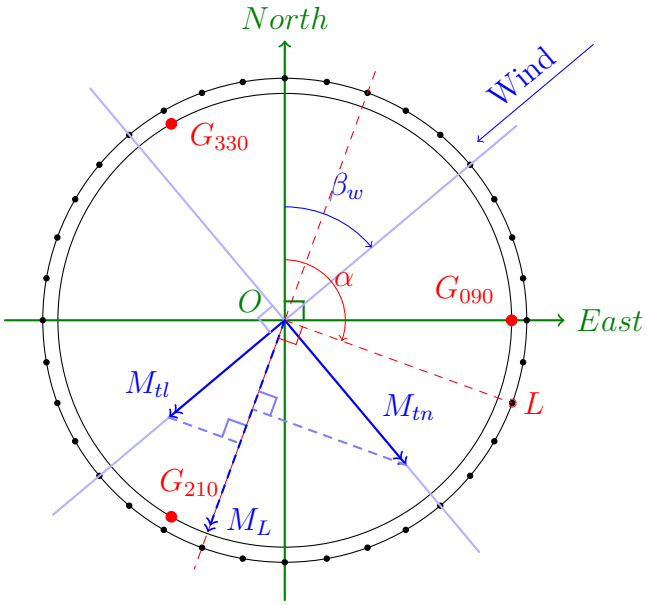

Figure 4.4.: Cross section of the tower. G_{090}, G_{210} and G_{330} are locations of the three strain gauges. M_L is the resultant moment caused by the wind direction β_w acting at location L.

with R_0 and R_i represent the outer and inner radius of the tubular section, respectively.

Given N, M_{tl}, and M_{tn} calculated from Eq.4.19, an unique stress history needs to be derived for any location (for a given measuring level of the tower). Let L is a location on the outer circumference (Fig. 4.4), the stress history at L is calculated as:

$$\sigma_L = -\frac{N}{A} + \frac{M_L}{I_c} R_o \tag{4.22}$$

where M_L is the resultant moment caused by each wind direction. M_L can be obtained by projecting M_{tn} and M_{tl} on the radial direction that is perpendicular to the line OL:

$$M_L = M_{tl} \sin(\alpha - \beta_w) + M_{tn} \cos(\alpha - \beta_w) \tag{4.23}$$

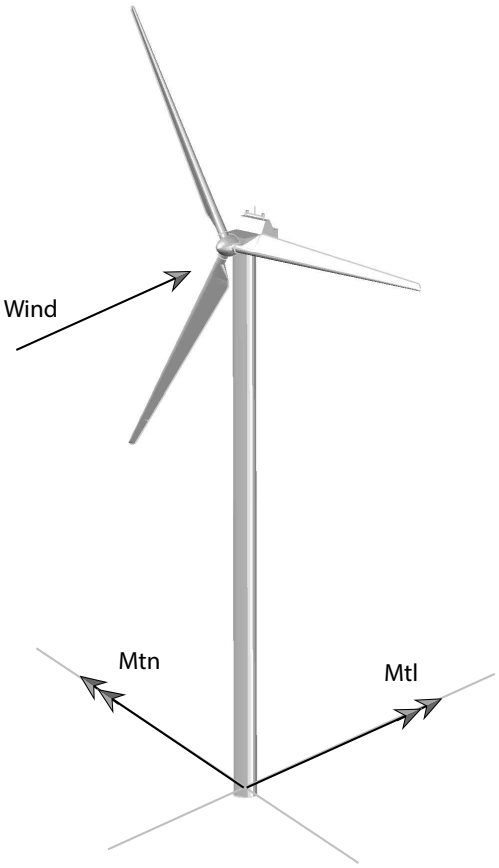

Figure 4.5.: Definition of M_{tn} and M_{tl}

4.4.3. The Potential Hot-spot Location

Stress history at any location on the outer circumference can be obtained using Eq.(4.22) for any 10-minute wind speed record. By calculating fatigue damage at every location on the outer circumference, the most probable hot-spot location is the one with highest fatigue damage. It is worth mentioning that the real potential hot-spot location also depends on the distance of the weld with respect to the seabed. As illustrated in Fig. 4.4, there are 36 locations used to compare fatigue damage for the case study. Once the most probable hot-spot location is found, its stress-range data will be used for distribution fitting as shown in sec. 4.4.5.

For each of these 36 locations, the procedure to find total fatigue damage can be summarized as following:

a) Calculating the resultant moment M_L corresponding to each set of three strain values in each 10-minute record, using Eq.(4.23),

b) Using Eq.(4.22) to find a stress history σ_L corresponding to each 10-minute record,

c) Using rain-flow counting for each 10-minute stress history σ_L,

d) The fatigue damage contributed by each 10-minute wind speed to location L is calculated using the S-N curve as in Eq.(4.24).

e) The total fatigue damage at the location L is found by summing up all the fatigue damage caused by each 10-minute wind speed.

$$\begin{cases} \log K_{1c} = 11.764; & m_1 = 3 \\ \log K_{2c} = 15.606; & m_2 = 5 \end{cases} \tag{4.24}$$

4.4.4. Oceanographic Data

Concurrent with strain data, the oceanographic data including wind speed, wind direction, significant wave height, wave period, and wave direction during 1 year is available. However, only wind speed is considered at the place of the oceanographic data in the limit state function due to the limited strain measuring duration. As explained in sec. 4.3.2.3, the number of stress cycles in each bin of load combination should be sufficiently large. To deploy the proposed method, the current available data is not enough to fit stress range distributions for all combinations of U_{10}, H_s, and T_p, and therefore in the case study only combinations for wind speed (U_{10}) are considered with all waves pooled together for the respective wind bins.

For the purpose of updating wind speed distribution using 3-year measured data, the 15-year data of U_{10} from the nearby measurement station Wandelaar has been used (IVA MDK - afdeling Kust - Meetnet Vlaamse Banken) to estimate the prior coefficient of variation of the scale parameter k_w.

By keeping the shape parameter obtained from the 15-year data fitting, the scale parameter is found for each year data by the least squares method. The scale parameters of the wind speed distributions are shown in Tab. 4.3 and Fig. 4.6. The coefficient of variation of (k_w) is found to be 0.0418 by using Eq.(4.25).

$$\mathrm{CoV}_{k_w} = \frac{\sigma_{k_w}}{\mu_{k_w}} \tag{4.25}$$

Year	2002	2003	2004	2005	2006	2007	2008	2009	2010	2011	2012	2013	2014	2015	2016
k_w	8.39	7.55	8.24	7.57	8.54	8.43	8.18	7.94	7.90	8.44	7.73	8.21	7.64	8.22	7.87

Table 4.3.: The fitted 15-year scale parameters of the similar site [m/s]

Together with the variation of k_w, the design wind speed data is utilized as prior information since the observed wind data before construction is not available at the

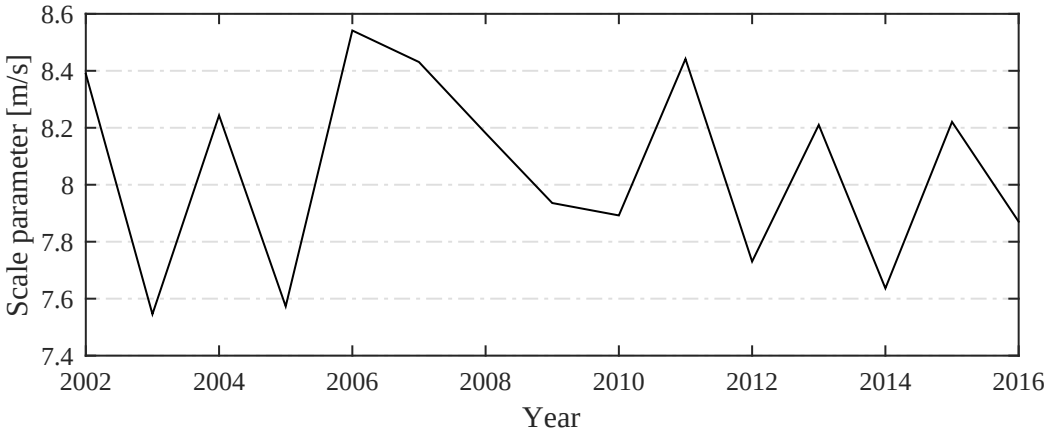

Figure 4.6.: The 15-year scale parameters of the similar site

considered site. The design wind speed data is given by Eq. (4.26) in the form of mean value and shape parameter. They are used to calculate the scale parameter in Eq. (4.27).

$$\begin{cases} \bar{U}_{10}^{design} & = 9.24\ (m/s) \\ \lambda_w^{design} & = 2.31 \end{cases} \tag{4.26}$$

$$k_w^{design} = \frac{\bar{U}_{10}^{design}}{\Gamma\left(1 + \frac{1}{\lambda_w^{design}}\right)} = 10.4294\ (m/s) \tag{4.27}$$

The same fitting method is applied to the three year data of U_{10} at the considered site to find the vector of 'measured' data $\hat{\mathbf{k}}_w$ for updating k_w distribution. The only difference is that the shape parameter is taken from the design wind speed distribution. The results are shown in Fig. 4.7. Due to the confidentiality of the wind data, some information is hidden. The fitted scale parameters constitute the components of the vector of the 'measured' data, given by Eq.(4.28) for updating random variable k_w.

$$\hat{\mathbf{k}}_w = \begin{bmatrix} 10.005 & 9.993 & 8.176 \end{bmatrix}\ \text{m/s} \tag{4.28}$$

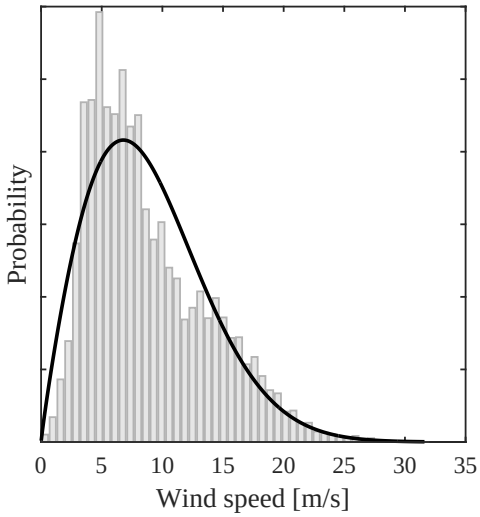

(a) The 1^{st} year

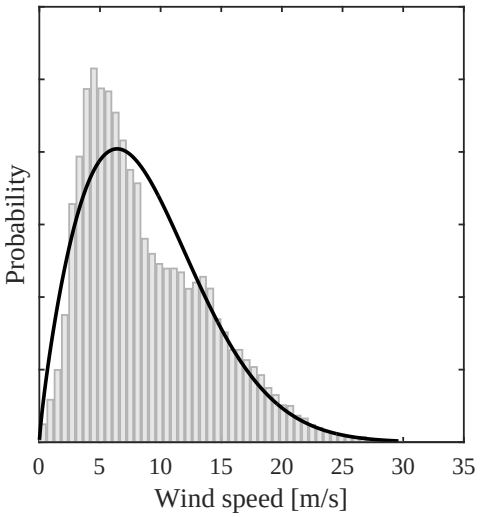

(b) The 2^{nd} year

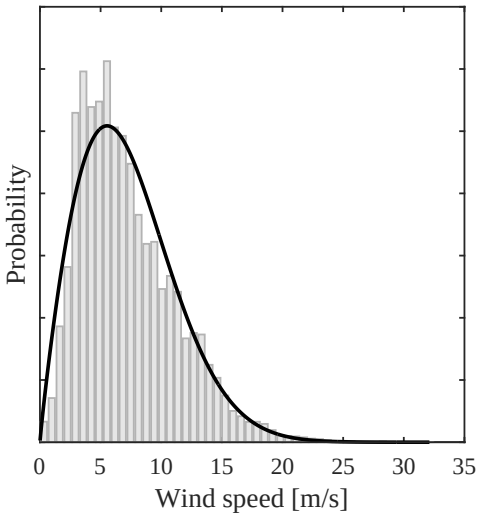

(c) The 3^{rd} year

Figure 4.7.: Fitted wind speed distributions

4.4.5. Fitted Stress-range Distribution

For each bin of wind speeds, stress-ranges obtained by rain-flow counting are fitted into a Weibull distribution model. The results are shown in figures from Fig. 4.8 to Fig. 4.12. The fitted scale and shape parameters are not shown due to data confidentiality. Since the fitted scale and shape parameters are found from an optimization procedure, as shown in Eq.(4.6), it can happen that the optimal result is local, not global. So the total fatigue damage calculated from those fitted stress-range distribution (using Eq.(4.9)) needs to be verified with the damage calculated

directly from the 'measured' stress-ranges.

Validation of the fitted parameters: The total fatigue damage calculated directly from the measured stress-ranges is 0.0084 with a load factor $\alpha_f = 5$. The total fatigue damage calculated using the fitted parameters of stress-range distributions is shown in Eq.(4.29). The result shows that the fatigue calculated from the fitted parameters of stress-range distributions is the same as the damage calculated directly from the measured stress-ranges.

$$\begin{aligned} D_{1year} &= \sum_{i=1}^{5} n_{m_i} \frac{\alpha_f^m}{K_c} \left[k_{s1}^m \, \Gamma\left(\frac{m}{\lambda_{s1}} + 1\right) \, p_1 \, \frac{n_{c_1}}{n_{m_1}} + k_{s2}^m \, \Gamma\left(\frac{m}{\lambda_{s2}} + 1\right) \, p_2 \, \frac{n_{c_2}}{n_{m_2}} + \right. \\ &\quad k_{s3}^m \, \Gamma\left(\frac{m}{\lambda_{s3}} + 1\right) \, p_3 \, \frac{n_{c_3}}{n_{m_3}} + k_{s4}^m \, \Gamma\left(\frac{m}{\lambda_{s4}} + 1\right) \, p_4 \, \frac{n_{c_4}}{n_{m_4}} + \\ &\quad \left. k_{s5}^m \, \Gamma\left(\frac{m}{\lambda_{s5}} + 1\right) \, p_5 \, \frac{n_{c_5}}{n_{m_5}} \right] \\ &= 0.0084 \end{aligned} \tag{4.29}$$

In Eq. (4.29), the input data is taken from Tab. 4.4, where the probability of each wind speed bin (p) is calculated using Eq.(4.31).

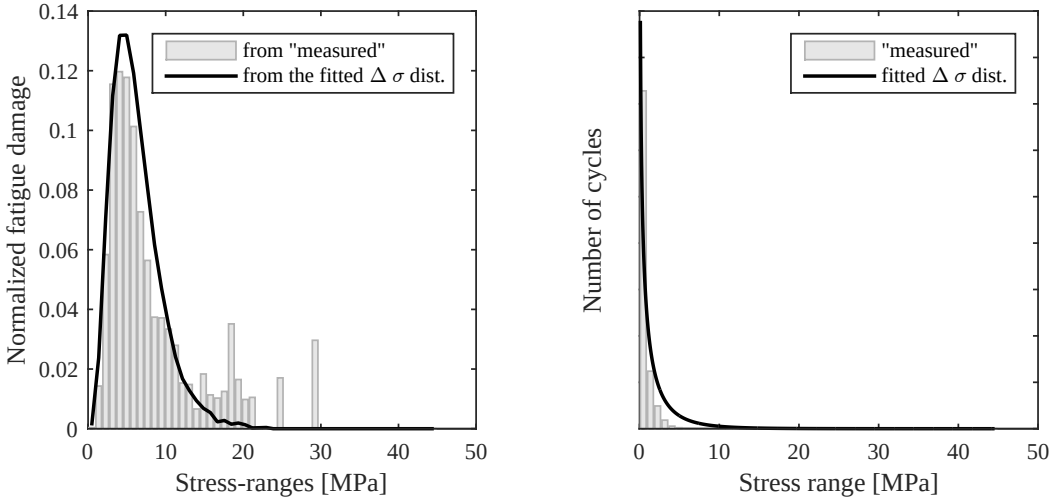

(a) Distribution of fatigue damage **(b)** Distribution of stress-range

Figure 4.8.: Fitting stress-range in wind class [0 to 5 m/s]

Quality of the stress-range fitting: The fitted stress-range distribution is plotted on the histogram of the raw data to see the fitness (Fig. 4.8b to Fig. 4.12b). It can

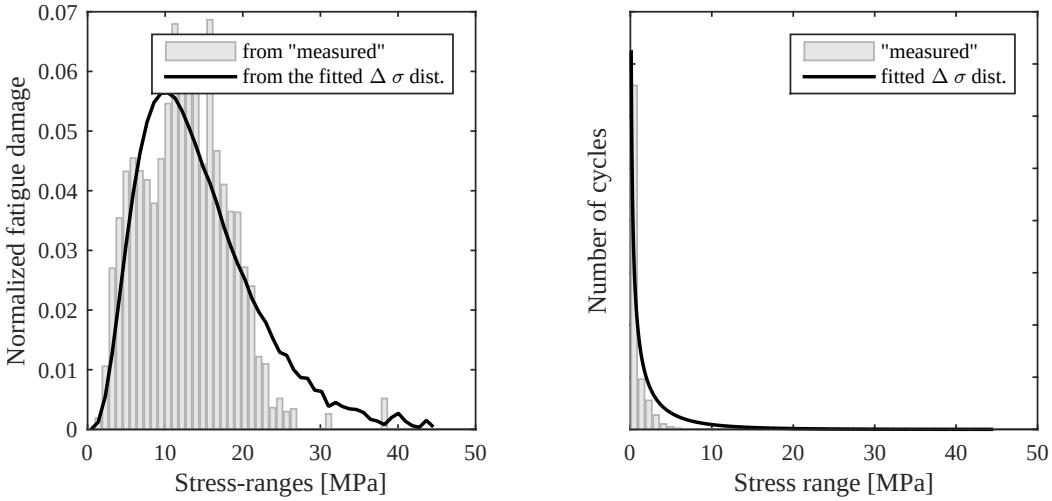

(a) Distribution of fatigue damage **(b)** Distribution of stress-range

Figure 4.9.: Fitting stress-range in wind class [5 to 10 m/s]

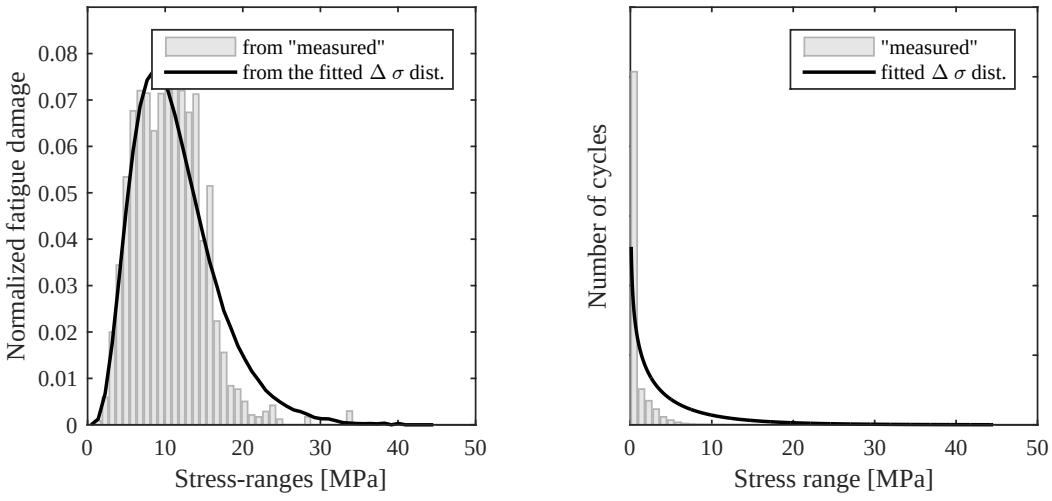

(a) Distribution of fatigue damage **(b)** Distribution of stress-range

Figure 4.10.: Fitting stress-range in wind class [10 to 15 m/s]

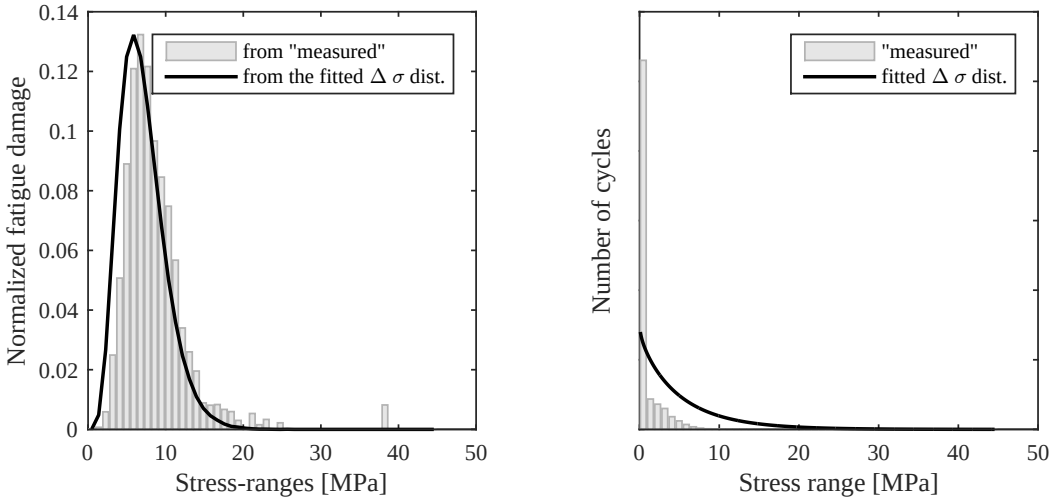

(a) Distribution of fatigue damage **(b)** Distribution of stress-range

Figure 4.11.: Fitting stress-range in wind class [15 to 20 m/s]

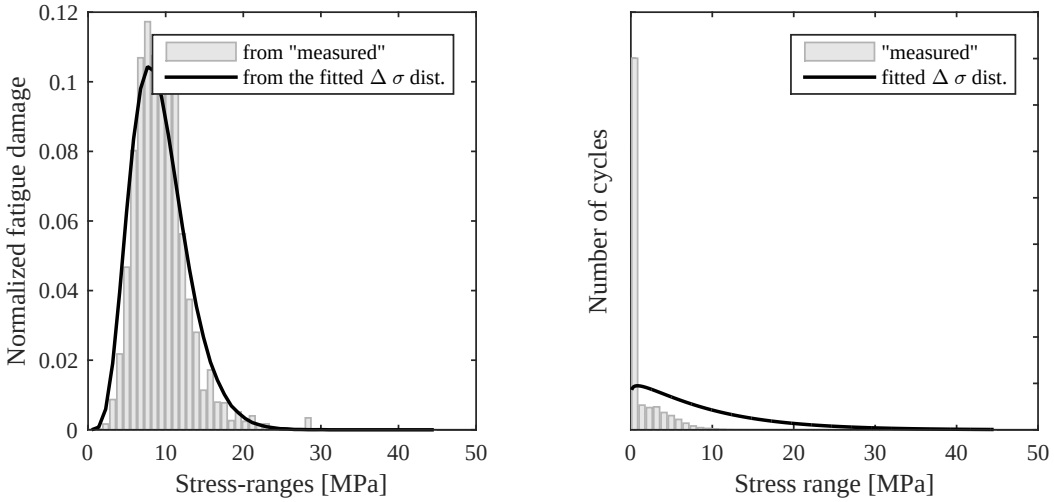

(a) Distribution of fatigue damage **(b)** Distribution of stress-range

Figure 4.12.: Fitting stress-range in wind class [20 to 30 m/s]

U_{10} (m/s)	$0 \div 5$	$5 \div 10$	$10 \div 15$	$15 \div 20$	$20 \div 30$
n_c	4640093	8575900	6418338	3423974	1075344
n_m	8256	13362	9007	4843	1639
p	0.2069	0.3678	0.2656	0.1170	0.0416

Table 4.4.: The input data for damage verification in Eq. (4.29).

be seen that the Weibull distribution is generally not very good for fitting stress-ranges in each bin of wind speed for the given data. However, the integrated fatigue damage for the considered bin is quite accurate since it is the objective of the fitting procedure described in sec. 4.3.2.3. The probability density distribution of stress-ranges is only important if contributions to the accumulated fatigue damage from both slopes of a bilinear SN-curve are important.

4.4.6. Limit State Equation

Since the 10-minute mean wind speed U_{10} is the only parameter used to link oceanographic data to fatigue damage for the application, the limit state function in Eq.(4.10) is simplified as:

$$g(T) = \Delta - \sum_{i=1}^{T} \sum_{j=1}^{n_{U_{10}}} \frac{(\alpha_f X_m X_{SCF})^{m_2}}{K} k_{s,j}^{m_2} \Gamma\left(\frac{m_2}{\lambda_{s,j}} + 1\right) \mathrm{P}\left(U_{10,j} | k_{w,i}\right) \frac{n_{c,j}}{n_{m,j}} n_m^*, \quad (4.30)$$

where

$n_{m,j}$ is number of 10-minute mean wind speed records in the j^{th} bin,

$n_m^* = \sum_{j=1}^{n_{cl}} n_{m,j}$ is number of 10-minute mean wind speed records in the i^{th} year,

$\mathrm{P}\left(U_{10,j} | k_{w,i}\right)$ is probability of 10-minute mean wind speed in the j^{th} bin in the i^{th} year. It can be calculated based on the distribution function in Eq. (4.2). If the lower and upper bound of the j^{th} bin is a_j and b_j, respectively, the value of $P_{ij}(U_{10})$ is calculated as shown in Eq. (4.31). It is noted that in this equation, λ_w is the shape parameter of the design wind speed distribution, k_{wi} is the random variable representing the scale parameter of the wind speed distribution at the i^{th} year.

$$\begin{aligned} \mathrm{P}\left(U_{10,j} | k_{w,i}\right) &= F_W\left(a_j \leq U_{10} < b_j;\ k_{w,i}, \lambda_w\right) \\ &= \exp\left(-\left(\frac{a_j}{k_{w,i}}\right)^{\lambda_w}\right) - \exp\left(-\left(\frac{b_j}{k_{w,i}}\right)^{\lambda_w}\right) \end{aligned} \quad (4.31)$$

4.4.7. Predicting Remaining Fatigue Life

The definition of remaining fatigue life used in this chapter is the time to reach the annual target reliability. It is noted that reliability index and failure probability are interchangeable. For the limit state function defined as in Eq. (4.30), the relationship between the probability of failure and the reliability index is:

$$P_f = P\left(g\left(T\right) \leq 0\right) \approx \Phi\left(\beta\right) \tag{4.32}$$

where β is the reliability index and $\Phi\left(\right)$ is the standard Normal distribution function.

The annual failure probability in year i given survival up to year $(i-1)$ is calculated as:

$$\Delta P_f\left(i\right) = \frac{P_f\left(i\right) - P_f\left(i-1\right)}{1 - P_f\left(i-1\right)} \tag{4.33}$$

As discussed in sec. 2.3, the target safety level for existing structures should be smaller than for the new designs. The recommended approach in current standards and recommendations to find the target safety level is to solve a decision problem based on an optimization of generalized benefits and cost including expected failure costs.

In this chapter, for the purpose of illustration, the target safety level is chosen to be the same as the design requirement. Details about choosing the target annual reliability for a new design can be found in [106]. The predicted remaining life, therefore, is found by using a target annual reliability of 3.3 (or a maximum annual failure probability of 5×10^{-4}).

4.5. Results & Discussion

4.5.1. Effects of the Measured Data and the Load Factor

The measured data may represent a mild or severe period of the loading condition, and in any case, the loading distribution (e.g. the U_{10} distribution) can be updated accordingly. In Fig. 4.13, the scale parameter of the 10-minute mean wind speed distribution is updated using 3 year measurement data. The annual failure probability is updated by considering the new loading distribution as can be seen in Fig. 4.14, implying the predicted remaining life, therefore, is changed because it is

interpolated from the annual failure probability curve using the maximum annual allowable failure probability value, as illustrated in Fig. 4.15.

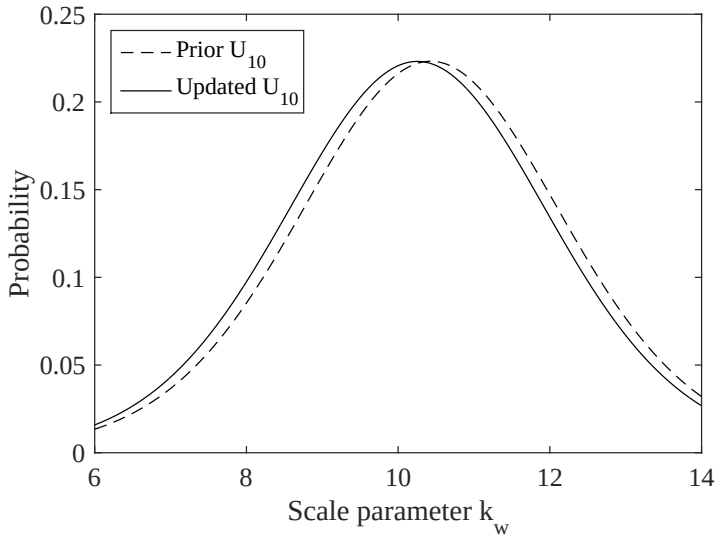

Figure 4.13.: The Student's t-distribution of k_w (the scale parameter of wind speed distribution), before and after updating, considering 3 year measured data of 10-minute mean wind speed U_{10}.

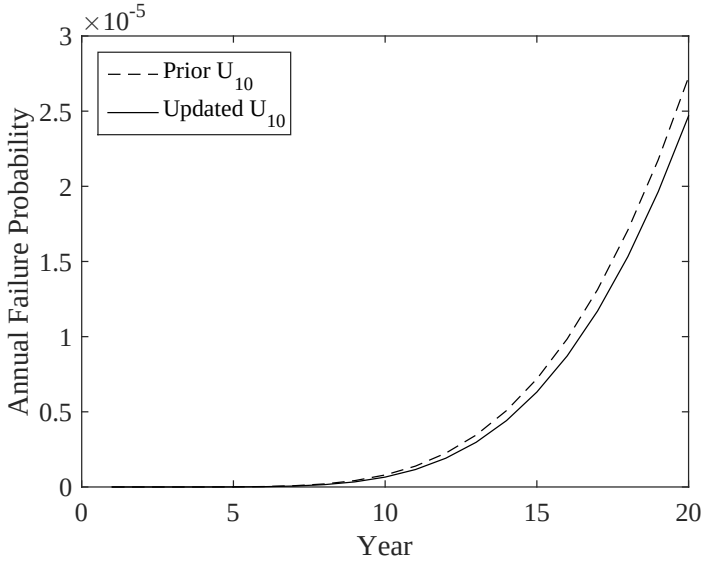

Figure 4.14.: Example of the updated annual failure probability considering 3 year measured data of 10-minute mean wind speed ($\alpha_f = 5$, $CoV_{X_m} = 0.05$, $CoV_{X_{SCF}} = 0.05$, $CoV_{k_s} = 0.1$). The annual updated failure probabilities starts at year 3 assuming that information up to year 3 has been used to update the failure probability.

The load factor may change during the service life because of corrosion or reassessing the SCF. This is especially the case when the measured strain is interpolated

to the interested location under corrosion. According to [107], the stress-range value at the interested location is higher than the interpolated value due to a reduced cross-section caused by corrosion. Hence, it is helpful to see the predicted remaining life in relation with load factors as shown in Fig. 4.16.

For the current application, the predicted remaining life is longer than before updating because the measured loading condition is milder. The magnitude of the difference depends on the duration of time that the mild loading condition lasts.

It can be seen that the predicted remaining fatigue life is very sensitive to the load factor, so great care is needed when calculating SCF as well as stress interpolating factor for corroded locations.

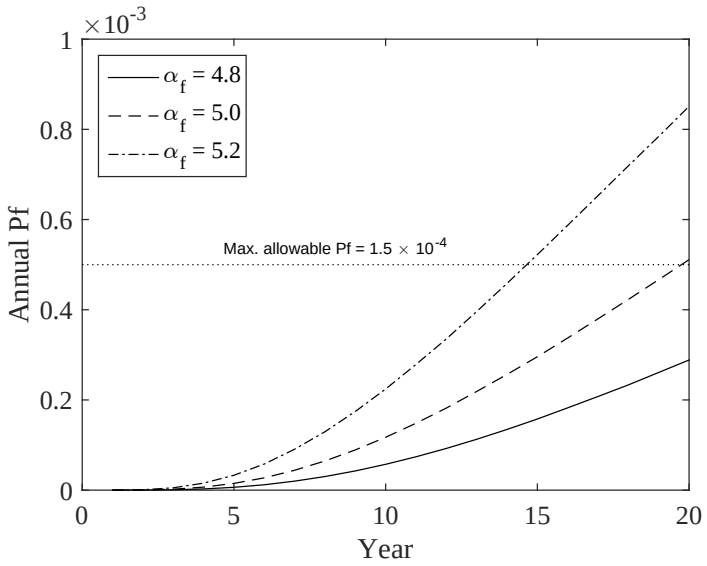

Figure 4.15.: Assessment of remaining fatigue life. Annual P_f curves are drawn with different values of load factor (α_f), given $CoV_{X_m} = 0.05$, $CoV_{X_{SCF}} = 0.15$, and $CoV_{k_s} = 0.1$.

The difference in the remaining fatigue life is not constant, but getting smaller when the load factor becomes larger. This is because the effect of having mild loading condition on the failure probability is less important when load factors are high.

4.5.2. About the Effect of Corrosion

The measures to protect the OWT support structure from corrosion (i.e. cathodic protection, coating) might become inefficient after some years in service, leading to a free corrosion condition for the structure. Because of the corrosive environment,

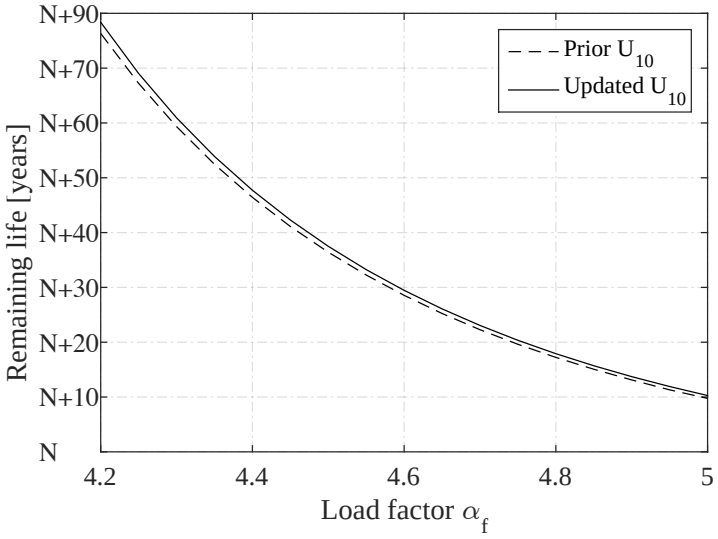

Figure 4.16.: Variation of the remaining fatigue life regarding Load Factor and measured data, given $CoV_{X_m} = 0.05$, $CoV_{X_{SCF}} = 0.15$, and $CoV_{k_s} = 0.1$.

a corresponding S-N curve for free corrosion is suggested, for example, by DNV-GL [100] for the design stage. Nevertheless, more research is needed to model what happens when corrosion starts at a given point in time during operation.

4.5.3. Effect of Wind Measurement Duration

To see the effect of wind measurement duration on the updated remaining fatigue life, more wind data is needed. In this section, it is assumed that six-year wind data is available and the fitted scale parameters of the year 4^{th}, 5^{th}, and 6^{th} equal to the mean value of the three measured years. This is an assumption to assess the future trend of the predicted remaining life, and the results are to be considered conditional on the assumption. The 'measured' vector of k_w becomes:

$$\hat{\mathbf{k}}_w = \begin{bmatrix} 10.005 & 9.993 & 8.176 & 9.391 & 9.391 & 9.391 \end{bmatrix} \text{ (m/s)}$$

The effect of wind measurement duration is shown in Fig. 4.17. This relationship is obtained by assuming that the load factor is $\alpha_f = 4.8$. With this load factor, the remaining fatigue life increases about 0.68 year after updating using the three-year wind data. This increment is not constant but slowly reduced with the increase of measurement duration if the loading condition remains the same as in the three observed years.

The predicted remaining fatigue life depends on the assumptions that are made on

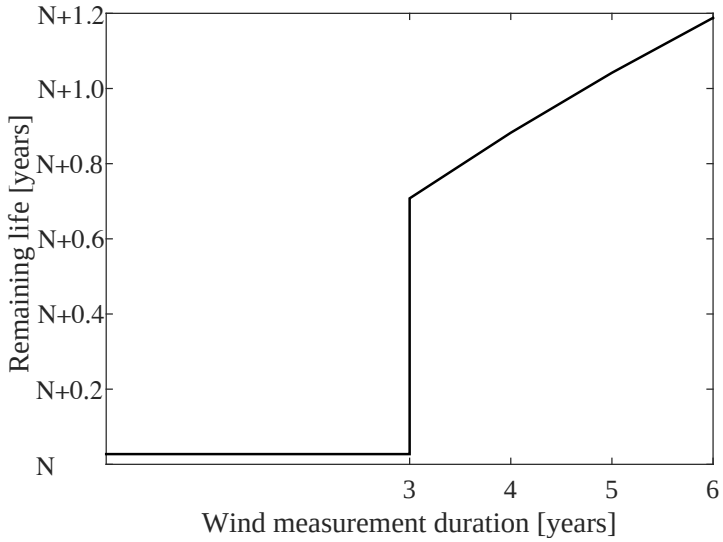

Figure 4.17.: Effects of wind measurement duration. Before 3 years, the curve is estimated using the prior U_{10} distribution. After the 3^{rd} year, the updated distribution of U_{10} is used. Data for the 4^{th}, 5^{th}, and 6^{th}years is assumed to be the mean of the real measured data. $\alpha_f = 4.8$, $CoV_{X_m} = 0.05$, $CoV_{X_{SCF}} = 0.15$, $CoV_{k_s} = 0.1$.

the load factor and its uncertainty. A sensitivity analysis will then be very useful to illustrate the assumptions.

4.5.4. The Importance Factors

As mentioned in sec. 4.3.4, by assessing the importance factor of each random variable, it is possible to justify which random variables can be considered as deterministic and which random variables need to be quantified carefully.

Year-to-year variation is represented by considering the scale parameters of the wind speed distributions ($k_{w,i}$, where $i = 1 \cdots \infty$ denoting the year in service) are uncorrelated random variables. As seen from Fig. 4.18, the year to year variation is important at the beginning of the service life and becomes negligible at the end. This is quite intuitive because the coefficient of variation of the accumulated fatigue damage in the limit state function decreases with time after some years. However, for predicting remaining fatigue life, this uncertainty is important for the first years of operation.

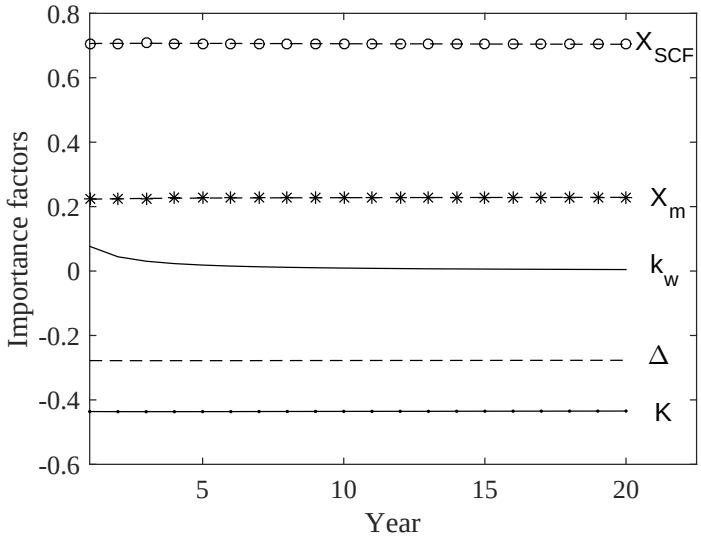

Figure 4.18.: Variations of Importance Factors over years. These curve are obtained with $\alpha_f = 4.8$, $CoV_{X_m} = 0.05$, $CoV_{X_{SCF}} = 0.15$, and $CoV_{k_s} = 0.1$.

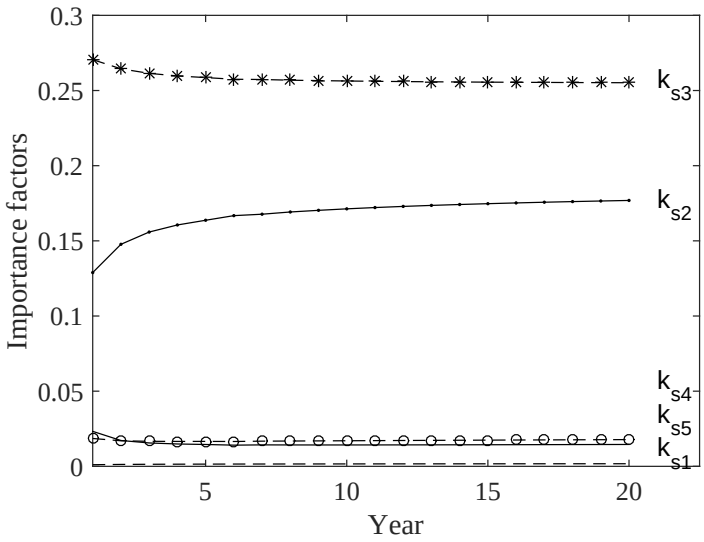

Figure 4.19.: Importance factors of scale parameters k_s of stress-range distributions. These curves are obtained with $\alpha_f = 4.8$, $CoV_{X_m} = 0.05$, $CoV_{X_{SCF}} = 0.15$, and $CoV_{k_s} = 0.1$.

Importance factors of random variables k_s—the scale parameter of the Weibull stress-range distributions—are shown separately in Fig. 4.19. Random variables k_{s1}, k_{s2}, k_{s3}, k_{s4}, k_{s5} are corresponding to wind speeds in the bin $0 \div 5$, $5 \div 10$, $10 \div 15$, $15 \div 20$, and $20 \div 30$ m/s, respectively. The obtained curves reveal the fact that fatigue damage caused by wind speed in the range from 5 to 15 m/s is the most significant.

4.5.5. Sensitivity to Measurement Uncertainty

Variation of measurement uncertainty is quantified by the coefficient of variation (CoV_{X_m}), also known as relative standard deviation. In the interested range of CoV_{X_m}, remaining fatigue life varies non-linearly. In general, for coefficient of variation values smaller than 5%, a change of 1% of CoV_{X_m} results in 1-year difference; for larger CoV_{X_m} the remaining life is reduced 2 years for each 1% increase of CoV_{X_m} (Fig. 4.20).

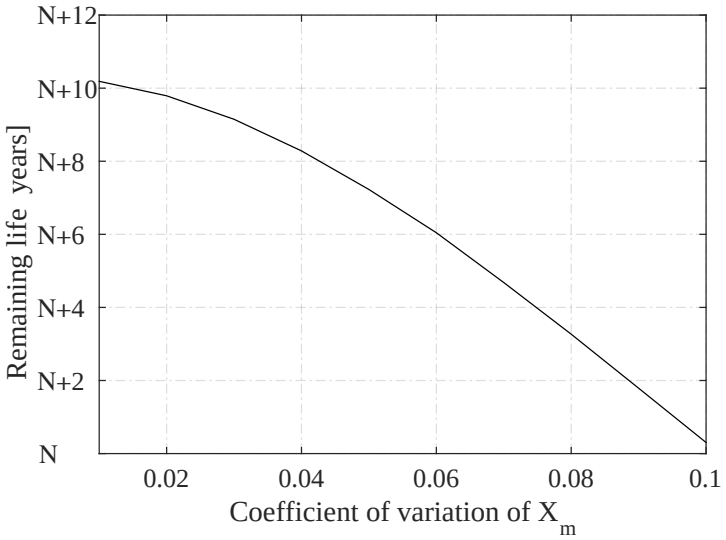

Figure 4.20.: Variation of the remaining fatigue life regarding CoV_{X_m}. The variation is obtained with $\alpha_f = 4.8$, $CoV_{X_{SCF}} = 0.15$, and $CoV_{k_s} = 0.1$.

4.5.6. Sensitivity to SCF Uncertainty

As seen in Fig. 4.21, the uncertainty in stress concentration factor (SCF) and the predicted remaining fatigue life have a linear relationship. Every 1 % reduction of the coefficient of variation of the SCF uncertainty ($CoV_{X_{SCF}}$) leads to an increase of about 3.5 years in the remaining fatigue life.

4.5.7. Sensitivity on the Scale Parameter of Stress-range Distributions

The uncertainty in the scale parameter of stress-range distribution in each bin of wind speed is denoted as k_s. The predicted remaining fatigue life varies with the assumed coefficient of variation of k_s, denoted (CoV_{k_s}), is shown in Fig. 4.22. It can

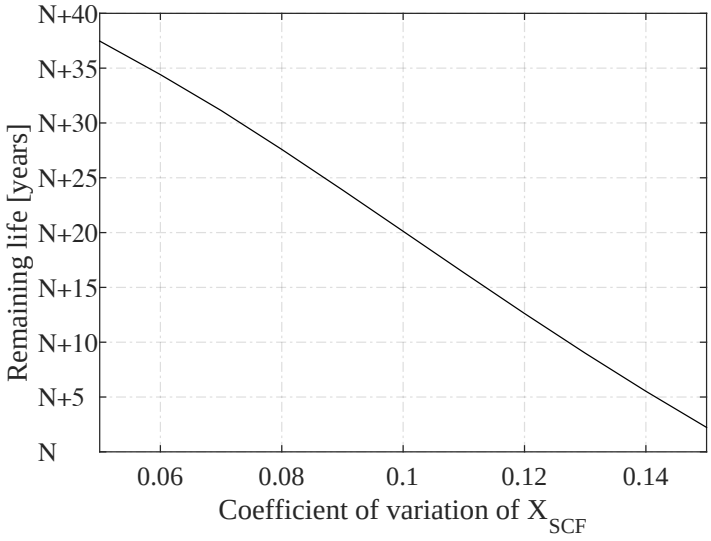

Figure 4.21.: Variation of the remaining fatigue life regarding CoV of X_{SCF}. The curve is obtained with $\alpha_f = 4.8$, $CoV_{X_m} = 0.05$, and $CoV_{k_s} = 0.1$.

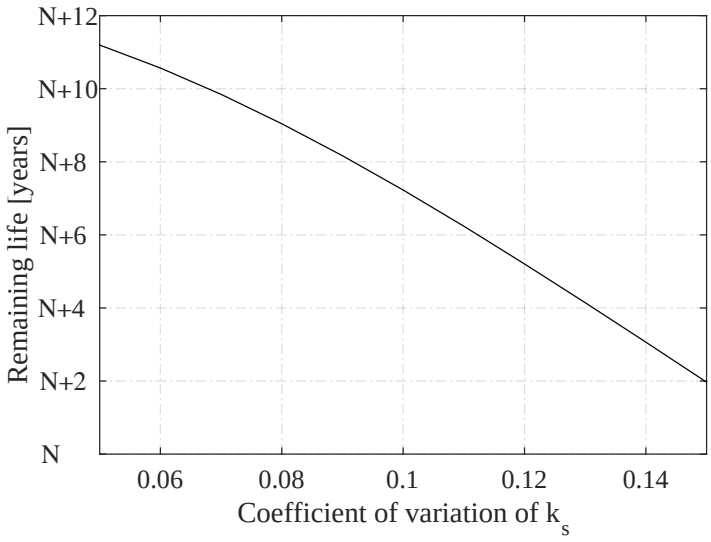

Figure 4.22.: Variation of the remaining fatigue life regarding CoV of k_s. The curve is obtained with $\alpha_f = 4.8$, $CoV_{X_m} = 0.05$, and $CoV_{X_{SCF}} = 0.15$.

be seen that the predicted remaining fatigue life is less sensitive to the uncertainty in the scale parameter (k_s) than the uncertainty in SCF.

4.5.8. About The Effect of Parked Condition

An attempt was made to have more insight into fatigue damage in the downtime of a wind turbine. This can be useful for making operational decisions in harsh

loading condition.

By separating data into 'Power production' and 'Parked' conditions, the mean fatigue damage per 10-minute can be compared (Fig. 4.23). A sudden jump at $U_{10} = 11.3$ (m/s) is due to the fact that there are only two records for this wind speed bin and one of them contains error on strain values.

For wind speed larger than 16.5 (m/s), the 10-minute mean fatigue damage in 'Parked' condition is larger than in the 'Power production' condition. This can be the result of lack of aerodynamic damping when the turbine is idle but can also be the result of high wave loads. Unfortunately, more data on 'Parked' condition is needed for each combination of wave height and wave period to observe the effect of 'Parked' condition to fatigue damage.

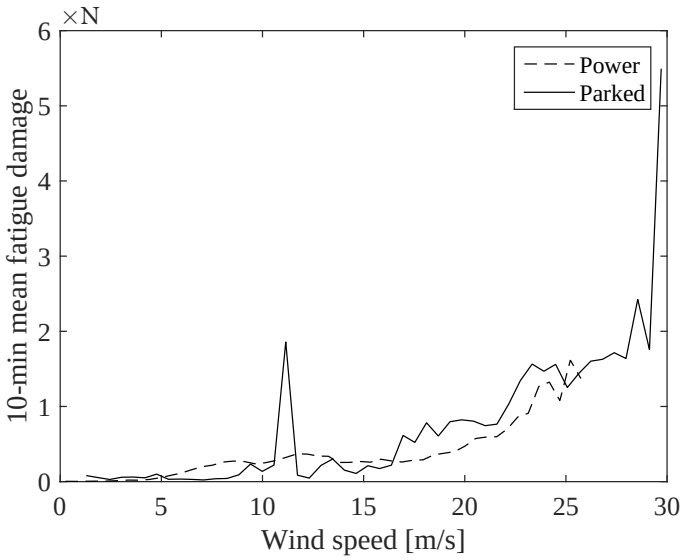

Figure 4.23.: Comparison of mean fatigue damage per 10 minutes in 'Power production' and 'Parked' conditions.

4.6. Conclusion

The proposed methodology works well in combining measured strain with oceanographic data to stochastically predict the remaining fatigue life of OWT support structures. The main influence on the remaining fatigue life comes from the magnitude of stress-ranges at the hot-spot. So the SCF, the interpolating factor (for stresses at under water locations, for example), the correction factor for corrosion effects (if any), and their uncertainties should be estimated with great care.

The measured oceanographic data have a significant effect in adjusting the predicted probability of failure and eventually the remaining fatigue life. The duration of strain measurement should be long enough to be combined with oceanographic data. The longer strain measurement duration, the greater number of parameters in the oceanographic data can be considered for the failure probability updating.

The value of the predicted remaining fatigue life obtained from the present methodology can be useful for decision making to down-rate, curtail, or to extend the lifetime of the wind turbine support structures.

The updated failure probability considering real loading conditions and structural responses can be further used with risk-based inspection planning to minimize the levelized cost of energy of offshore wind farms.

4.7. Perspectives

Critical fatigue locations are normally expected to be near the sea bed, where maximum stress and corrosion occurs. Nevertheless, strain gauges are hard to install under-water, and corrosion inspections are costly and not easy to do in deep water. Predicting fatigue failure of those locations therefore becomes valuable. To apply the present methodology for under-water locations, a proper structural identification method is needed for each type of support structure.

A sudden, unrealistic change in the annual reliability curve might be obtained if the SN-curve in corrosive environment is used at the year when corrosion is detected. So a proper fatigue model is needed to consider corrosion.

Chapter 5.

Conclusion

5.1. General

In this thesis, updating failure probability of a welded joint in existing OWT support structures considering new information is studied. Depending on the nature of the collected information and the updating purpose, different approaches to update failure probabilities can be used. In chapter 3, the reliability of the joint is updated considering crack inspection events, and in chapter 4, it is updated through a random variable. Using well-known techniques in reliability analyses, this thesis humbly tackles the issues of the failure criteria and how to incorporate monitoring data into reliability assessments.

Updating failure probability considering crack inspection data is studied in chapter 3. In this chapter, new information comes from the crack inspection results (no detection or detected) and possible interventions (repair or not, repair quality). The new information is used directly to update failure probability of the considered welded joint.

Failure probabilities are calculated using the Fracture Assessment Diagram (FAD) and then compared with those obtained from the conventional limit state function (LSF), i.e. the critical crack size. The simulation-based approach is used to calculate and update the failure probability. The reason for choosing this simulation-based approach is that it allows to simulate simultaneously crack depth and length, to consider the effects of these crack dimensions in the reference stress of the FAD, and to integrate easily the intervention actions and crack inspection results into crack samples. The crack propagations are calculated using a bi-linear Paris' law with stress-range value varying over time. Uncertainties come from the

crack growth parameter (C), initial crack sizes, fracture toughness, yield and ultimate strengths, FAD formula, stress intensity factor, stress-range values, and the detectable crack size.

The results show that by integrating fracture toughness into failure criteria, the estimated failure probability of the welded joint is significantly increased in comparison to the case where only the critical crack size is considered in the LSF. In comparison with a failure criteria that includes both the critical crack size and fracture toughness, the FAD approach gives similar reliability results when the applied peak tensile stress is small.

The estimated failure probability increases when fracture toughness decreases. This trend is consistent in both FAD and the traditional approach. However, when the applied peak tensile stress is high—the ratio between the applied peak tensile stress and the yield strength is more than 65%—the FAD approach predicts a higher failure probability. In this case, it is clear that the FAD approach is more conservative.

The FAD uncertainty does not affect significantly the failure probability of the joint as compared to the uncertainties in the ultimate and yield strength. This is because the latter affects directly the cut-off location of the FAD curve where the plastic failure is defined. So the FAD uncertainty can be neglected in using FAD failure criteria, but variances of ultimate and yield strengths of the material are decisive.

The FAD approach can be used to update failure probability considering crack inspections and intervention actions. The calculation shows that reliability of the welded joint increases when no crack is detected, or when a crack is detected and repaired. In comparison with a perfect repair, an imperfect repair assumption reduces significantly reliability of the joint.

Updating failure probability can also be done through basic random variables in the LSF, as shown in chapter 4. Instead of updating a random variable considering crack inspections, the characteristics of its distribution are updated using monitoring data. The updated random variable is then used in a reliability analysis to obtain the updated failure probability. The LSF is based on the Miner's rule and solved using the first order reliability method (FORM). A multivariate random variable whose components are 10-minute mean wind speed, significant wave height, and wave period is used to update failure probability.

Fatigue damage is summed up from all load combinations, i.e. from all the dis-

cretized components of the joint distribution of the multivariate random variable (wind and wave). The measured strain data is used to calculate fatigue damage in each load combination. The probability of each load combination is calculated using the joint distribution which, in turn, can be updated using monitoring data.

The 10-minute mean wind speed is assumed to follow a Weibull distribution and can be updated using Bayesian approach. Assuming that the scale Weibull's parameter is a normally distributed random variable with unknown mean and standard deviation, the predictive distribution of this random variable becomes a student's t-distribution.

The proposed methodology has been applied to a monopile support structure in a wind farm in Belgium. The measured strain is used to find the potential hot-spot location. Stresses are derived at the hot-spot location for fatigue analyses. It is assumed that stress-ranges of each load combination follow a Weibull distribution. The stress-range distribution parameters are found by performing least squares fitting method on the fatigue damage.

The results show that the Weibull distribution is generally not very good for fitting stress-ranges in each wind-speed bin using the considered data. However, the integrated fatigue damage for the considered load combination is quite accurate since it is the objective of the fitting procedure.

The main governing parameter on the remaining fatigue life is the magnitude of stress-ranges at the hot-spot. So the stress concentration factor, the interpolating factor (for example to obtain stresses at under water locations), the correction factor for corrosion effects (if any), and their uncertainties should be estimated with great care.

The measured oceanographic data have a significant effect in adjusting the predicted probability of failure and eventually the remaining fatigue life. The duration of strain measurement should be long enough to be combined with oceanographic data. Longer strain measurement duration, greater number of parameters in the oceanographic data can be considered for the failure probability updating.

It can be concluded that the research targets are sucessfully achieved. Updating failure probability of a welded joint is done considering crack inspections and intervention actions. Oceanographic data and measured strain can be used together to update failure probabilities. If they are measured simultaneously for at least one or few years, oceanographic data can also be used alone to update failure probability of the joint in the following years.

5.2. Practical Implications

- ◇ The failure probability results are higher when fracture toughness is included in the LSF, implying it is an important variable to be included in the failure criteria (to be conservative). Indeed, the fracture toughness has no effect if the fracture mechanics model is calibrated to the SN model for predicting inspection plans at the design stage, but it is crucial for updating reliability of existing structure and life extension purposes.
- ◇ The peak tensile stress affects the safety state of any crack size, so the time when a high peak tensile stress occurs is important. Therefore, in real applications, it should be modelled by a stochastic process.
- ◇ FAD approach predicts higher failure probability values when the applied peak tensile stress is larger than 65% the yield strength, in comparison to the traditional approach. This means the use of FAD should be recommended for reliability assessment of existing OWT support structures with high peak tensile stress. Therefore the risk-based inspection plan might proposes a shorter inspection interval for those cases.
- ◇ When FAD approach is utilized, the uncertainties in yield and ultimate strengths are important because they define the region of plastic collapse. Information about these material properties should therefore be investigated to improve the reliability of the structure.
- ◇ It is always better for the reliability of the structure to have more information about cracks and also corrosion states, provided that necessary intervention actions are done. The present work concentrated on using available inspection outcomes and intervention actions to update failure probability of existing structures. The proposed methodology can be further applied in a decision problem to justify the necessity of investing on inspections and possible repair actions.
- ◇ A normal repair leads to a smaller reliability than a perfect repair. So a normal repair should be considered in the decision tree for a conservative inspection plan.
- ◇ In updating reliability using monitoring data, the impact of the year-to-year variation of the annual mean wind speed becomes neglectible after 4 years. This means it can be ignored in the LSF. This can reduce significantly calculation time and give a chance to consider a finer discretized load combination.

- ◇ The value of the predicted remaining fatigue life obtained from the present methodology can be useful for decision making to down-rate, curtail, or extend the lifetime of the wind turbine support structures.
- ◇ In this thesis, the method to link oceanographic data to fatigue damage is based on the mean fatigue damage per cycle in each discretized load combination. So the accuracy of the fatigue damage solution depends largely on number of stress cycles in each load combination. To decide how many load combination to discretize, a sensitivity analysis is needed for each specific problem.

5.3. Main Outcomes

- ◇ The critical crack size criterion is not always conservative for reliability assessment of welded joints. It should be combined with fracture toughness criterion for the reliability assessment of existing structures to consider the effects of peak tensile stress.
- ◇ When peak tensile stress in the structure is larger than 65% the yield strength, the FAD should be used for reliability assessment. This threshold is found with a degree of bending (DOB) of 0.5 and specific parameters of the FAD curve (i.e. fracture toughness, yield strength).
- ◇ A procedure to consider FAD in reliability updating using simulation-based approach is proposed.
- ◇ A methodology to fit stress-range distribution for the case where the stress-range histogram is distorted by a large number of cycles of small stress-ranges.
- ◇ A methodology to consider monitoring data into reliability updating of a welded joint is proposed.

5.4. Future Works

- ◇ The updated failure probability considering real loading conditions and structural responses can be further studied with risk-based inspection planning to minimize the levelized cost of energy of offshore wind farms.
- ◇ The measures to protect the OWT support structure from corrosion (i.e. cathodic protection, coating) might become inefficient after some years in

service, leading to a free corrosion condition for the structure. To update the failure probability considering corrosion information, more research is needed to model what happens when corrosion starts at a given point (in time) during operation.

- ◇ Measurement uncertainty of strain data obtained from optic fiber sensors should be quantified.
- ◇ Strain gauges are hard to install under-water, and corrosion inspections are costly and not easy to do in deep water. Therefore, predicting fatigue failure of those locations becomes valuable. To apply the present methodology (Chapter 4) for under-water locations, a proper calibrated finite element model is needed to derive strain from measuring location.
- ◇ Quantifying uncertainty of load extrapolation methods, i.e. assessing the uncertainty of the stress-range of welded joints that are not monitored.
- ◇ A method combining monitoring data with crack inspection data should be considered for optimizing inspection plans and life extension of existing structures.

Bibliography

[1] GL Garrad Hassan, A guide to uk offshore wind operations and maintenance, Scottish Enterprise and The Crown Estate (2013) 21.

[2] A. A. Cornell, Some thoughts on maximum probable loads and structural safety insurance, Memorandum to Members of ASCE Structural Safety Committee, Massachusetts Institute of Technology.

[3] O. Ditlevsen, Structural reliability and the invariance problem, University of Waterloo, Solid Mechanics Division, 1973.

[4] L. I. N. D. NIELS C, The design of structural design norms, Journal of Structural Mechanics 1 (3) (1972) 357–370.

[5] A. M. Hasofer, N. C. Lind, Exact and invariant second-moment code format, Journal of the Engineering Mechanics division 100 (1) (1974) 111–121.

[6] A. Harbitz, Efficient and accurate probability of failure calculation by use of the importance sampling technique, 1983, pp. 825–836.

[7] M. Shinozuka, Basic analysis of structural safety, Journal of Structural Engineering 109 (3) (1983) 721–740.

[8] S. Engelund, R. Rackwitz, A benchmark study on importance sampling techniques in structural reliability, Structural safety 12 (4) (1993) 255–276.

[9] R. Rackwitz, Reliability analysis–a review and some perspectives, Structural safety 23 (4) (2001) 365–395.

[10] C. Bucher, T. Most, A comparison of approximate response functions in structural reliability analysis, Probabilistic Engineering Mechanics 23 (2-3) (2008) 154–163.

[11] R. H. Myer, D. C. Montgomery, Response surface methodology: process and product optimization using designed experiment, John Wiley and Sons, New York.

[12] S. Reh, J.-D. Beley, S. Mukherjee, E. H. Khor, Probabilistic finite element analysis using ansys, Structural safety 28 (1-2) (2006) 17–43.

[13] M. Kleiber, J. Knabel, J. Rojek, Response surface method for probabilistic assessment of metal forming failures, International journal for numerical methods in engineering 60 (1) (2004) 51–67.

[14] S. Thöns, M. H. Faber, W. Rücker, Support structure reliability of offshore wind turbines utilizing an adaptive response surface method, American Society of Mechanical Engineers, 2010, pp. 407–416.

[15] C. Bucher, Asymptotic sampling for high-dimensional reliability analysis, Probabilistic Engineering Mechanics 24 (4) (2009) 504–510.

[16] A. Naess, B. J. Leira, O. Batsevych, System reliability analysis by enhanced monte carlo simulation, Structural safety 31 (5) (2009) 349–355.

[17] S. O. Rice, Mathematical analysis of random noise, Bell Labs Technical Journal 23 (3) (1944) 282–332.

[18] E. H. Vanmarcke, On the distribution of the first-passage time for normal stationary random processes, J. of applied Mech. (1975) 215–220.

[19] H. Cramér, M. R. Leadbetter, Stationary and related stochastic processes: Sample function properties and their applications, Courier Corporation, 2013.

[20] O. Ditlevsen, P. Bjerager, Methods of structural systems reliability, Structural Safety 3 (3-4) (1986) 195–229.

[21] R. E. Melchers, A. T. Beck, Structural reliability analysis and prediction, John Wiley & Sons, 2018.

[22] ISO, 19902: 2008-07: Petroleum and natural gas industries-fixed steel offshore structures (iso 19902: 2007), English version EN ISO 19902 (2007) 182–202.

[23] API, Recommended practice for planning, designing and constructing fixed offshore platforms-working stress design, Vol. 21, American Petroleum Institute, 2000.

[24] API RP 2SIM, Structural integrity management of fixed offshore structures, American Petroleum Institute (2014).

[25] M. Faber, Reliability based assessment of existing structures, Progress in Structural Engineering and Materials 2 (2) (2000) 247–253.

[26] Joint Committe on Structural Safety (JCSS), Probabilistic Assessment of Existing Structures, RILEM Publications S.A.R.L., 2001.

[27] G. Ersdal, Assessment of existing offshore structures for life extension, Department of Mechanical and Structural Engineering and Material Sciences, University of Stavanger, Norway.

[28] S. Th ons, Monitoring based condition assessment of offshore wind turbine support structures, IBK Bericht 345.

[29] M. Sykora, D. Diamantidis, M. Holicky, K. Jung, Target reliability for existing structures considering economic and societal aspects, Structure and Infrastructure Engineering 13 (1) (2017) 181–194.

[30] R. G. Bea, Reliability-based requalification criteria for offshore platforms, Vol. 2, ASME, 1993, pp. 351–361.

[31] W. D. Iwan, C. C. Thiel, G. W. Housner, C. A. Cornell, A reliability-based approach to seismic reassessment of offshore platforms, 1993.

[32] D. Diamantidis, P. Bazzurro, Safety acceptance criteria for existing structures, 2007, pp. 26–27.

[33] T. Vrouwenvelder, N. Scholten, Assessment criteria for existing structures, Structural Engineering International 20 (1) (2010) 62–65.

[34] E. Rosenblueth, E. Mendoza, Reliability optimization in isostatic structures, Journal of the Engineering Mechanics Division 97 (6) (1971) 1625–1642.

[35] A. M. Hasofer, R. Rackwitz, Time-dependent models for code optimization, Vol. 99, 2000, pp. 151–158.

[36] ISO 13822:2010, Bases for design of structures: assessment of existing structures (2010).

[37] M. H. Faber, J. D. Sørensen, J. Tychsen, D. Straub, Field Implementation of RBI for Jacket Structures, Journal of Offshore Mechanics and Arctic Engineering 127 (3) (2005) 220.

[38] EN 1990: 2002, Eurocode-basis of structural design (2002).

[39] IEC 16400-1 ed4., FDIS, 2018, Wind turbines part 1: Design requirements (2018).

[40] DNV-GL, Recommended practice rp-c210: Probabilistic methods for planning of inspection for fatigue cracks in offshore structures. (2015).

[41] BSI Standards Publication, BS 7910:2015 Guide to methods for assessing the acceptability of flaws in metallic structures (1).

[42] H. O. Madsen, Model updating in reliability theory, Vol. 5, 1987, pp. 564–577.

[43] G. Jiao, T. Moan, Methods of reliability model updating through additional events, Structural Safety 9 (2) (1990) 139–153.

[44] Z. Zhao, A. Haldar, F. L. Breen Jr, Fatigue-reliability updating through inspections of steel bridges, Journal of Structural Engineering 120 (5) (1994) 1624–1642.

[45] H. O. Madsen, J. D. Sørensen, R. Olesen, Optimal inspection planning for fatigue damage of offshore structures, American Society of Civil Engineers, 1990, pp. 2099–2106.

[46] H. O. Madsen, Stochastic modeling of fatigue crack growth and inspection, Springer, 1997, pp. 59–83.

[47] T. D. Righiniotis, Influence of management actions on fatigue reliability of a welded joint, International Journal of Fatigue 26 (2004) 231–239.

[48] T. Anderson, Fracture Mechanics: Fundamentals and Applications, 2004.

[49] T. D. Righiniotis, M. K. Chryssanthopoulos, Fatigue and fracture simulation of welded bridge details through a bi-linear crack growth law.

[50] W. Weijtens, N. Noppe, T. Verbelen, A. Iliopoulos, C. Devriendt, Offshore wind turbine foundation monitoring, extrapolating fatigue measurements from fleet leaders to the entire wind farm, in: Journal of Physics: Conference Series, Vol. 753, IOP Publishing, 2016, p. 092018.

[51] JCSS, Probabilitic Model Codes: Part 3 Resistance Models (2011).

[52] B. Yeter, Y. Garbatov, C. G. Soares, Fatigue Reliability of an Offshore Wind Turbine Supporting Structure Accounting for Inspection and Repair, in: G. Soares, Shenoi" (Eds.), *Analysis and Design of Marine Structures*, Taylor & Francis Group, London, 2015, pp. 737–747.

[53] S. Webster, A. Bannister, Structural integrity assessment procedure for Europe of the SINTAP programme overview, Engineering Fracture Mechanics 67 (6) (2000) 481–514.

[54] I. Milne, K. Avenue, S. Kt, R. a. Ainsworth, a. R. Dowling, a. T. Stewart, Background to and Validation of CEGB Report R / H / R 6 Revision 3 32 (1988) 105–196.

[55] A. E1049-85, Standard practices for cycle counting in fatigue analysis (1997).

[56] P. Paris, F. Erdogan, A critical analysis of crack propagation laws, Journal of Basic Engineering 85 (1963) 528.

[57] DNV-GL, Recommended Practice RP-0001: Probabilistic methods for planning of inspection for fatigue cracks in offshore structures (2015).

[58] A. Hobbacher, Recomendations for Fatigue Design of Welded Joints and Components, Tech. Rep. IIW document IIW-1823-07 ex XIII-2151r4-07/XV-1254r4-07, International Institute of Welding (IIW) (2008).

[59] Aker Offshore Partner A.S, Target Levels for Reliability-based Assessment of Offshore Structures During Design and Operation, Tech. Rep. 1999/060, Health & Safety Executive (HSE) (1999).

[60] E. H. Niccolls, A correlation for fatigue crack growth rate, Scripta Metallurgica 10 (4) (1976) 295–298.

[61] P. E. Irving, L. N. Mccartney, Prediction of fatigue crack growth rates: theory, mechanisms, and experimental results, Metal Science 11 (8-9) (1977) 351–361.

[62] V. Radhakrishnan, Quantifying the parameters in fatigue crack propagation, Engineering Fracture Mechanics 13 (1) (1980) 129–141.

[63] T. Lassen, Experimental investigation and stochastic modelling of the fatigue behaviour of welded steel joints, Thesis, Department of Building Technology and Structural Engineering (1997).

[64] A. Almar-Næss, Fatigue handbook: offshore steel structures, Akademika Publishing, 1985.

[65] DNV, Guideline for Offshore Structural Reliability Analysis: Application to Jacket Platforms, Tech. rep. (1996).

[66] Det Norske Veritas, DNV-OS-J101 Offshore Standard: Design of Offshore Wind Turbine Structures (2014).

[67] T. R. Gurney, An analysis of some recent fatigue crack propagation data for steels subjected to pulsating tension loading, Report 1978E, UK: The Welding Institute TWI.

[68] D. Straub, Generic approaches to risk based inspection planning for steel structures, Thesis (2004).

[69] M. H. Faber, S. Engelund, J. D. Sørensen, A. Bloch, Simplified and generic risk based inspection planning, Simplified and Generic Risk Based Inspection Planning.

[70] J. Newman Jr, I. Raju, An empirical stress-intensity factor equation for the surface crack, Engineering Fracture Mechanics 15 (1) (1981) 185–192.

[71] I. Kountouris, M. Baker, Reliability of Non-destructive Examination of Welded Joints, Imperial College of Science and Technology Engineering Structures Laboratories, 1989.

[72] A. Muhammed, H. G. Pisarski, R. M. Sanderson, Calibration Of Probability Of Failure Estimates Made From Probabilistic Fracture Mechanics Analysis, Tech. rep., Health & Safety Executive (HSE) (2002).

[73] British Energy, R6: Assessment of the Integrity of Structures Containing Defects, revision 4 Edition, British Energy Generation Ltd., Gloucester, 2001.

[74] P. Dillstrom, Probabilistic Safety Evaluation-Development of Procedures with Applications on Components Used in Nuclear Power Plants, SKi Report 00.

[75] F. Burdekin, W. Hamour, SINTAP, Contribution to Task 3.5, Safety Factors and Risk, UMIST, 25p.

[76] K. Wallin, Probabilistisk sakerhetsvardering PROPSE-Materialparametrar, Rapport VALC444, VTT Tillverkningsteknik (1998) 22.

[77] A. S. M. Handbook, Fatigue and fracture, Vol. 19, 1996.

[78] R. G. Forman, V. Shivakumar, J. C. Newman Jr, Fatigue-crack-growth computer program, Tech. rep. (1991).

[79] K. Wallin, The master curve method: a new concept for brittle fracture, International Journal of Materials and Product ....

[80] F. Burdekin, W. Hamour, Partial safety factors for the SINTAP procedure, Offshore technology report.

[81] N. V. Challenger, R. Phaal, S. J. Garwood, Fracture mechanics assessment of industrial pressure vessel failures, International Journal of Pressure Vessels and Piping 61 (2-3) (1995) 433–456.

[82] F. A. Simonen, Nondestructive Examination Reliability, in: C. R. Sundarajan (Ed.), *Probabilistic Structural Mechanics Handbook*, Springer, 1995, pp. 238–260.

[83] R. Skjong, E. Bitner-Gregersen, E. Cramer, A. Croker, Ø. Hagen, G. Korneliussen, S. Lacasse, I. Lotsberg, F. Nadim, K. O. Ronold, Guidelines for offshore structural reliability analysis-general, Tech. rep., Det Norske Veritas (1995).

[84] T. Moan, O. Vårdal, In-service Observations of Cracks in North Sea Jackets. A Study on Initial Crack Depth and POD Values, in: *Proceeding on*

16th OMAE conference, Yokohama, Japan., American Society of Mechanical Engineers (ASME), 1997, pp. 189–198.

[85] J. Goyet, D. Straub, M. H. Faber, Risk-based inspection planning of offshore installations, Structural Engineering International: Journal of the International Association for Bridge and Structural Engineering (IABSE) 12 (3) (2002) 200–208.

[86] D. Straub, Reliability updating with equality information, Probabilistic Engineering Mechanics 26 (2011) 254–258.

[87] H. O. Madsen, J. D. Sørensen, Probability-based optimization of fatigue design, inspection and maintenance, Integrity of Offshore Structures, Volume 4 (1990) 421–432.

[88] K. Maes, A. Iliopoulos, W. Weijtjens, C. Devriendt, G. Lombaert, Dynamic strain estimation for fatigue assessment of an offshore monopile wind turbine using filtering and modal expansion algorithms, Mechanical Systems and Signal Processing 76-77 (2016) 592–611.

[89] S. Thöns, Monitoring Based Condition Assessment of Offshore Wind Turbine Support Structures, Ph.D. thesis, ETH Zurich (2012).

[90] D. Straub, Value of information analysis with structural reliability methods, Structural Safety 49 (2014) 75–85.

[91] S. Thöns, R. Schneider, M. H. Faber, Quantification of the Value of Structural Health Monitoring Information for Fatigue Deteriorating Structural Systems.

[92] B. P. Alduse, S. Jung, O. A. Vanli, S.-D. Kwon, Effect of uncertainties in wind speed and direction on the fatigue damage of long-span bridges, Engineering Structures 100 (2015) 468–478.

[93] H. Karadeniz, Uncertainty modeling in the fatigue reliability calculation of offshore structures, Reliability Engineering & System Safety 74 (3) (2001) 323–335.

[94] S. Ambühl, J. P. Kofoed, J. D. Sørensen, Determination of Wave Model Uncertainties used for Probabilistic Reliability Assessments of Wave Energy Devices Definition of Wave States Quantification of Uncertainties 3 (2) (2014) 508–515.

[95] K. Johannessen, T. S. Meling, S. Haver, Joint distribution for wind and waves in the Northern North Sea, International Journal of Offshore and Polar Engineering 12 (1) (2002) 1–8.

[96] P. H. Wirsching, a. M. Shehata, Fatigue Under Wide Band Random Stresses Using the Rain-Flow Method, Journal of Engineering Materials and Technology 99 (3) (1977) 205–211.

[97] M. Miner, Cumulative fatigue damage, Journal of applied mechanics (1945) A159–A164.

[98] N. E. Dowling, Fatigue failure predictions for complicated stress-strain histories, Report, DTIC Document (1971).

[99] P. H. Wirsching, Fatigue reliability for offshore structures, Journal of Structural Engineering 110 (10) (1984) 2340–2356.

[100] DNVGL, Recommended Practice RP-C203: Fatigue design of offshore steel structures (2014).

[101] S. Thöns, R. Schneider, M. H. Faber, Quantification of the value of structural health monitoring information for fatigue deteriorating structural systems, 12th International Conference on Applications of Statistics and Probability in Civil Engineering (ICASP12) (2015) 1–8.

[102] J. D. Sørensen, Reliability-based Calibration of Fatigue Safety Factors For Offshore Wind Turbines, International Society of Offshore and Polar Engineers.

[103] R. Folsø, S. Otto, G. Parmentier, Reliability-based calibration of fatigue design guidelines for ship structures, Marine Structures 15 (6) (2002) 627–651.

[104] H. O. Madsen, S. Krenk, N. C. Lind, Methods of structural safety, Courier Dover Publications, 2006.

[105] RCP GmbH, Statrel: Users Manual - Statistical Analysis of Data for Reliability Applications, Munich, Germany, 2007.

[106] J. D. Sørensen, H. S. Toft, Background document IEC 61400-1 ed.4: Safety Factors, Vol. 0066, 2014.

[107] T. Moan, E. Ayala-Uraga, Reliability-based assessment of deteriorating ship structures operating in multiple sea loading climates, Reliability Engineering & System Safety 93 (3) (2008) 433–446.

Appendix A.

Data Cleaning for Rain-flow Counting

A.1. Overview

A high resolution monitoring system is valuable to capture accurately the structural responses. However, redundant and duplicated measured strain values in the collected data may lead to a underestimated number of cycles of large stress-ranges. This section shows the procedure to clean the data and then applies it on a real piece of measured strain data to see the efffect of cleaning.

A.2. Cleaning Procedure

The rain-flow counting procedure described in [55] is applied only for peaks and troughs on the stress time series. Cleaning the redundant and duplicated points is therefore necessary. The following procedure is applied to a set of three consecutive points in the time series.

A.2.1. Check the Extreme

Strain value at time 2 is the extreme when:

$$\Delta\sigma_{1-2} \times \Delta\sigma_{2-3} \leq 0$$

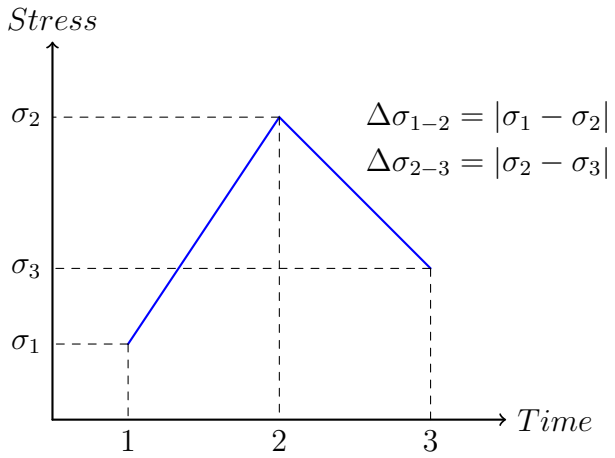

Figure A.1.: Three arbitrary stress values in the time series

A.2.2. Delete Replication

Triple replication when:

$$\begin{cases} \Delta\sigma_{1-2} & = 0 \\ \Delta\sigma_{2-3} & = 0 \end{cases}$$

Double replication when:

$$\Delta\sigma_{1-2} = 0$$

A.2.3. Check the Extreme Again

After deleting duplication, the extreme checking as in **??** should be done again to delete any remaining redundancy.

A.3. Effect of Cleaning

The effect of cleaning is shown in Tab. A.1 for a 10-minute measured strain record. It is clear that without data cleaning, number of cycles of large stress-ranges is very small, and most of the counted cycles are for unimportant stress-ranges.

	Original	Cleaned
No. of points	7500	2121
Max. strain range [$\mu\varepsilon$]	43.73	83.43
Min. strain range [$\mu\varepsilon$]	10^{-4}	0.01
No. of cycles in $10 \leq \varepsilon \leq$ max	5.5	50
No. of cycles in $0 < \varepsilon < 10$	3744	1010

Table A.1.: Effects of cleaning on a 10-minute measured strain record

Appendix B.

Derivation of Fatigue Damage Formula

B.1. Linear S-N Curve Case

For a linear S-N curve, the relationship between applied stress-range and its corresponding fatigue life (in cycles) are shown as in Eq. (B.1), where K_c and m are parameters of the S-N curve.

$$N_i = K_c \, S_i^{-m} \tag{B.1}$$

Fatigue damage contributed by one load cycle is calculated as:

$$\begin{aligned} D_i &= \frac{1}{N_i} \\ &= \frac{1}{K_c} S_i^m \end{aligned} \tag{B.2}$$

For a large number of load cycle, the expected fatigue damage is described as:

$$\begin{aligned} \mathrm{E}\left[D_i\right] &= \frac{1}{K_c} \sum_0^\infty S_i^m \, \mathrm{P}\left(S_i\right) \\ &= \frac{1}{K_c} \int_0^\infty S^m \, f\left(S\right) dS \end{aligned}$$

where $f\left(S\right)$ is the probability density function of the stress-range distribution, assumed to be Weibull as shown in Eq. (B.3), where k and λ are scale and shape

parameters.

$$f(S) = \frac{\lambda}{k}\left(\frac{S}{k}\right)^{\lambda-1} \exp\left(-\left(\frac{S}{k}\right)^{\lambda}\right) \tag{B.3}$$

Set: $t = \left(\frac{S}{k}\right)^{\lambda}$

$\rightarrow dt = \frac{\lambda}{k}\left(\frac{S}{k}\right)^{\lambda-1} dS$

$\rightarrow S = k \cdot t^{1/\lambda} \Rightarrow S^m = k^m \cdot t^{m/\lambda}$

then:

$$\begin{aligned} \mathrm{E}[D_i] &= \frac{1}{K_c} \int_0^{\infty} k^m\, t^{m/\lambda} \exp(-t)\, dt \\ &= \frac{1}{K_c}\, k^m \Gamma\left(\frac{m}{\lambda} + 1\right) \end{aligned}$$

The total fatigue damage at year t, given number of load cycle per year is ν:

$$\begin{aligned} D_{tot} &= T\,\nu\,\mathrm{E}[D_i] \\ &= T\,\nu\,\frac{1}{K_c}\, k^m \Gamma\left(\frac{m}{\lambda} + 1\right) \end{aligned}$$

B.2. Bi-linear S-N Curve Case

A bi-linear S-N curve is defined as in Eq. (B.4) where S_q is the stress-range value at the knee point, calculated as in Eq. (B.5); K_{1c}, $m_1$and K_{2c}, m_2 are parameters of the bi-linear S-N curve for the upper and lower branches, respectively.

$$N_i = \begin{cases} K_{1c}\, S_i^{-m_1} & \text{if } S_i \geq S_q \\ K_{2c}\, S_i^{-m_2} & \text{otherwise} \end{cases} \tag{B.4}$$

$$S_q = \left(\frac{K_{2c}}{K_{1c}}\right)^{1/(m_2 - m_1)} \tag{B.5}$$

The fatigue damage index contributed by a single stress-range can be written as:

$$D_i = \begin{cases} \dfrac{1}{K_{1c}}\, S_i^{m_1} & \text{if } S_i \geq S_q \\ \\ \dfrac{1}{K_{2c}}\, S_i^{m_2} & \text{otherwise} \end{cases}$$

Then, the expected value of fatigue damage per stress-range can be estimated as:

$$\begin{aligned} \mathrm{E}\left[D_i\right] &= \frac{S_i^{m_1}}{K_{1c}}\, \mathrm{P}\left(S_i \geq S_q\right) + \frac{S_i^{m_2}}{K_{2c}}\, \mathrm{P}\left(S_i < S_q\right) \\ &= \frac{1}{K_{1c}} \int_{S_q}^{\infty} S_i^{m_1}\; f\left(S\right) dS + \frac{1}{K_{2c}} \int_{0}^{S_q} S_i^{m_2}\; f\left(S\right) dS \end{aligned} \tag{B.6}$$

where $f\left(S\right)$ is the probability density function as shown in Eq. (B.3). Using the change of variable as for the linear S-N curve case above, we have:

$$\begin{aligned} \mathrm{E}\left[D_i\right] &= \frac{1}{K_{1c}} \int_{\left(\frac{S_q}{k}\right)^{\lambda}}^{\infty} k^{m_1}\, t^{m_1/\lambda}\, \exp\left(-t\right) dt + \frac{1}{K_{2c}} \int_{0}^{\left(\frac{S_q}{k}\right)^{\lambda}} k^{m_2}\, t^{m_2/\lambda}\, \exp\left(-t\right) dt \\ &= \frac{1}{K_{1c}}\, k^{m_1}\, \Gamma\left(\frac{m_1}{\lambda} + 1,\, \left(\frac{S_q}{k}\right)^{\lambda}\right) + \frac{1}{K_{2c}}\, k^{m_2}\, \gamma\left(\frac{m_2}{\lambda} + 1,\, \left(\frac{S_q}{k}\right)^{\lambda}\right) \end{aligned} \tag{B.7}$$

where $\gamma\left(\ ,\ \right)$ and $\Gamma\left(\ ,\ \right)$ are lower and upper incomplete gamma functions, respectively.

Appendix C.

Minimum Number of Stress Cycles

For a given Weibull distribution of stress-range, different sets of n generated stress-ranges results in different values of fatigue damage D. A larger value of n will lead to a smaller variation of D. This Appendix show a method to find a minimum value of n for a given value of error threshold.

a) To quantify the variation of D, let's generate m sets of n stress-ranges.

b) The 95% confidence intervals:

$$UpperLimit = mean\,(D) + Z_{95\%} \times S_{meanD}$$

$$LowerLimit = mean\,(D) - Z_{95\%} \times S_{meanD}$$

where S_{meanD} is the standard error of the mean of D:

$$S_{meanD} = \frac{std\,(D)}{\sqrt{m}}$$

the value of $Z_{95\%}$ can be estimated using a Student t-distribution with $m = 100$:

$$Z_{95\%} = 1.9842$$

c) The error of fatigue damage can be defined as:

$$a = \frac{UpperLimit - LowerLimit}{mean\,(D)}\,(\%)$$

d) **Conclusion**: For the given stress-range data, if the error threshold of fatigue damage is set to 5%, number of cycles n should be larger than 10^7.

The results of calculation are shown in the table below Tab. C.1, considering:

- $m = 100$,
- n is varied to see the effect on the error of fatigue damage
- Weibull parameters (scale = k, shape = λ) of stress-range distributions in:
  - Case 1: wind speed range from 5 to 10 m/s: $k = 1.922$, $\lambda = 0.6172$
  - Case 2: wind speed range from 10 to 15 m/s: $k = 4.2385$, $\lambda = 0.7793$
  - Case 3: wind speed range from 20 to 30 m/s: $k = 9.408$, $\lambda = 1.0774$
- SN curve: $\log a_2 = 15.606$; $\log a_1 = 11.764$; $m_1 = 3$; $m_2 = 5$

No. of cycles (n)	Case 1	Case 2	Case 3
10^7	5.5%	3.4%	1.4%
5×10^6	7.3%	4.5%	1.7%
10^6	19.5%	9.3%	4.3%

Table C.1.: Error in fatigue damage

Appendix D.

Stress Intensity Factor Solutions

The content of this Appendix is based on BS 7910:2013+A1:2015.

The general form of the stress intensity factors solution are:

$$K_{I(a)} = (Y\sigma)\sqrt{\pi a} \tag{D.1}$$

$$K_{I(c)} = (Y\sigma)\sqrt{\pi c} \tag{D.2}$$

The stress intensity factor range $\Delta K_{I(a)}$ and $\Delta K_{I(c)}$ are calculated as:

$$\Delta K_{I(a)} = (Y\Delta\sigma)\sqrt{\pi a} \tag{D.3}$$

$$\Delta K_{I(c)} = (Y\Delta\sigma)\sqrt{\pi c} \tag{D.4}$$

The components $(Y\sigma)$ and $(Y\Delta\sigma)$ are calculated as followings:

$$(Y\sigma) = Mf_w\left\{k_{tm}M_{km}M_mP_m + k_{tb}M_{kb}M_b\left[P_b + (k_m - 1)\,P_m\right]\right\} \tag{D.5}$$

$$(Y\Delta\sigma) = Mf_w\left\{k_{tm}M_{km}M_m\Delta\sigma_m + k_{tb}M_{kb}M_b\left[\Delta\sigma_b + (k_m - 1)\,\Delta\sigma_m\right]\right\} \tag{D.6}$$

where:

- ◇ P_m and P_b are
- ◇ $\Delta\sigma_m$ and $\Delta\sigma_b$ are
- ◇ k_{tm}, k_{tb}, and k_m are the stress concentration factors for membrane stress, bending stress, and misalignment, respectively.
- ◇ M_{km} and M_{kb} are correction factors for membrane and bending loading, applied when the flaw is in a region of local stress concentration, such as the weld toe.
- ◇ M, f_w, M_m, and M_b are calculated as in ... for surface crack and in .... for through-thickness cracks.

L is the overall length of the attachment, measured from weld toe to weld toe, assumed to be $L = 120\ mm$

D.1. Surface Cracks

D.1.1. General

This section show the solutions of components in equations from (D.1) to (D.6), where:

$$M = 1,$$

$$f_w = \left\{ \sec\left[\left(\frac{\pi c}{W}\right) \left(\frac{a}{B}\right)^{0.5} \right] \right\}^{0.5} \quad \text{which equals 1.0 if } a/2c = 0$$

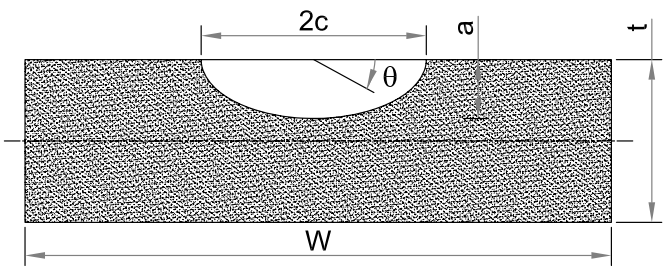

Figure D.1.: Dimensions of a surface crack

D.1.2. Membrane Loading:

D.1.2.1. The following conditions apply:

$$0 < a/2c \leq 1.0$$

$$0 \leq \theta \leq \pi$$

and:

$$a/t < 1.25\,(a/c + 0.6) \quad \text{for } 0 < a/2c \leq 0.1$$

$$a/t < 1.0 \quad \text{for } 0.1 < a/2c \leq 1.0$$

D.1.2.2. Solution

$$M_m = \left[M_1 + M_2 \left(\frac{a}{B}\right)^2 + M_3 \left(\frac{a}{B}\right)^4\right] \frac{g\ f_\theta}{\Phi} \tag{D.7}$$

where:

$$M_1 = 1.13 - 0.09\left(\frac{a}{c}\right) \quad \text{for } 0 < a/2c \leq 0.5\ ;$$

$$M_1 = \left(\frac{c}{a}\right)^{0.5}\left[1 + 0.04\left(\frac{c}{a}\right)\right] \quad \text{for } 0.5 < a/2c \leq 1.0;$$

$$M_2 = \left[\frac{0.89}{0.2 + (a/c)}\right] - 0.54 \quad \text{for } 0 < a/2c \leq 0.5;$$

$$M_2 = 0.2\left(\frac{c}{a}\right)^4 \quad \text{for } 0.5 < a/2c \leq 1.0;$$

$$M_3 = 0.5 - \frac{1}{0.65 + \left(\frac{a}{c}\right)} + 14\left(1 - \frac{a}{c}\right)^{24} \quad \text{for } 0 < a/2c \leq 0.5;$$

$$M_3 = -0.11\left(\frac{c}{a}\right)^4 \quad \text{for } 0.5 < a/2c \leq 1.0;$$

$$g = 1 + \left[0.1 + 0.35\left(\frac{a}{B}\right)^2\right](1 - \sin\theta)^2 \quad \text{for } 0 < a/2c \leq 0.5;$$

$$g = 1 + \left[0.1 + 0.35\left(\frac{c}{a}\right)\left(\frac{a}{B}\right)^2\right](1 - \sin\theta)^2 \quad \text{for } 0 < a/2c \leq 1.0;$$

$$f_\theta = \left[\left(\frac{a}{c}\right)^2 \cos^2\theta + \sin^2\theta\right]^{0.25} \quad \text{for } 0 < a/2c \leq 0.5;$$

$$f_\theta = \left[\left(\frac{c}{a}\right)^2 \sin^2\theta + \cos^2\theta\right]^{0.25} \quad \text{for } 0.5 < a/2c \leq 1.0;$$

$$\Phi = \left[1 + 1.464\left(\frac{a}{c}\right)^{1.65}\right]^{0.5} \qquad \text{for } 0 \leq a/2c \leq 0.5;$$

$$\Phi = \left[1 + 1.464\left(\frac{c}{a}\right)^{1.65}\right]^{0.5} \qquad \text{for } 0.5 < a/2c \leq 1.0;$$

dfsdf

D.1.3. Bending Loading

D.1.3.1. Conditions

The same conditions as in sec. D.1.2.1 are applied for surface cracks in bending loading condition.

D.1.3.2. Solutions

$$M_b = HM_m$$

where:

M_m is calculated from equation (D.7),

$H = H_1 + (H_2 - H_1)\sin^q\theta$

where:

$q = 0.2 + (a/c) + 0.6\,(a/B)$ for $0 < a/2c \leq 0.5$,

$q = 0.2 + (c/a) + 0.6\,(a/B)$ for $0.5 < a/2c \leq 1.0$,

$H_1 = 1 - 0.34\,(a/B) - 0.11\,(a/c)\,(a/B)$ for $0 < a/2c \leq 0.5$,

$H_1 = 1 - [0.04 + 0.41\,(c/a)]\,(a/B) + \cdots$
$\left[0.55 - 1.93\,(c/a)^{0.75} + 1.38\,(c/a)^{1.5}\right](a/B)^2$ for $0.5 < a/2c \leq 1.0$,

$H_2 = 1 + G_1\,(a/B) + G_2\,(a/B)^2$.

where:

$G_1 = -1.22 - 0.12(a/c)$ for $0 < a/2c \leq 0.5$,

$G_1 = -2.11 + 0.77\,(c/a)$ for $0.5 < a/2c \leq 1.0$,

$G_2 = 0.55 - 1.05\,(a/c)^{0.75} + 0.47\,(a/c)^{1.5}$ for $0 < a/2c \leq 0.5$,

$G_2 = 0.55 - 0.72\,(c/a)^{0.75} + 0.14\,(c/a)^{1.5}$ for $0.5 < a/2c \leq 1.0$.

D.2. Correction Factors of Local Stress Concentration

The solution used in this thesis is based on 2D finite element analysis. The general formula for M_{kb} and M_{km} is:

$$M_k = v\,(z/B)^w \tag{D.8}$$

down to $M_k = 1$

where v and w have the values given in Tab. D.1; z is the through-thickness distance from the weld toe to crack unity; B is the wall thickness; L is the overall length of the attachment, measured from weld toe to weld toe.

It is noted that when it is used to calculate $\Delta K_{I(c)}$and $K_{I(c)}$, $z = 0.15\ mm$ should be used because Eq.(D.8) is not applicable for $z = 0$.

Loading mode	L/B	z/B	v	w
Axial	≤ 2	$\leq 0.05(L/B)^{0.55}$	$0.51(L/B)^{0.27}$	-0.31
		$> 0.05(L/B)^{0.55}$	0.83	$-0.15(L/B)^{0.46}$
	> 2	≤ 0.073	0.615	-0.31
		> 0.073	0.83	-0.21
Bending	≤ 1	$\leq 0.03(L/B)^{0.55}$	$0.45(L/B)^{0.21}$	-0.31
		$> 0.03(L/B)^{0.55}$	0.68	$-0.19(L/B)^{0.21}$
	> 1	≤ 0.03	0.45	-0.31
		> 0.03	0.68	-0.19

Table D.1.: Values of v and w for axial and bending loading